Title
MyD88-dependent signaling in prostate cancer: Regulation of immune populations in the tumor microenvironment

Author
Peek, Elizabeth Marie

Publication Date
2016

Peer reviewed|Thesis/dissertation

UNIVERSITY OF CALIFORNIA

Los Angeles

MyD88-dependent signaling in prostate cancer:

Regulation of immune populations in the tumor microenvironment

A dissertation submitted in partial satisfaction

of the requirements for the degree

Doctor of Philosophy in Molecular Biology

By

Elizabeth Marie Peek

2016

ABSTRACT OF THE

DISSERTATION

MyD88-dependent signaling in prostate cancer:

Regulation of immune populations in the tumor microenvironment

by

Elizabeth Marie Peek

Doctor of Philosophy in Molecular Biology

University of California, Los Angeles, 2016

Professor Arnold I. Chin, Co-Chair

Professor Genhong Cheng, Co-Chair

Abstract

The role of immune signaling in cancer is complex and conflicting. Inflammatory signaling can drive an anti-tumor response, but copious evidence suggests that chronic inflammation also promotes tumorigenesis. The most well-characterized of inflammatory pathways is the Toll-like receptor (TLR) pathway, which promotes downstream NF-κB activation. Mutations in TLRs are associated with a higher risk of prostate cancer.

Using the TRAMP model of prostate cancer, we report the impact of TLR signaling disruption on tumor growth and progression. The adaptor protein MyD88 is an essential

component of signaling for almost all TLRs, so loss of MyD88 abrogates most TLR signaling. Absence of MyD88-dependent signaling in TRAMP prostate tumors resulted in a more aggressive disease, as determined by histology. Analysis of infiltrating immune cells revealed an increase in $CD11b^{+}Gr\text{-}1^{+}$ MDSCs (myeloid-derived suppressor cells) in $MyD88^{-/-}$ tumors when compared to $MyD88^{+/+}$ tumors, both in number and in functional output. $MyD88^{-/-}$ tumors also displayed increased expression of some chemokines involved in MDSC recruitment.

An explicit link between MyD88-dependent signaling and MDSC accumulation was suggested by the expression of S100A9, a chemokine and a TLR4 ligand. Specifically, this indicates that MyD88-dependent signaling may play a role within the MDSCs themselves. *In vitro* differentiation of MDSCs from bone marrow skewed towards the granulocytic subset (gMDSCs) in $MyD88^{-/-}$ cells, supporting an internal role for MyD88 signaling. $MyD88^{-/-}$ MDSCs also showed an increased sensitivity to chemotaxis mediated by S100A9 and an increase in Arg-1 expression following S100A9 stimulation. We conclude that MyD88-dependent signaling may play an essential role in regulating the population of tumor-infiltrating cells by reducing MDSC activity and MDSC response to S100A9-mediated chemotaxis, thus limiting prostate tumor progression.

The dissertation of Elizabeth Marie Peek is approved.

Matthew B. Rettig

Arnold I. Chin, Committee Co-Chair

Genhong Cheng, Committee Co-Chair

University of California, Los Angeles

2016

TABLE OF CONTENTS

LIST OF TABLES AND FIGURES

Chapter I

Chapter II

Chapter III

Chapter IV

Chapter V

LIST OF ABBREVIATIONS

Akt	Protein kinase B (PKB)
AR	Androgen receptor
Arg-1	Arginase-1 enzyme
CCL2/MCP1	Chemokine (C-C motif) ligand 2; monocyte chemoattractant protein 1
CCL3/MIP-1α	Chemokine (C-C motif) ligand 3; macrophage inflammatory protein-1α
CCL5/RANTES	Chemokine (C-C motif) ligand 5; regulated on activation, normal T cell expressed and secreted
CD11b	Cluster of differentiation molecule 11b
CpG	5'-Cytosine-phosphate-Guanine-3' linear DNA sequence
CTLA-4	Cytotoxic T-lymphocyte-associated protein 4
CXCL1/KC	Chemokine (C-X-C motif) ligand 1; keratinocyte chemoattractant
DAMP	Damage-associated molecular pattern
ERK1/2 (MAPK3/1)	Extracellular signal-regulated kinase 1/2; mitogen-activated protein kinase 3/1
G-CSF	Granulocyte colony-stimulating factor
GM-CSF	Granulocyte and monocyte colony-stimulating factor
gMDSC	Granulocytic myeloid-derived suppressor cell
Gr-1	Granulocyte marker 1
H&E	Hematoxylin and eosin histological stains
HMGB1	High mobility group box 1 protein
IκBα	Inhibitor of NF-κB, alpha
IKK-β	IκB kinase, subunit beta
IL-1β/LAF	Interleukin 1β; lymphocyte-activating factor
IL-4	Interleukin 4
IL-10	Interleukin 10

IL-13	Interleukin 13
iNOS	Inducible nitric oxide synthase
JAK/STAT	Janus kinase/signal transducer and activator of transcription
LPS	Lipopolysaccharide
Ly-6C/G	Leukocyte antigen-6 complex, locus C/G
M-CSF	Macrophage colony-stimulating factor
MAPK	Mitogen-activated protein kinase
mCRPC	Metastatic castration-resistant prostate cancer
MDSC	Myeloid-derived suppressor cell
mMDSC	Monocytic myeloid-derived suppressor cell
MyD88	Myeloid differentiation primary response gene 88
NF-κB	Nuclear factor κ-light-chain-enhancer of activated B cells
NK cell	Natural killer cell
PAMP	Pathogen-associated molecular pattern
PD-1	Programmed cell death protein 1
PD-L1	Programmed death-ligand 1
PIN	Prostatic intraepithelial neoplasia
PolyI:C	Polyinosinic:polycytidylic acid
RAGE	Receptor for advanced glycation endproducts
Rb	Retinoblastoma protein
S100A9/MRP14/CalB	S100 calcium-binding protein A9; migration inhibitory factor-related protein 14; calgranulin B
SV40 TAg	Simian vacuolating virus 40 large T antigen
TLR	Toll-like receptor
TRAMP	Transgenic adenocarcinoma of the mouse prostate

VITA

2007-2011	B.S., Biology
	With Highest Distinction
	University of Virginia
2010	Ingrassia Family Echols Scholar Research Grant
	University of Virginia
2011	2nd Place
	Richard D. Katz Undergraduate Research Symposium
	University of Virginia
Fall 2012	Teaching Assistant, Molecular Parasitology
	Department of Microbiology, Immunology, and Molecular Genetics
	University of California, Los Angeles
Fall 2013	Teaching Assistant, Molecular Parasitology
	Department of Microbiology, Immunology, and Molecular Genetics
	University of California, Los Angeles
2014-2015	Whitcome Fellowship
	Molecular Biology Interdepartmental Doctoral Program (MBIDP)
	University of California, Los Angeles
2015	Poster Presentation Award
	MBIDP Retreat
	University of California, Los Angeles

2015-2016 Whitcome Fellowship

UCLA Molecular Biology Interdepartmental Doctoral Program (MBIDP)

University of California, Los Angeles

PUBLICATIONS

Hanwei Zhang, Kris Prado, Kelvin X. Zhang, Elizabeth M. Peek, Jane Lee, Xiaoyan Wang, Jiaoti Huang, Gang Li, Matteo Pellegrini, and Arnold I. Chin (2016). Biased expression of the FOXP33 isoform in aggressive bladder cancer mediates differentiation and cisplatin chemotherapy resistance. *Clinical Cancer Research* Epub ahead of print May 17 2016.

David R. Li, Hanwei Zhang, Elizabeth M. Peek, Wang Song, Lin Du, Gang Li, Arnold I. Chin (2015). Synergy of histone-deacetylase inhibitor AR-42 with cisplatin in bladder cancer. *Journal of Urology* 194(2):547-55.

Elizabeth M. Peek, Wang Song, Hanwei Zhang, Jiaoti Huang, and Arnold I. Chin (2015). Loss of MyD88 leads to more aggressive TRAMP prostate cancer and influences tumor infiltrating lymphocytes. *Prostate* 75(5):463-73.

Elizabeth M. Peek, David R. Li, Hanwei Zhang, Hyun Pyo Kim, Baohui Zhang, Isla P. Garraway, and Arnold I. Chin (2012). Stromal modulation of bladder cancer-initiating cells in a subcutaneous tumor model. *American Journal of Cancer Research* 2(6): 745-751.

Paul V. Beum*, Elizabeth M. Peek*, Margaret A. Lindorfer, Frank J. Beurskens, Patrick J. Engelberts, Paul W.H.I. Parren, Jan G.J. van de Winkel, and Ronald P. Taylor (2011). Loss of CD20 and bound CD20 antibody from opsonized B cells occurs more rapidly because of trogocytosis mediated by Fc receptor-expressing effector cells than direct internalization by the B cells. *Journal of Immunology* 187: 3438-3447.

Paul V. Beum, Margaret A. Lindorfer, Elizabeth M. Peek, P. Todd Stukenberg, Michel de Weers, Frank J. Beurskens, Paul W.H.I. Parren, Jan G.J. van de Winkel, Ronald P. Taylor (2011). Penetration of antibody-opsonized cells by the membrane attack complex of complement promotes Ca(2+) influx and induces streamers. *European Journal of Immunology* 41(8): 2436-2446.

Margaret A. Lindorfer, Andrew W. Pawluczkowycz, Elizabeth M. Peek, Kimberly Hickman, Ronald P. Taylor, and Charles J. Parker (2010). A novel approach to preventing the hemolysis of paroxysmal nocturnal hemoglobinuria: both complement-mediated cytolysis and C3 deposition are blocked by a monoclonal antibody specific for the alternative pathway of complement. *Blood* 115: 2283-2291

CHAPTER I

INTRODUCTION

PROSTATE CANCER

Incidence and treatment. Prostate cancer is the most common cancer in men, representing 26% of new cases of cancer[1-2]. Currently, 2.9 million men are living with prostate cancer in the US, and 1 in 6 men will be diagnosed within their lifetime. However, prostate cancer constitutes only 9% of male cancer deaths in the US. Patients' 5-year relative survival depends heavily on the progression of their disease: for localized and regional tumors, survival is 100%; for metastatic disease, 5-year survival is merely 29.3%[1].

The first line therapeutics for patients with metastatic disease are typically anti-androgen therapies. As part of the male reproductive system, the prostate responds to growth signals from testosterone and other hormones through the androgen receptor (AR)[3]. Tumors can stimulate their own growth by increasing activity of the AR pathway, so therapeutics are used to inhibit androgen-AR binding and suppress androgen production. Typically, this castration therapy results in rapid tumor regression and reduction in metastatic lesions, and patients may be treated simultaneously with radiotherapy or prostatectomy.

Castration-resistant disease. Eventually, many tumors become resistant to androgen deprivation therapy and are then termed castration-resistant prostate cancer (CRPC). This stage represents a particular focus for the research community. While most prostate tumors initially respond to androgen deprivation, CRPC therapeutic responses are more measured. In recent years, several therapies (of varying efficacy) have been developed: abiraterone, enzalutamide, docetaxel, and sipuleucel-T[4]. Both abiraterone and enzalutamide are anti-androgens- abiraterone inhibits androgen synthesis and partially blocks AR, while enzalutamide blocks AR with very high affinity

and inhibits effectors of downstream AR signaling. Sipuleucel-T, the first cell-based cancer immunotherapy approved by the FDA, involves the removal and priming of patient dendritic cells with a common prostate cancer protein[5]. The activated cells are then re-infused and stimulate an anti-tumor immune response.

Barriers to immunotherapy. Despite the success of sipuleucel-T in mCRPC, prostate cancer notoriously responds poorly to immunotherapies. While promising results were seen with nivolumab (anti-PD-1) in non-small cell lung cancer, renal cell carcinoma, and melanoma, no objective response was seen in patients with mCRPC[6-7]. Similarly, a phase III trial of ipilimumab (anti-CTLA-4) in mCRPC with almost 800 patients showed no significant difference in overall survival[8].

Given previous efficacy with cell-based therapies, adoptive T cell therapies have been proposed, but advanced prostate cancer lacks tumor-specific markers needed to direct those T cells. For example, increased PSA levels have long been associated with prostate cancer, but PSA is prostate-specific and not tumor-specific. Additionally, PSA is a secreted protein. While the non-coding PCA3 transcript is tumor-specific, it lacks a surface protein for immune cells to target[9]. At this point, the most promising immunotherapies appear to be mostly ineffective with CRPC. Understanding the tumor and its interactions with immune cells may elucidate novel targets and ways to enhance susceptibility to existing therapies.

Mouse models. Mice do not spontaneously develop prostate cancer, limiting the design of potential research models. Most of the early models of prostate cancer were in rats: the Lobund-Wistar rat

developed spontaneous disease at 26 months (earlier with chemical treatment)[10]; the Fischer F344 rat developed non-metastatic tumors after chemical treatment[11]; the Dunning R-3327 system used cell lines derived from the spontaneous tumor of a Copenhagen rat[12].

An autochthonous mouse model of prostate cancer called TRAMP (transgenic adenocarcinoma of the mouse prostate) was developed using a prostate-specific transgene[13]. A rat probasin promoter drives the expression of the SV40 large T antigen, a viral protein that targets and inhibits the Rb/p53 family of tumor suppressors. Over time, the mice develop prostate tumors that mimic the histology and progression of human disease[14-15]. In addition, several TRAMP cell lines derived from the transgenic tumors have been established and characterized[16]. These cell lines can be grown subcutaneously in C57Bl/6 mice, though they do not recapitulate the prostate histology seen in patients.

TOLL-LIKE RECEPTOR SIGNALING

Activation of immune pathways. Toll-like receptors (TLRs) are an essential part of the innate immune system, recognizing foreign or unusual molecules and triggering a humoral response[17]. TLRs are transmembrane proteins that each recognize a conserved molecular pattern and, upon recognition, transduce a signal across the cell membrane. TLRs 1-10 have been identified in humans, and TLRs 1-9 plus 11-13 have been identified in mice[18].

Following activation of the TLR, an adaptor protein MyD88 associates with the intracellular domain, leading to phosphorylation of IRAK1 (**Figure 1.1**). IRAK1 attracts TRAF6, which then forms a complex with TAK1, TAB1, and TAB2. TRAF6 is ubiquitinylated, activating TAK1, which phosphorylates IKK and MAPK. Phosphorylated IKK promotes degradation of IκB, which releases its inhibition of NF-κB. After translocation to the nucleus, NF-κB modifies expression of its target genes. Through this canonical TLR-NF-κB pathway, TLR activation promotes inflammation and innate immune activation. Not all the TLRs use MyD88 as an adapter molecule. TLR3 uses TRIF exclusively, while TLR4 uses both MyD88 and TRIF.

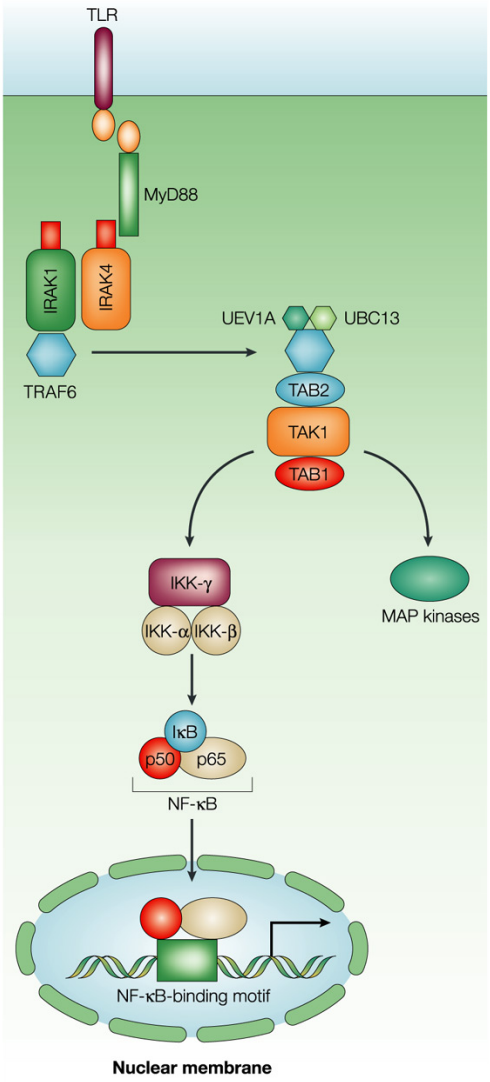

Figure 1.1. Toll-like receptor signaling. Adapted from Akira & Takeda (2004).

Ligands. Individual TLRs can recognize multiple ligands, but there are two main categories: pathogen-associated molecular patterns (PAMPs) and damage-associated molecular patterns (DAMPs). The PAMPs are better-studied, as most of the early research on TLRs focused on response to infection[19]. For example, TLR3 binds to dsRNA and TLR9 binds CpG DNA, both unique structures of viral or bacterial pathogens. TLR4 meanwhile binds to LPS, a component of Gram-negative bacterial cell walls.

DAMPs, meanwhile, are released from or near necrotic cells, indicating that tissue damage has occurred. These molecules can also bind TLRs and activate inflammatory signaling. HMGB1 is a nuclear protein that is only released into the extracellular space following cell necrosis, but not apoptosis[20-21]. HMGB1 can bind TLR2, TLR4, and RAGE. S100A8 and S100A9 are calcium-binding molecules specifically secreted by some cells following damage or stress. They can homo- or hetero-dimerize to activate their receptors, TLR4 and RAGE[22-23].

TLRs in cancer. Activation of TLRs is intended to drive an immune response to fight off invading pathogens and/or rebuild damaged tissue. Therefore, one could expect TLR activity in or around a tumor would promote an anti-tumor response. The class of immune checkpoint inhibitors (anti-PD-1/PD-L1) have been successful by specifically removing suppressive forces on infiltrating T cells[24-25]. However, chronic inflammation, particularly through NF-ϰB, has been consistently tied to tumorigenesis[26-27]. Specifically in prostate cancer, areas of chronic inflammation are common surrounding prostatic intraepithelial neoplasia (PIN) lesions[28-29]. Additionally, a series of SNPs have been identified within the TLR gene cluster that indicate an increased prostate cancer risk[30].

This duality of inflammation also plays out in various tumor models when TLR signaling is perturbed (**Table 1.1**). In colorectal[31-33], gastric[34], breast[35], and prostate models[36], disruption of TLR signaling produces an anti-tumor effect. However, additional studies in colorectal[37-38], lymphoma[39], pancreatic[40], and prostate[41] models show that disruption of TLR signaling enhances tumor growth and progression. No obvious conclusion can be drawn, as the same mutation in different disease models, or even different mutations within the same disease model show varying results. We hope to gain a deeper understanding of how TLR signaling affects different tissue types.

Modification	Ref	Model	Tumor Effect
TLR3$^{-/-}$	41	Prostate (TRAMP)	↑
IKK-β$^{-/-}$	36	Prostate (TRAMP)	↓
TLR2$^{-/-}$ or MyD88$^{-/-}$	35	Breast (xenograft)	↓
MyD88$^{-/-}$	40	Pancreatic (Kras^{G12D})	↑
MyD88 L265P	39	DLBCL patients	↑
MyD88$^{-/-}$	37	Colitis (DSS)	↑
TLR2$^{-/-}$	34	Intestinal (DSS)	↓
Mal (TIRAP)$^{-/-}$	38	Colorectal (CAC)	↑
IKK-β$^{-/-}$	31	Colorectal (CAC)	↓
MyD88 inhibitor	33	Colorectal (CAC)	↓
MyD88$^{-/-}$	32	Colon (APC)	↓
MyD88$^{-/-}$	34	Gastric (*Gan*)	↓

Table 1.1. TLR disruption in cancer models.

MYELOID-DERIVED SUPPRESSOR CELLS

MDSC markers and function. The immune system employs several mechanisms to regulate non-specific or self immune activation and prevent the emergence of autoimmune disease. Distinct cell types with regulatory functions have been identified, including Tregs and myeloid-derived suppressor cells (MDSCs)[42]. In mice, MDSCs are defined as a heterogeneous group of $CD11b^+$ $Gr\text{-}1^+$ cells and can be subdivided into populations of granulocytic and monocytic lineages[43]. Granulocytic MDSCs (gMDSCs) are $Ly6G^+$ $Ly6C^{mid/lo}$, while monocytic MDSCs are $Ly6G^-$ $Ly6C^{hi}$, and they are currently identified as immature cells from different myeloid lineages that share a similar functional output[44-45]. Human MDSCs have not been fully characterized, and there are no markers to correspond with the murine subpopulations, but the current identification is $CD11b^+$ $CD33^+$ $HLA\text{-}DR^{lo}$ [46].

Generally, MDSCs are important for suppressing T cell function, particularly blocking the cytotoxic action of $CD8^+$ cells, by producing arginase-1 and inducible nitric oxide synthase (iNOS)[47-48]. Arginase-1 depletes the amino acid L-arginine, which is central to T cell proliferation[49], and iNOS uses L-arginine to produce nitric oxide (NO) and reactive oxygen species (ROS) that react to form peroxynitrites[50]. Peroxynitrites are powerful oxidants that will then promote nitration of T cell receptors and CD8 molecules, preventing antigen-specific T cell activation[48]. Though they ultimately perform the same function, the two MDSC subsets prefer different oxidant species: gMDSCs produce ROS, while mMDSCs produce NO[51]. This is the only confirmed functional difference in the subpopulations, and it does not cause differences in the T cell suppressive activity of MDSCs[45]. MDSCs can also function to suppress NK cells, both in

differentiation and in activity[52-54], and some effects on dendritic cell development have been observed[55].

MDSCs in cancer. MDSCs have recently been identified as an important barrier to the success of cancer immunotherapies[56]. Present in the tumor microenvironment of mice and circulating in the bloodstream of most human patients, these cells promote escape from immune surveillance[57-59]. For example, in breast cancer, more circulating MDSCs correlated with increased clinical stage, larger metastatic burden, and decreased response to chemotherapy[60]. Similar results are seen in prostate cancer[61] and a host of other cancers[62-64]. The tumors themselves, as part of an immune escape mechanism, will often secrete or promote the expression of chemokines that recruit MDSCs[65-67]. Notably, a reduction in tumor inflammation delays MDSC recruitment to the tumor microenvironment, consequently slowing tumor progression[68]. Given our current understanding of MDSC-tumor interactions, targeting MDSC recruitment and activity should reduce tumor growth and increase the efficacy of immunotherapies[69].

Many signaling molecules that regulate aspects MDSC function have been well-characterized[70]. Several members of the colony-stimulating factor family[71] are important for MDSC generation and differentiation: G-CSF[72-75], GM-CSF[76-78], and M-CSF[79-80]. While these proteins are not directly involved in recruitment, they drive production of MDSCs and regulate differentiation into the g- and m-MDSC populations. The cytokines IL-1β and IL-13 play a role in MDSC activation, as IL-1β promotes inflammation in the tumor that indirectly induces MDSCs, and IL-13 drives a Th2 immune response and increases Arg-1 expression in MDSCs [81-85]. Members of the CC and CXC chemokine families are shown to play the most direct role in MDSC accumulation in the tumor[86-

[89]. Chemokines CCL2, CCL3, CCL5, CCL7, CXCL1, CXCL8, CXCL12, and CX3CL1 have all been identified as potential recruiters of MDSCs. However, CCL2 activity has been studied in more depth, as MDSCs express its receptor, CCR2, and CCL2-CCR2 binding directly recruits MDSCs to tumors[90-93]. Additionally, blockade of CCL2 or inhibition of its synthesis has been shown to augment immunotherapies and induce tumor regression[92,94].

S100A9

Inflammatory activity. As described previously, DAMPs (damage-associated molecular patterns) are endogenous proteins that activate Toll-like receptors (TLRs) following tissue damage or necrosis. One of the best-studied DAMPs is S100A9, a member of the S100 calcium binding pathway that is often hetero-dimerized with S100A8[95]. S100A9 binds to two surface receptors: TLR4[95-98] and RAGE[99]. Downstream of TLR4, S100A9 signaling activates the MyD88-dependent NF-κB pathway[97,100], while MAPK pathways are activated downstream of RAGE[99,101-102].

S100A9 expression and activation of both receptors has been repeatedly documented in a variety of cancers, where S100A9 signaling appears to promote tumor growth[103-109]. This is particularly true in prostate cancer, where S100A9 is considered a diagnostic marker due to its close association with more proliferative, more aggressive tumors[110-113]. Notably, S100A9 is also a chemokine that recruits MDSCs[114-116]. It is therefore unsurprising that high expression of S100A9, leading to increased MDSC infiltration, would be correlated with more advanced tumors.

REFERENCES

1. Howlader, N. et al. SEER Cancer Statistics Review, 1975-2013, National Cancer Institute. Bethesda, MD, http://seer.cancer.gov/csr/1975_2013/, based on November 2015 SEER data submission, posted to the SEER web site, April 2016.

2. Siegel, R.L. et al. (2015). Cancer statistics, 2015. CA: A Cancer Journal for Clinicians, 65(1), 5-29.

3. Heinlein, C.A. & Chang, C. (2004). Androgen receptor in prostate cancer. Endocrine Reviews, 25(2), 276-308.

4. Cookson, M.S. et al. (2015). Castration-resistant prostate cancer: AUA guideline. https://www.auanet.org/education/guidelines/castration-resistant-prostate-cancer.cfm.

5. Kantoff, P.W. et al. (2010). Sipuleucel-T immunotherapy for castration-resistant prostate cancer. NEJM, 363(5), 411-22.

6. Topalian, S.L. et al. (2012). Safety, activity, and immune correlates of anti-PD-1 antibody in cancer. NEJM, 366(26), 2443-54.

7. Brahmer, J.R. et al. (2010). Phase I study of single-agent anti-programmed death-1 (MDX-1106) in refractory solid tumors: safety, clinical activity, pharmacodynamics, and immunologic correlates. JCO, 28(19), 3167-75.

8. Kwon, E.D. et al. (2014). Ipilimumab versus placebo after radiotherapy in patients with metastatic castration-resistant prostate cancer that had progressed after docetaxel chemotherapy (CA184-043): a multicenter, randomized, double-blind, phase 3 trial. The Lancet Oncology, 15(7), 700-12.

9. Neves, A.F. et al. (2008). Combined analysis of multiple mRNA markers by RT-PCR assay for prostate cancer diagnosis. Clinical Biochemistry, 41(14-15), 1191-1198.

10. Pollard, M. (1992). The Lobund-Wistar rat model of prostate cancer. Journal of Cellular Biochemistry, 16H, 84-88.

11. Masui, T. et al. (1995). Ki-*ras* mutations with frequent normal allele loss versus absence of *p53* mutations in rat prostate and seminal vesicle carcinomas induced with 3,2'-dimethyl-4-aminobiphenyl. Molecular Carcinogenesis, 13(1), 21-26.

12. Dunning, W.F. (1963). Prostate cancer in the rat. National Cancer Institute monograph, 12, 351-69.

13. Greenberg, N. et al. (1995). Prostate cancer in a transgenic mouse. PNAS, 92(8), 3439-43.

14. Hurwitz, A. et al. (2001). The TRAMP mouse as a model for prostate cancer. Current Protocols in Immunology, chapter 20.

15. Kaplan-Lefko, P. et al. (2003). Pathobiology of autochthonous prostate cancer in a pre-clinical transgenic mouse model. Prostate, 55(3), 219-37.

16. Foster, B.A. et al. (1997). Characterization of prostatic epithelial cell lines derived from transgenic adenocarcinoma of the mouse prostate (TRAMP) model. Cancer Research, 57(16), 3325-30.

17. Medzhitov, R. et al. (1997). A human homologue of the *Drosophila* Toll protein signals activation of adaptive immunity. Nature, 388, 394-7.

18. Akira, S. & Takeda, K. (2004). Toll-like receptor signaling. Nature Reviews Immunology, 4, 499-511.

19. Borden, E.C. et al. (2007). Interferons at age 50: past, current, and future impact on biomedicine. Nature Reviews Drug Discovery, 6, 975-90.

20. Tsung, A. et al. (2007). HMGB1 release induced by liver ischemia involves Toll-like receptor 4-dependent reactive oxygen species production and calcium-mediated signaling. JEM 204(12), 2913-23.

21. Yu, M. et al. (2006). HMGB1 signals through toll-like receptor (TLR) 4 and TLR2. Shock 26(2), 174-9.

22. Chen, B. et al. (2015). S100A9 induced inflammatory responses are mediated by distinct damage associated molecular patterns (DAMP) receptors in vitro and in vivo. PLoS One, 10(2), e0115828.

23. Ehrchen, J. M. et al. (2009). The endogenous Toll-like receptor 4 agonist S100A8/S100A9 (calprotectin) as innate amplifier of infection, autoimmunity, and cancer. J. Leukoc. Biol. 86, 557–566.

24. Woo, S.-R. et al. (2015). Innate immune recognition of cancer. Annual Review of Immunology, 33, 445-74.

25. Liu, Y. et al. (2012). Cancer and innate immune system interactions: translational potentials for cancer immunotherapy. Journal of Immunotherapy, 35(4), 299-308.

26. Lu, H. et al. (2006). Inflammation, a key event in cancer development. Molecular Cancer Research, 4, 221.

27. Smyth, M.J. et al. (2001). A fresh look at tumor immunosurveillance and immunotherapy. Nature Immunology, 2(4), 293-9.

28. Sfanos et al. *The role of inflammation in prostate cancer*. (2014)

29. Davidsson et al. (2011) Inflammation, focal atrophic lesions, and PIN with respect to risk of lethal prostate cancer. Cancer Epidemiol Biomarkers Prev, 20(10), 2280-7.

30. Stevens, V.L. et al. (2008). Genetic variation in the toll-like receptor gene cluster (TLR10-TLR1-TLR6) and prostate cancer risk. International Journal of Cancer, 123(11), 2644-50.

31. Greten, F.R. et al. (2004). IKKbeta links inflammation and tumorigenesis in a mouse model of colitis-associated cancer. Cell, 118(3), 285-96.

32. Rakoff-Nahoum, S. & Medzhitov, R. (2007). Regulation of spontaneous intestinal tumorigenesis through the adaptor protein MyD88. Science, 317(5834), 124-7.

33. Xie, L. et al. (2015). Targeting of MyD88 homo-dimerization by novel synthetic inhibitor TJ-M2010-5 in preventing colitis-associated colorectal cancer. Journal of the National Cancer Institute, 108(4).

34. Maeda, Y. et al. (2016). Myeloid differentiation factor 88 signaling in bone marrow-derived cells promotes gastric tumorigenesis by generation of inflammatory microenvironment. Cancer Prevention Research, 9(3), 253-63.

35. Scheeren, F.A. et al. (2014). A cell-intrinsic role for TLR2-MyD88 in intestinal and breast epithelia and oncogenesis. Nature Cell Biology, 16(12), 1238-48.

36. Ammirante, M. et al. (2010). B-cell-derived lymphotoxin promotes castration-resistant prostate cancer. Nature, 464(7286), 302-5.

37. Araki, A. et al. (2005). MyD88-deficient mice develop severe intestinal inflammation in dextran sodium sulfate colitis. Journal of Gastroenterology, 40(1), 16-23.

38. Aviello, G. et al. (2013). MyD88 adaptor-like (Mal) regulates intestinal homeostasis and colitis-associated colorectal cancer in mice. Gastrointestinal and Liver Physiology, 306(9), G769-78.

39. Rovira, J. et al. (2016). *MYD88* L265P mutations, but no other variants, identify a subpopulation of DLBCL patients of activated B-cell origin, extranodal involvement and poor outcome. Clinical Cancer Research, e-pub.

40. Ochi, A. et al. (2012). MyD88 inhibition amplifies dendritic cell capacity to promote pancreatic carcinogenesis via Th2 cells. JEM, 209(9), 1671-87.

41. Chin, A.I. et al. (2010). Toll-like receptor 3-mediated suppression of TRAMP prostate cancer demonstrates the critical role of Type I interferons in tumor immune surveillance. Cancer Research, 70(7), 2595-2603.

42. Wood, K.J. et al. (2012). Regulatory immune cells in transplantation. Nature Reviews Immunology, 12, 417-30.

43. Mantovani, A. (2010). The growing diversity and spectrum of action of myeloid-derived suppressor cells. European Journal of Immunology, 40(12), 3317-20.

44. Damuzzo, V. et al. (2015). Complexity and challenges in defining myeloid-derived suppressor cells. Cytometry. Part B, Clinical Cytometry, 88(2), 77–91.

45.

46. Solito, S. et al. (2011). A human promyelocytic-like population is responsible for the immune suppression mediated by myeloid-derived suppressor cells. Blood, 118(8), 2254–2265.

47. Highfill, S. et al. (2010). Bone marrow myeloid-derived suppressor cells (MDSCs) inhibit graft-versus-host disease (GVHD) via an arginase-1-dependent mechanism that is up-regulated by interleukin-13. Blood, 116(25), 5738-47.

48. Gabrilovich, D.I. & Nagaraj, S. (2009). Myeloid-derived-suppressor cells as regulators of the immune system. Nature Reviews Immunology, 9(3), 162-174.

49. Raber, P. et al. (2013). Metabolism of L-arginine by myeloid-derived suppressor cells in cancer: mechanisms of T cell suppression and therapeutic perspectives. Immunological Investigations, 41(6-7), 614-34.

50. Zhao, K. et al. (2010). Induction of inducible nitric oxide synthase increases the production of reactive oxygen species in RAW264.7 macrophages. Bioscience Reports, 30(4).

51. Vlachou, K. et al. (2015). Elimination of granulocytic myeloid-derived suppressor cells in lupus-prone mice due to ROS-dependent extracellular trap formation. Arthritis & Rheumatology, 68(2), 449-61.

52. Elkabets, M. et al. (2010). IL-1b regulates a novel myeloid-derived suppressor cell subset that impairs NK cell development and function. European Journal of Immunology, 40(12), 3347-57.

53. Li, H. et al. (2008). Cancer-expanded myeloid-derived suppressor cells induce anergy of NK cells through membrane-bound TGF-1. Journal of Immunology, 182(1), 240-249.

54. Liu, C. et al. (2007). Expansion of spleen myeloid suppressor cells represses NK cell cytotoxicity in tumor-bearing host. Blood, 109(10), 4336-42.

55. Greifenberg, V. et al. (2009). Myeloid-derived suppressor cell activation by combined LPS and IFN-gamma treatment impairs DC development. European Journal of Immunology, 39(10), 2865-76.

56. Ostrand-Rosenberg, S. & Sinha, P. (2009). Myeloid-derived suppressor cells: linking inflammation and cancer. Journal of Immunology, 182(8), 4499-506.

57. Almand, B. et al. (2001). Increased production of immature myeloid cells in cancer patients: a mechanism of immunosuppression in cancer. Journal of Immunology, 166(1), 678-89.

58. Sevko, A. & Umansky, V. (2013). Myeloid-Derived Suppressor Cells Interact with Tumors in Terms of Myelopoiesis, Tumorigenesis and Immunosuppression: Thick as Thieves. J. Cancer 4, 3–11.

59. Wesolowski, R. et al. (2013). Myeloid derived suppressor cells - a new therapeutic target in the treatment of cancer. J. Immunother. cancer 1, 10.

60. Diaz-Montero, C.M. et al. (2009). Increased circulating myeloid-derived suppressor cells correlate with clinical cancer stage, metastatic tumor burden, and doxorubicin-cyclophosphamide chemotherapy. Cancer Immunology and Immunotherapy, 58(1), 49-59.

61. Vuk-Pavlovic, S. et al. (2010). Immunosuppressive CD14+HLA-DRlow/- monocytes in prostate cancer. Prostate, 70(4), 443-55.

62. Feng, P.-H. et al. (2012). CD14(+)S100A9(+) monocytic myeloid-derived suppressor cells and their clinical relevance in non-small cell lung cancer. Am. J. Respir. Crit. Care Med. 186, 1025–36.

63. Gros, A. et al. (2012). Myeloid cells obtained from the blood but not from the tumor can suppress T-cell proliferation in patients with melanoma. Clinical Cancer Research, 18(19), 5212-23.

64. Filipazzi, P. et al. (2012). Phenotype, function, and clinical implications of myeloid-derived suppressor cells in cancer patients. Cancer Immunology and Immunotherapy, 61(2), 255-63.

65. Hiratsuka, S. et al. (2006). Tumor-mediated upregulation of chemoattractants and recruitment of myeloid cells predetermines lung metastasis. Nat. Cell Biol. 8, 1369–75.

66. Allan, S. (2008). Tumor immunology: Regulating MDSC recruitment. Nat. Rev. Immunol. 8, 828–828 (2008).

67. Wang, G. et al. (2016). Targeting YAP-dependent MDSC infiltration impairs tumor progression. Cancer Discovery, 6(1), 80-95.

68. Bunt, S. et al. (2007). Reduced inflammation in the tumor microenvironment delays the accumulation of myeloid-derived suppressor cells and limits tumor progression. Cancer Research, 67(20), 10019-26.

69. Gabrilovich & Hurwitz. (2014). Tumor-Induced Immune Suppression: Mechanisms and Therapeutic Reversal.

70. Kusmartsev, S., & Gabrilovich, D. I. (2006). Effect of tumor-derived cytokines and growth factors on differentiation and immune suppressive features of myeloid cells in cancer. Cancer Metastasis Reviews, 25(3), 323–31.

71. Barreda, D. et al. (2004). Regulation of myeloid development and function by colony stimulating factors. Developmental and Comparative Immunology, 28(5), 509-54.

72. Numata, A. et al. (2005). Signal transducers and activators of transcription 3 augments the transcriptional activity of CCAAT/enhancer-binding protein alpha in granulocyte colony-stimulating factor signaling pathway.

73. Panopoulous, A. & Watowich, S. (2008). Granulocyte colon-stimulating factor: molecular mechanisms of action during steady state and "emergency" hematopoiesis. Cytokine, 42(3), 277-88.

74. Waight, J. et al. (2011). Tumor-derived G-CSF facilitates neoplastic growth through a granulocytic myeloid-derived suppressor cell-dependent mechanism. PLoS One, 6(11), e27690.

75. De La Luz Sierra, M. et al. (2007). Transcription factor Gfi-1 induced by G-CSF is a negative regulator of CXCR4 in myeloid cells. Blood, 110(7), 2276-85.

76. Bot, F. et al. (1990). Synergistic effects between GM-CSF and G-CSF or M-CSF on highly enriched human marrow progenitor cells. Leukemia, 4(5), 325-8.

77. Dolcetti, L. et al. (2010). Hierarchy of immunosuppressive strength among myeloid-derived suppressor cell subsets is determined by GM-CSF. European Journal of Immunology, 40(1), 22–35.

78. Morales, J. et al. (2010). GM-CSF is one of the main breast tumor-derived soluble factors involved in the differentiation of CD11b-Gr1-bone marrow progenitor cells into myeloid-derived suppressor cells. Breast Cancer Research and Treatment, 123(1), 39-49.

79. Sawanobori, Y. et al. (2008). Chemokine-mediated rapid turnover of myeloid-derived suppressor cells in tumor-bearing mice. Blood, 111(12), 5457-66.

80. Stanley, E. et al. (1997). Biology and action of colony-stimulating factor-1. Molecular Reproduction and Development, 46(1), 4-10.

81. Apte, R. and Voronov, E. (2002). Interleukin-1- a major pleiotropic cytokine in tumor-host interactions. Seminars in Cancer Biology, 12(4), 277-290.

82. Bunt, S. et al. (2007). Reduced inflammation in the tumor microenvironment delays the accumulation of myeloid-derived suppressor cells and limits tumor progression. Cancer Research, 67(20), 10019-26.

83. Song, X. et al. (2005). CD11b+/Gr-1+ immature myeloid cells mediate suppression of T cells in mice bearing tumors of IL-1-secreting cells. Journal of Immunology, 175(12), 8200-8208.

84. Boneberg, E. & Hartung, T. (2003). Febrile temperatures attenuate IL-1 release by inhibiting proteolytic processing of the preform and influence Th1/Th2 balance by favoring Th2 cytokines. Journal of Immunology, 171(2), 664-668.

85. Gabitass, R. et al. (2011). Elevated myeloid-derived suppressor cells in pancreatic, esophageal, and gastric cancer are an independent prognostic factor and are associated with significant elevation of the Th2 cytokine interleukin-13. Cancer Immunology & Immunotherapy, 60(10), 1419-30.

86. Ichikawa, M. et al. (2011). S100A8/A9 activate key genes and pathways in colon tumor progression. Molecular Cancer Research, 9(2), 133-48.

87. Lesokhin, A. et al. (2012). Monocytic CCR2+ myeloid-derived suppressor cells promote immune escape by limiting activated CD8 T-cell infiltration into the tumor microenvironment. Cancer Research, 72(4), 876-86.

88. Loetscher, P. et al. (1996). Activation of NK cells by CC chemokines: chemotaxis, Ca2+ mobilization, and enzyme release. Journal of Immunology, 156(1), 322-7.

89. Molon, B. et al. (2011). Chemokine nitration prevents intratumoral infiltration of antigen-specific T cells. Journal of Experimental Medicine, 208(10), 1949-62.

90. Allavena, P. et al. (1994). Induction of natural killer cell migration by monocyte chemotactic protein-1, -2, and -3. European Journal of Immunology, 24(12), 3233-6.

91. Carr, M. et al. (1994). Monocyte chemoattractant protein 1 acts as a T-lymphocytes chemoattractant. PNAS, 91(9), 3652-6.

92. Fridlender, Z. et al. (2010). CCL2 blockade augments cancer immunotherapy. Cancer Research, 70(1), 109-18.

93. Huang, B. et al. (2007). CCL2/CCR2 pathway mediates recruitment of myeloid suppressor cells to cancers. Cancer Letters, 252(1), 86-92.

94. Zollo, M. et al. (2012). Targeting monocyte chemotactic protein-1 synthesis with bindarit induces tumor regression in prostate and breast cancer animal models. Clinical & Experimental Metastasis, 29(6), 585-601.

95. Chen, B. et al. (2015). S100A9 induced inflammatory responses are mediated by distinct damage associated molecular patterns (DAMP) receptors in vitro and in vivo. PLoS One, 10(2), e0115828.

96. Ehrchen, J. M. et al. (2009). The endogenous Toll-like receptor 4 agonist S100A8/S100A9 (calprotectin) as innate amplifier of infection, autoimmunity, and cancer. J. Leukoc. Biol. 86, 557–566.

97. Tsai, S.-Y. et al. (2014). DAMP molecule S100A9 acts as a molecular pattern to enhance inflammation during influenza A virus infection: role of DDX21-TRIF-TLR4-MyD88 pathway. PLoS Pathog. 10, e1003848.

98. Vogl, T. et al. (2007). Mrp8 and Mrp14 are endogenous activators of Toll-like receptor 4, promoting lethal, endotoxin-induced shock. Nature Medicine, 13(9), 1042-9.

99. Hermani, A. et al. (2008). S100A8 and S100A9 activate MAP kinase and NF-kappaB signaling pathways and trigger translocation of RAGE in human prostate cancer cells. Experimental Cell Research, 312(2), 184-97.

100. Simard, J.-C. et al. (2013). S100A8 and S100A9 induce cytokine expression and regulate the NLRP3 inflammasome via ROS-dependent activation of NF-κB(1.). PLoS One 8, e72138.

101. Ghavami, S. et al. (2008). S100A8/A9 at low concentration promotes tumor cell growth via RAGE ligation and MAP kinase-dependent pathway. Journal of Leukocyte Biology, 83(6), 1484-92.

102. Wagner, E. & Nebreda, A. (2009). Signal integration by JNK and p38 MAPK pathways in cancer development. Nature Reviews Cancer, 9(8), 537-49.

103. Kallberg, E. et al. (2012). S100A9 interaction with TLR4 promotes tumor growth. PLoS One, 7(3), e34207.

104. Leanderson, T. & Ivars, F. (2014). S100A9 and tumor growth. Oncoimmunology 1, 1404–1405.

105. Gebhardt, C. et al. (2008). RAGE signaling sustains inflammation and promotes tumor development. JEM, 205(2), 275-85.

106. Riehl, A. et al. (2009). The receptor RAGE: bridging inflammation and cancer. Cell Communication and Signaling, 7(1), 12.

107. Taguchi, A. et al. (2000). Blockade of RAGE-amphoterin signaling suppresses tumor growth and metastases. Nature, 405(6784), 354-60.

108. Ichikawa, M. et al. (2011). S100A8/A9 activate key genes and pathways in colon tumor progression. Molecular Cancer Research, 9(2), 133-48.

109. Turovskaya, O. et al. (2008). RAGE, carboxylated glycans and S100A8/A9 play essential roles in colitis-associated carcinogenesis. Carcinogenesis, 29(10), 2035-43.

110. Hermani, A. et al. (2005). Calcium-binding proteins S100A8 and S100A9 as novel diagnostic markers in human prostate cancer. Clinical Cancer Research, 11, 5146.

111. Tidehag, V. et al. (2014). High density of S100A9 positive inflammatory cells in prostate cancer stroma is associated with poor outcome. Eur. J. Cancer 50, 1829–35.

112. Bao, J. et al. (2015). AGE/RAGE/Akt pathway contributes to prostate cancer cell proliferation by promoting Rb phosphorylation and degradation. Am J Cancer Res, 5(5), 1741-50.

113. Ishiguro, H. et al. (2005). Receptor for advanced glycation end products (RAGE) and its ligand, amphoterin, are overexpressed and associated with prostate cancer development. Prostate, 64(1), 92-100.

114. Manitz, M.-P. et al. (2003). Loss of S100A9 (MRP14) results in reduced interleukin-8-induced CD11b surface expression, a polarized microfilament system, and diminished responsiveness to chemoattractants in vitro. Mol. Cell. Biol. 23, 1034–43.

115. Sinha, P. et al. (2008). Proinflammatory S100 proteins regulate the accumulation of myeloid-derived suppressor cells. J. Immunol. 181, 4666–75.

116. Cheng, P. et al. (2008). Inhibition of dendritic cell differentiation and accumulation of myeloid-derived suppressor cells in cancer is regulated by S100A9 protein. Journal of Experimental Medicine. 205(10), 2235-49.

CHAPTER II

LOSS OF MYD88 LEADS TO MORE AGGRESSIVE TRAMP PROSTATE CANCER AND INFLUENCES TUMOR-INFILTRATING LYMPHOCYTES

Elizabeth M. Peek, Wang Song, Hanwei Zhang, Jiaoti Huang, and Arnold I. Chin (2015). Loss of MyD88 leads to more aggressive TRAMP prostate cancer and influences tumor infiltrating lymphocytes. *Prostate* 75(5):463-73.

Loss of MyD88 Leads to More Aggressive TRAMP Prostate Cancer and Influences Tumor Infiltrating Lymphocytes

Elizabeth M. Peek,[1] Wang Song,[2] Hanwei Zhang,[3] Jiaoti Huang,[4] and Arnold I. Chin[1,3,5,6]*

[1]*Molecular Biology Institute, UCLA, Los Angeles, California*
[2]*Urology Center, First Hospital of Jilin University, Changchun, China*
[3]*Department of Urology, UCLA, Los Angeles, California*
[4]*Department of Pathology, UCLA, Los Angeles, California*
[5]*Eli & Edythe Broad Stem Cell Research Center, UCLA, Los Angeles, California*
[6]*Jonsson Comprehensive Cancer Center, UCLA, Los Angeles, California*

BACKGROUND. The influence of pattern recognition receptor (PRR) signaling in the prostate tumor microenvironment remains unclear. Although there may be a role for PRR agonists as adjuvants to therapy, prior evidence suggests tumor promoting as well as tumor inhibiting mechanisms. The purpose of this study is to examine the role of the key Toll-like receptor (TLR) signaling adaptor protein myeloid differentiation primary response gene 88 (MyD88) in prostate cancer development.

METHODS. MyD88$^{-/-}$ mice in a C57Bl6 background were crossed with transgenic adenocarcinomas of the mouse prostate (TRAMP) mice to create MyD88$^{-/-}$ TRAMP$^{Tg+/-}$ animals, which were compared to MyD88$^{+/+}$ TRAMP$^{Tg+/-}$ animals and their non-transgenic counterparts at 30 weeks. Prostates were examined histologically, by immunohistochemistry and immunofluorescence staining, and by qPCR, to characterize tumor-infiltrating immune populations as well as activation of the downstream NF-κB pathway and androgen receptor (AR) expression. Splenocytes were examined for development of distinct immune cell populations.

RESULTS. Absence of MyD88 led to increased prostatic intraepithelial neoplasm (PIN) and areas of well-differentiated adenocarcinoma in TRAMP transgenic mice. Analysis of infiltrating immune populations revealed an increase in CD11b^{+} Gr1^{+} myeloid-derived suppressor cells (MDSCs), as evidenced by increased expression of prostatic arginase-1 and iNOS as well as the cytokine IL-10, and a deficiency in NK cells in prostates from MyD88$^{-/-}$ TRAMP$^{Tg+/-}$ compared to MyD88$^{+/+}$ TRAMP$^{Tg+/-}$ mice, whereas a decrease in splenocytic NK cell differentiation was observed in MyD88$^{-/-}$ mice. Prostate tumors revealed no significant differences in NF-κB or AR expression in MyD88$^{+/+}$ TRAMP$^{Tg+/-}$ compared to MyD88$^{-/-}$ TRAMP$^{Tg+/-}$ mice.

CONCLUSIONS. During prostate cancer development in the TRAMP model, MyD88 may play a role in limiting prostate tumorigenesis by altering tumor-infiltrating immune populations. This suggests that in the context of specific cancers, distinct PRRs and signaling

Grant sponsor: Department of Defense Grant; Grant number: PC1010917; Grant sponsor: STOP Cancer; Grant sponsor: Broad Stem Cell Research Center Scholars in Translational Medicine; Grant sponsor: UCLA Broad Stem Cell Research Center Flow Cytometry Core; Grant sponsor: UCLA Translational Pathology Core Laboratory.

Elizabeth M. Peek and Wang Song made an equal contribution to this manuscript.

The authors have nothing to disclose.

*Correspondence to: Arnold I. Chin, MD, PhD, Department of Urology, UCLA, 10833 Le Conte Ave, PO Box 951738, Los Angeles, CA 90095-1738. E-mail: aichin@ucla.edu

Received 6 August 2014; Accepted 22 October 2014
DOI 10.1002/pros.22932
Published online in Wiley Online Library (wileyonlinelibrary.com).

pathways of innate immune signaling may influence the tumor microenvironment and represent a novel therapeutic strategy. *Prostate*

KEY WORDS: **MyD88; prostate cancer; TRAMP; Toll-like receptors; NF-κB; tumor-infiltrating lymphocytes**

INTRODUCTION

Inflammation within the prostate cancer microenvironment is often observed adjacent to areas of focal atrophy and adenocarcinoma, although the contribution of distinct subsets of tumor infiltrating lymphocytes (TILs) to prostate cancer development, growth, and metastasis is unclear [1]. These inflammatory processes may promote anti-tumor responses, as clonal expansion and presence of circulating prostate-antigen specific $CD8^+$ T cells have been observed clinically [2]. Conversely, pro-tumor inflammation has been observed with the release of pro-inflammatory chemotactic agents from areas of tumor necrosis into the tumor microenvironment that stimulate angiogenesis and proliferation [3–5]. The prostate cancer microenvironment may be globally immunosuppressive, as studies have linked TGF-β production to a bias of $CD4^+$ T cells in the human prostate cancer microenvironment towards both $CD4^+CD25^+Foxp3^+$ regulatory T cells (T_{regs}) and Th17 cells [6,7]. Nonetheless, the clinical importance of the immune system in prostate cancer is borne out by the efficacy of the cancer vaccine sipuleucel-T, which justifies the necessity to parse out the contributions of distinct inflammatory pathways and to examine for adjuvants to tumor immunity.

Pathogens or cancerous cells alike can produce danger signals that elicit the activation of immune responses. These signals, consisting of conserved molecules termed pathogen-associated molecular patterns (PAMPs) or danger-associated molecular patterns (DAMPs), can be discriminated from self-antigens by a family of pattern-recognition receptors (PRRs) such as the Toll-like receptors (TLRs) of the innate immune system [8–12]. Thirteen mammalian TLRs have been identified to date with ligands ranging from lipopolysaccharide (LPS) found in gram-negative bacterial walls recognized by TLR4, double stranded RNA produced by viruses recognized by TLR3, viral CpG motifs by TLR9, to endogenous ligands, such as heat-shock protein 70 and chromatin component HMG-B1 [8,13]. TLRs recruit adaptor proteins that promote activation of downstream transcription factors such as NF-κB or interferon regulator factors (IRFs), mediating downstream development of adaptive immune effector cells such as cytotoxic T lymphocytes (CTLs) and dendritic cell (DC) maturation [14].

Although the majority of TLRs recruit the adaptor protein myeloid differentiation primary response gene 88 (MyD88), TLR3 exclusively interacts with the adaptor protein TIR-domain-containing adapter-inducing interferon-β (TRIF) to activate a MyD88-independent pathway leading to IRF3 activation and production of type I interferons. We have previously implicated the pattern recognition receptor TLR3 and type I interferons to play a critical role in prostate cancer immune surveillance in TRAMP mice, with increased tumor growth in absence of TLR3 [15]. Using polyI:C as a TLR3 agonist, we showed a marked reduction in prostate cancer growth which influenced the tumor microenvironment by creating an influx of $CD3^+$ T cells and NK cells [15]. The role of TLR signaling in the inherent development of prostate cancer has important clinical correlation, as sequence variants in a 3′-untranslated region of TLR4 and polymorphisms in the TLR gene cluster encoding TLR1, 6, 10, and the downstream signaling mediators IRAK1 and IRAK4, confer increased prostate cancer risk [16–19]. How distinct TLR signaling pathways modulate the prostate cancer tumor immune environment is an open question.

In this study, we investigated the role of MyD88 in prostate cancer development using the autochthonous TRAMP model. TRAMP mice express the SV40 large T antigen in the prostate epithelium under the control of the rat probasin promoter, and are a well-described immunocompetent prostate cancer model that develops histologic PIN by 8 to 12 weeks of age and adenocarcinoma by 24 to 30 weeks of age. We hypothesized that loss of MyD88 will promote prostate cancer development, as a result of alterations in tumor-infiltrating immune populations. This work complements our prior studies of TLR3 in prostate cancer and the intracellular Nod-like receptor pathway in bladder cancer, to extend the idea that distinct PRRs differentially mediate tumor immune surveillance [15,20].

MATERIALS AND METHODS

Mice

$TRAMP^{Tg+/-}$ mice (Jackson Laboratories) on a C57Bl/6 background were genotyped as previously

described [21,22]. MyD88$^{-/-}$ mice backcrossed to a C57Bl/6 background for 10 generations were bred with TRAMP transgenic mice to homozygosity generating MyD88$^{-/-}$ TRAMP$^{Tg-/-}$ and MyD88$^{-/-}$ TRAMP$^{Tg+/-}$ mice [23]. Mice were housed in pathogen-free conditions in accordance to UCLA Animal Research Committee protocols. All animal work was performed through the approved UCLA Institutional Animal Care and Use Committee protocol #2010–023-11C in accordance with the Public Health Service Policy on Human Care and Use of Laboratory Animals and USDA Animal Welfare Act Regulations.

Tumor Models

MyD88$^{+/+}$ TRAMP$^{Tg-/-}$, MyD88$^{+/+}$ TRAMP$^{Tg+/-}$, MyD88$^{-/-}$ TRAMP$^{Tg-/-}$, and MyD88$^{-/-}$ TRAMP$^{Tg+/-}$ male mice at 25 and 30 weeks of age were sacrificed, with lungs, liver, and abdominal lymph nodes grossly inspected for metastases. Whole prostates with seminal vesicles were removed, weighed, and a portion fixed in formalin or embedded in OCT. Spleens were removed and dispersed into single cell suspensions for flow cytometric analysis of immune populations.

Histology

Representative paraffin embedded, formalin-fixed tissues were sectioned at 0.4 μm and stained by hematoxylin and eosin. Images were assessed by light microscopy using an Axio Imager 2 (Zeiss).

Immunofluorescence and Immunohistochemistry

Immunofluorescence was performed on OCT-embedded tissue. Sections were fixed in 4% paraformaldehyde for 10 min and then blocked for 1 hr with either standard (5% BSA and 5% goat serum in PBS) or specific, when using mouse primary antibodies, (M.O.M kit block, Vector Labs) reagents. Sections were stained overnight at 4°C with anti-CD8 at 1:100 (53-6.7, R&D Systems), anti-CD11b at 1:400 (M1/70, R&D Systems), anti-Gr-1 at 1:300 (RB6-8C5, eBioscience), anti-CD49 at 1:300 (DX5, Biolegend), anti-Foxp3 at 1:300 (MF23, BD Biosciences), and anti-AR at 1:2000 (ab3510, Abcam). Secondary antibodies using goat anti-rat Al488 (Invitrogen) or goat anti-rabbit Al594 (Invitrogen) were incubated at 1:750 for 1 hr and sections counterstained with DAPI and mounted using Vectorshield (Vector Labs). Images were assessed by fluorescence microscopy using an Axio Imager 2 (Zeiss).

Immunohistochemistry was performed on formalin-fixed and paraffin embedded tissues. Sections were deparaffinized and rehydrated before blocking for one hour in 5% BSA and 5% goat serum in PBS. Sections were stained with anti-p40 at 1:50 (2073, BioSB), anti-MyD88 1:100 (ab2064, AbCam), anti-IL-10 at 1:100 (JESS-16E3, eBioscience), and anti-pIκB at 1:500 (S32/36, 5A5, Cell Signaling), followed by incubation with biotinylated goat anti-rabbit or goat anti-mouse secondary antibodies at 1:750 using the ABC kit (Vector Labs). Sections were developed using streptavidin-conjugated HRP and substrate, counterstained with hematoxylin, then dehydrated and mounted with Cytoseal 60 (Richard-Allan Scientific). Representative formalin-fixed tissues were stained by hematoxylin and eosin. Images were assessed by light microscopy using an Axio Imager 2 (Zeiss).

Quantitative RT-PCR

Total RNA from frozen prostate tissue was used to synthesize cDNA using High Capacity cDNA Reverse Transcription Kits (Applied Biosystems). Relative gene expression was determined using SYBR Green PCR Master Mix (Applied Biosystems) on a Bio-Rad iCycler, normalized to GAPDH as a gene reference with the comparative threshold cycle method. Primers sets for the following genes were used: Arginase-1, 5′-AGAGATACTTCCAACTGCCAGACT, 3′-ACCTGGCCTTTGTTGATGTCCCTA; iNOS, 5′-GCTGGAAGCCACTGACACTTCG, 3′-CGAGATGGTCAGGGTCCCCT; GAPDH, 5′-GACCCCTTCATTGACCTCAAC, 3′-CTTCTCCATGGTGGTGAAGA.

Flow Cytometry

Spleens were dispersed into single cell suspensions and stained with immune cell markers CD4-APC (RM4–5, BD Bioscience), CD8-FITC (53–6.7, BD Bioscience), B220-FITC (RA3–6B2, BD Bioscience), CD11b-FITC (M1/70, BD Bioscience), GR1-PE (RB6–8C5, BD Bioscience), Foxp3-PE (MF23, BD Bioscience), and NK1.1-PE (PK136, BD Biosciences). For Foxp3 staining, cells were fixed and permeabilized using an intracellular staining protocol per manufacturer's instructions (00–5523-00, eBioscience). Cells were analyzed on an LSRII flow cytometer (BD Biosciences).

RESULTS

More Extensive PIN and Adenocarcinoma in Prostates of MyD88$^{-/-}$ TRAMP$^{Tg+/-}$ Compared to MyD88$^{+/+}$ TRAMP$^{Tg+/-}$ Mice

To examine the role of MyD88 in prostate cancer development, we crossed TRAMP$^{Tg+/-}$ mice with MyD88$^{-/-}$ mice in a C57Bl/6 background to generate a

syngenic immune-competent prostate cancer model. Male MyD88$^{+/+}$ TRAMP$^{Tg-/-}$, MyD88$^{+/+}$ TRAMP$^{Tg+/-}$, MyD88$^{-/-}$ TRAMP$^{Tg-/-}$, and MyD88$^{-/-}$ TRAMP$^{Tg+/-}$ mice were sacrificed at 25 weeks and prostate sections were stained with hematoxylin and eosin and examined by light microscopy. Prostates from non-transgenic MyD88$^{+/+}$ and MyD88$^{-/-}$ mice showed normal prostate development, while comparable development of PIN without areas of adenocarcinoma were observed in prostates of TRAMP$^{Tg+/-}$ MyD88$^{+/+}$ and MyD88$^{-/-}$ animals (Fig. 1A). To better understand the role of MyD88 in development of adenocarcinoma, we elected to examine a cohort of animals at 30 weeks. In the absence of the TRAMP transgene, prostates from MyD88$^{+/+}$ TRAMP$^{Tg-/-}$ and MyD88$^{-/-}$ TRAMP$^{Tg-/-}$ mice showed similar glandular architecture. Interestingly, prostates from MyD88$^{-/-}$ TRAMP$^{Tg+/-}$ mice revealed larger and more densely packed glands then prostates from MyD88$^{+/+}$ TRAMP$^{Tg+/-}$ mice. These glands exhibited higher density of PIN as well as increased areas of well-differentiated adenocarcinoma, defined as loss of p40 staining and disruption of the basal cell layer, in MyD88$^{-/-}$ TRAMP$^{Tg+/-}$ compared to MyD88$^{+/+}$ TRAMP$^{Tg+/-}$ mice (Fig. 1B). In 60% of TRAMP transgenic mice in each genotype, a phyllodes-like tumor was observed arising from the seminal vesicles as previously described with an intact basal layer by p40 expression (Fig. 1C) [24]. Collectively, 30-week prostate and seminal vesicle weights were similar between TRAMP$^{Tg+/-}$ MyD88$^{+/+}$ and MyD88$^{-/-}$ mice (Fig. 1D). To quantitate the extent of PIN and adenocarcinoma, we assessed the percentage of glands harboring PIN and adenocarcinoma and found a significant increase in the prostates from MyD88$^{-/-}$ TRAMP$^{Tg+/-}$ compared to MyD88$^{+/+}$ TRAMP$^{Tg+/-}$ mice (Fig. 1E). The presence of lung metastases were examined histologically and there was no evidence in either MyD88$^{+/+}$ TRAMP$^{Tg+/-}$ or MyD88$^{-/-}$ TRAMP$^{Tg+/-}$ mice (data not shown).

Decreased NK Cells and Increased Myeloid Cells in Tumor Infiltrating Lymphocytes in MyD88$^{-/-}$ TRAMP$^{Tg+/-}$ Mice Compared to MyD88$^{+/+}$ TRAMP$^{Tg+/-}$ Mice

To investigate the role of MyD88 in programming the tumor infiltrating lymphocytes (TILs), we examined expression of distinct immune populations by immunofluorescence staining of prostate tissues. There were no significant differences in expression of the cytotoxic T cell marker CD8 or T regulatory cell marker Foxp3. However, significantly increased myeloid cells, denoted by expression of CD11b and Gr1, and decreased infiltration of NK cells, characterized by the expression of CD49, were observed in MyD88$^{-/-}$ TRAMP$^{Tg+/-}$ compared to MyD88$^{+/+}$ TRAMP$^{Tg+/-}$ animals (Fig. 2).

CD11b^{+} Gr1^{+} Myeloid Cells Represent Myeloid-Derived Suppressor Cells (MDSCs)

To assess the role of MyD88 in mediating tumorigenesis and tumor infiltrating lymphocytes in MyD88$^{-/-}$ TRAMP$^{Tg+/-}$ compared to MyD88$^{+/+}$ TRAMP$^{Tg+/-}$ animals, prostatic expression patterns of MyD88 were examined and found intensely localized in the stroma, along with diffuse expression in the prostate epithelium in MyD88$^{+/+}$ mice (Fig. 3A). Appropriately, no specific staining was found in MyD88$^{-/-}$ mice. MDSCs are early myeloid cells characterized by the surface markers CD11b^{+} and Gr1^{+} in mice, and produce cytokines such as IL-10, and arginase-1 and iNOS, to mediate its negative regulatory functions on T cells and NK cells [25]. We examined expression of IL-10 and found increased stromal IL-10 expression in MyD88$^{-/-}$ TRAMP$^{Tg+/-}$ compared to MyD88$^{+/+}$ TRAMP$^{Tg+/-}$ mice (Fig. 3B). Furthermore, whole prostates from MyD88$^{-/-}$ TRAMP$^{Tg+/-}$ mice produced significantly more arginase-1 and iNOS than MyD88$^{+/+}$ TRAMP$^{Tg+/-}$ mice, supporting the expansion of infiltrating MDSCs in MyD88$^{-/-}$ TRAMP$^{Tg+/-}$ mice (Fig. 3C).

Deficiency of NK Cells in Spleens of MyD88$^{-/-}$ TRAMP$^{Tg+/-}$ and MyD88$^{-/-}$ TRAMP$^{Tg-/-}$ Mice

As the absence of MyD88 biased the composition of the tumor microenvironment with respect to tumor infiltrating NK and myeloid cells, we were interested in characterizing the immune populations of spleens from MyD88$^{+/+}$ and MyD88$^{-/-}$ mice as a measure of the systemic influences in immune cell development. In 30-week old mice, no significant differences were observed in the myeloid, B cell, or T cell lineages of the various genotypes. However, a significant decrease in NK cells was observed in both MyD88$^{-/-}$ TRAMP$^{Tg-/-}$ and MyD88$^{-/-}$ TRAMP$^{Tg+/-}$ animals compared to their wild-type counterparts (Fig. 4).

Loss of MyD88 Results in No Significant Differences in NF-κB Signaling or AR Expression

Activation of TLRs through MyD88-dependent pathways leads to activation of canonical NF-κB pathways through the NEMO/IKKα/IKKβ complex resulting in phosphorylation of IκB, allowing translocation of p50/p65 subunits to the nucleus [26]. With a bias composition in the tumor infiltrating lymphocytes and increased areas of prostate adenocarcinoma

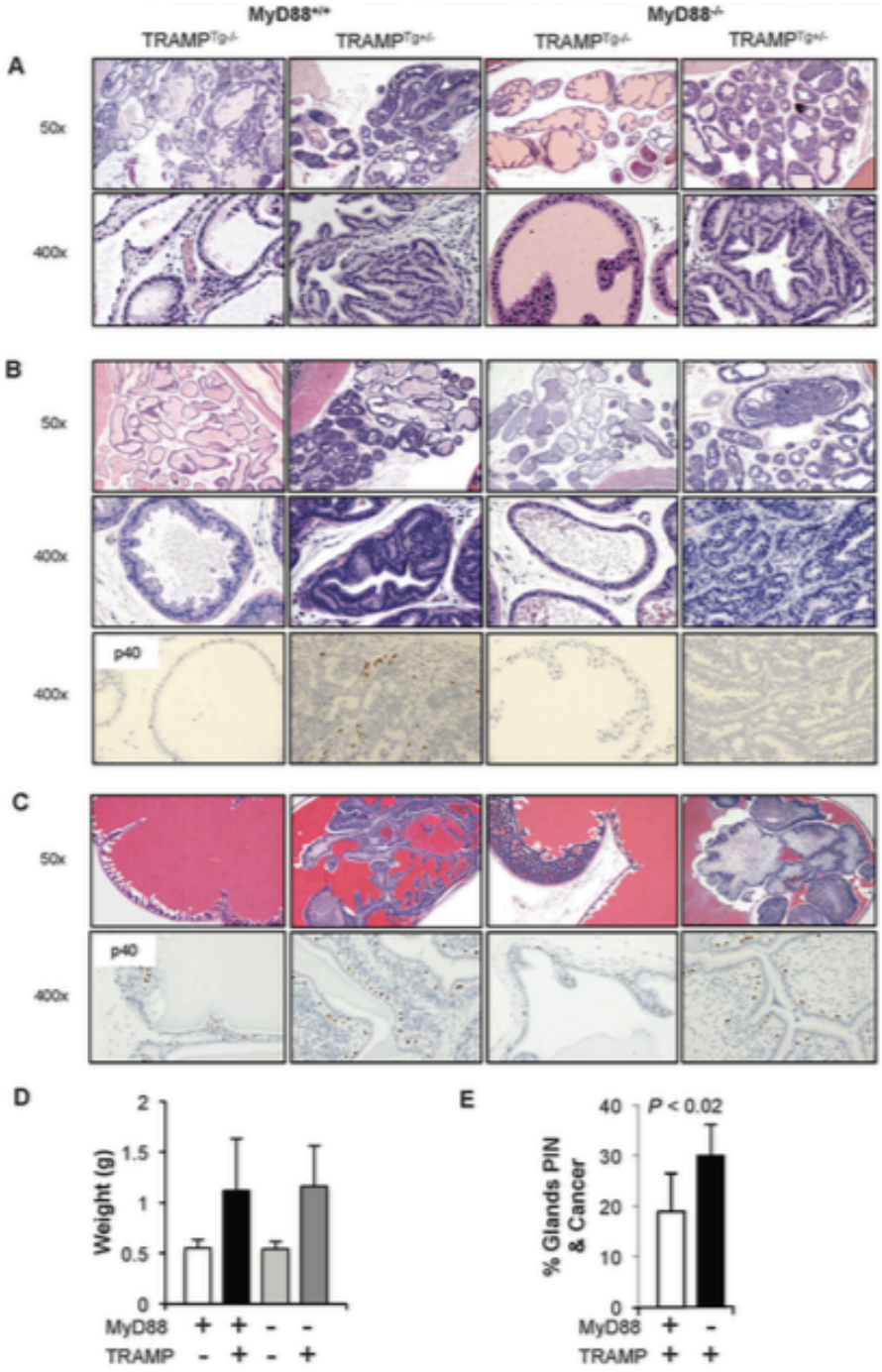

Fig. 1. MyD88$^{-/-}$ TRAMP$^{Tg+/-}$ mice show more aggressive prostate adenocarcinoma compared to MyD88$^{+/+}$ TRAMP$^{Tg+/-}$ mice. (A) Histology by H&E staining of prostates from mice as indicated at 25 weeks. Histology by H&E staining and immunohistochemistry by p40 staining of prostates (B) and seminal vesicles (C) from 30 week-old mice. (D) Prostate and seminal vesicle weights from mice at 30 weeks. (E) Percentage of glands containing PIN or adenocarcinoma. Magnification as indicated. Columns, mean of five animals; bars, standard deviations. Data are representative of five mice per group.

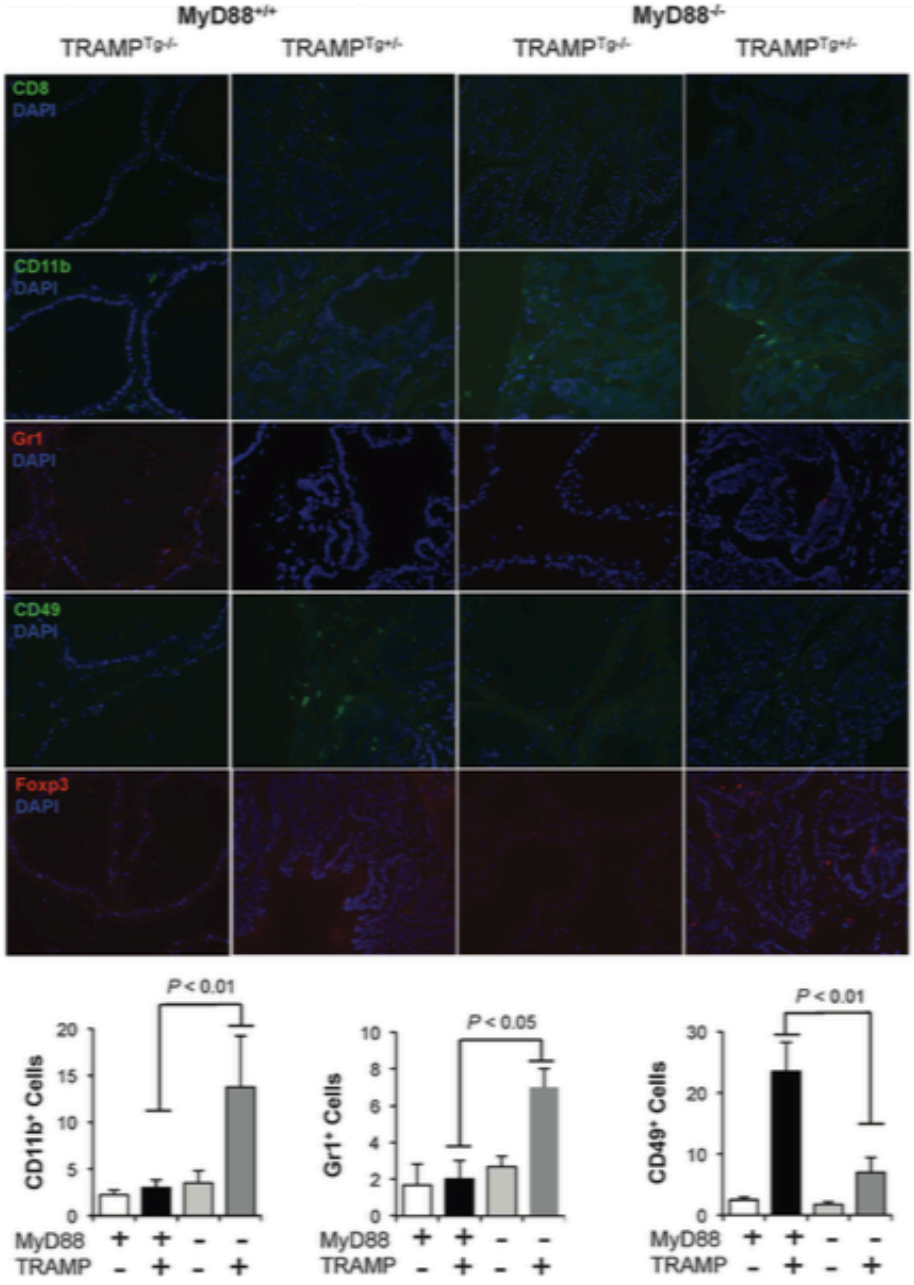

Fig. 2. MyD88$^{-/-}$ TRAMP$^{Tg+/-}$ prostates show distinct TIL populations when compared to MyD88$^{+/+}$ TRAMP$^{Tg+/-}$ mice. Prostate sections stained by immunofluorescence using immune cell markers as indicated to determine the infiltration of specific immune populations in 30 week MyD88$^{-/+}$ TRAMP$^{-/-}$, MyD88$^{+/+}$ TRAMP$^{Tg+/-}$, MyD88$^{-/-}$ TRAMP$^{-/-}$, MyD88$^{-/-}$ TRAMP$^{Tg+/-}$ mice as indicated. Representative merged fluorescence images are shown (400×). CD11b, Gr1, and CD49 quantified by mean positive staining cells in four high-powered field fields (400×); bars, standard deviations. All *P*-values were determined by two-tailed Student's *t*-test, with statistical significance defined as $P < 0.05$.

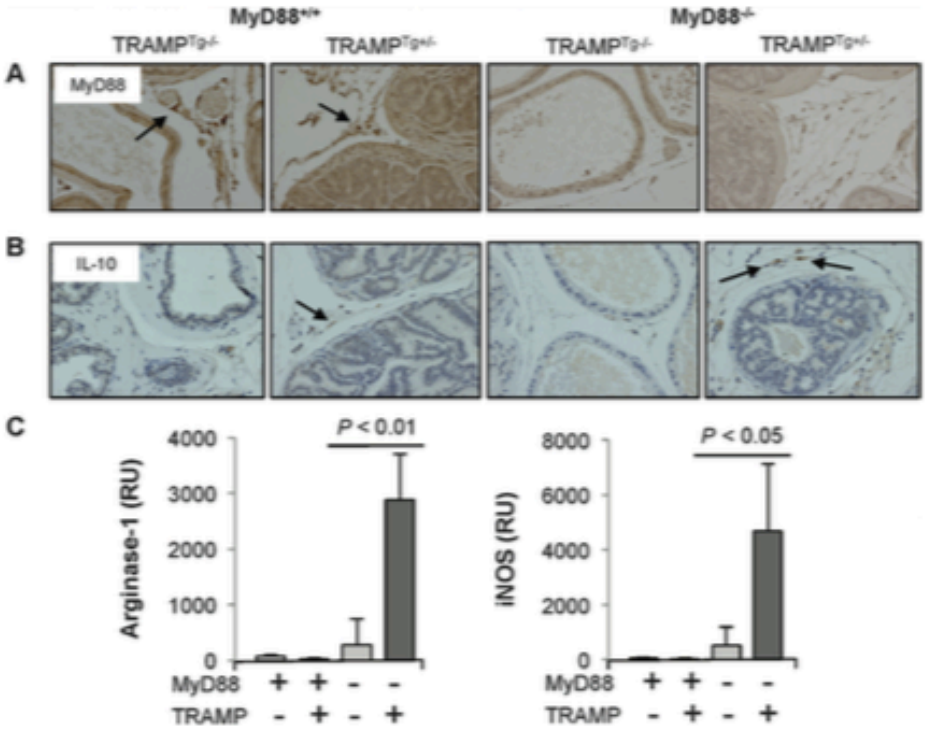

Fig. 3. Increased expression of IL-10, arginase-1, and iNOS from prostates of MyD88$^{-/-}$ TRAMP$^{Tg+/-}$ compared to MyD88$^{+/+}$ TRAMP$^{Tg+/-}$ mice. Prostate sections stained by immunohistochemistry using antibodies against MyD88 (A) and IL-10 (B). Representative images (400x) shown, with arrows highlighting representative stained cells. (C) Levels of arginase-1 and iNOS by quantitative PCR from prostate tissue of mice as indicated. Columns, mean of three animals; bars, standard deviations. All *P*-values were determined by two-tailed Student's *t* test, with statistical significance defined as $P < 0.05$.

in absence of MyD88, we asked whether this phenotype would be associated with altered activation of NF-κB. Staining of prostates from MyD88$^{+/+}$ TRAMP$^{Tg-/-}$, MyD88$^{+/+}$ TRAMP$^{Tg+/-}$, MyD88$^{-/-}$ TRAMP$^{Tg-/-}$, and MyD88$^{-/-}$ TRAMP$^{Tg+/-}$ animals revealed similar activation of canonical NF-κB in prostate epithelial cells manifested by detection of phosphorylated IκB (p-IκB) (Fig. 5A). As NF-κB has been linked with androgen receptor expression, we examined expression of AR, which appeared unchanged with the loss of MyD88 [27–30] (Fig. 5B).

DISCUSSION

Using the TRAMP autochthonous prostate cancer model, we have observed increased areas of PIN and adenocarcinoma of the prostate in the absence of MyD88. This result is consistent with our prior observations of PRRs TLR3 and the intracellular kinase Rip2 of Nod-like receptors in tumor surveillance and in programming distinct lymphocyte populations within the tumor microenvironment [15,20]. In each of these instances, the nature of the inflammatory microenvironment correlated with the response in tumorigenesis. The predominant stromal expression of MyD88 suggests that the prostate epithelium is responding to the altered tumor microenvironment rather than an intrinsic alteration. Similarly, MyD88 blockade has been shown to increase inflammation and progression in a murine model of TLR4-accelerated pancreatic carcinogenesis, thought to be in part mediated by dendritic cell induction of a Th2-polarizing response [31]. However, blockade of TRIF protected against this model of pancreatic carcinogenesis, which is not congruent with our observations of TLR3 signaling in prostate cancer [15]. The anti-tumor effect of TLRs and their signaling molecules is supported by the efficacy of TLR agonists as adjuvants to enhance host immunity with the TLR7 agonist imiquimod FDA approved for treatment of basal cell carcinoma and TLR9 agonists in clinical trials against malignancies including breast, melanoma, and lymphomas [32–36].

Nonetheless, the role of TLRs in tumor surveillance and modulating cancer is not clear, as reports have also supported tumor-promoting effects. For instance, deficiency in MyD88 has been shown to decrease the

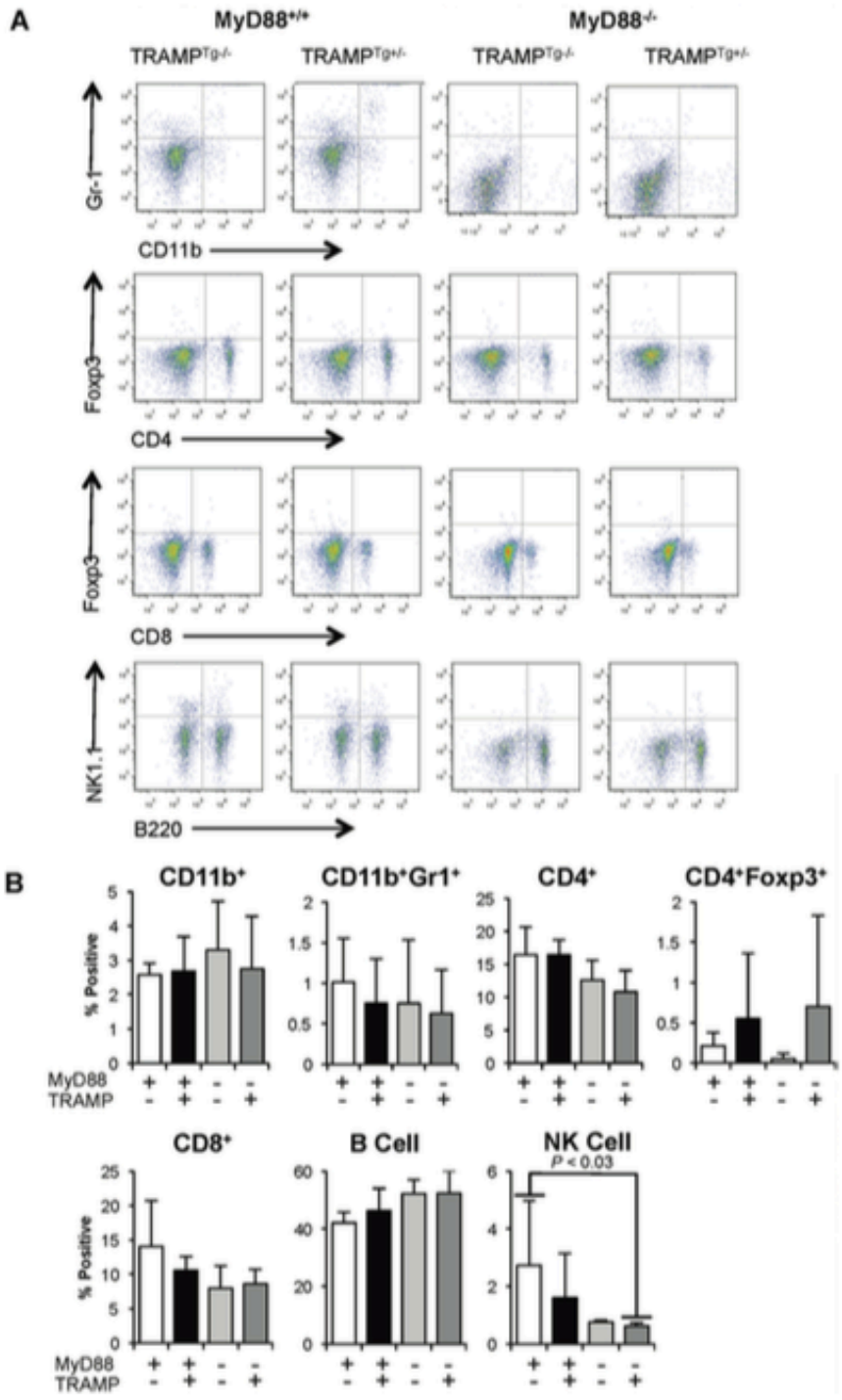

Fig. 4. Splenocytes from MyD88$^{-/-}$ TRAMP$^{-/-}$ and MyD88$^{-/-}$ TRAMP$^{Tg+/-}$ mice show a deficiency in NK cells. (A) Representative flow cytometry of splenic immune populations from mice as indicated. (B) The percentage of immune populations in total splenocytes is shown for each genotype as indicated. Columns, mean of five animals; bars, standard deviations. All *p* values were determined by two-tailed Student's *t*-test, with statistical significance defined as $P < 0.05$.

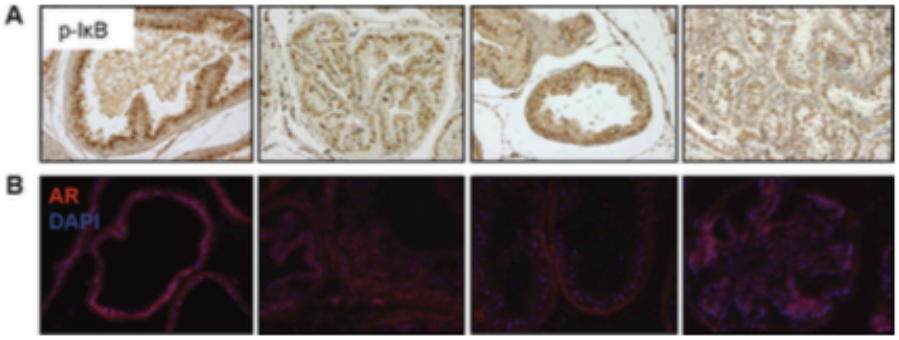

Fig. 5. Prostates of MyD88$^{+/+}$ TRAMP$^{Tg+/-}$ and MyD88$^{-/-}$ TRAMP$^{Tg+/-}$ mice show similar canonical NF-κB activation and AR expression. Representative prostates stained by immunohistochemistry with phospho-IκB and by immunofluorescence with AR, merged fluorescence images shown (400×).

development of tumors in mouse models of spontaneous colorectal cancer and diethylnitrosamine-induced hepatocellular tumors, through mechanisms including enhancing tumor evasion and tissue repair [37,38]. In immune- or tumor-specific knockouts of IKKβ using a colitis-associated cancer model, investigators showed that loss of IKKβ in the tumor epithelium decreased tumor incidence, while loss in myeloid cells led to decreased tumor size [39]. Previously, TLR4$^{-/-}$ TRAMP$^{Tg+/-}$ animals showed a delay in the onset of palpable tumor from 26 to 31 weeks compared to WT controls, however no histology or examination of TILs were performed [40]. This apparent discrepancy may be explained by the pleiotropic TLRs that utilize MyD88 to active NF-κB and MAP kinase pathways, the persistence of MyD88-independent pathways, and the cellular distribution of these receptors in the tumor microenvironment. Perhaps the distribution and bias between epithelial and stromal expression of PRRs and specificity of signaling remains a critical question. Despite these differences in specific knockouts of TLR signaling components, the influence of positive or negative immune regulators and tumor growth remain consistent.

In our study, we identified the decreased presence of tumor infiltrating NK cells and increased CD11b+ Gr1^{+} cells in the absence of MyD88 in TRAMP murine prostates at 30 weeks (Fig. 3). The loss of infiltrating NK cells in MyD88$^{-/-}$ prostates reinforces previously observed NK-mediated IFN-γ production in response to *Chlamydia trachomatis* infection [41]. Further characterization of the activity of NK cells and the subset of CD11b^{+} Gr1^{+} cells will be an important future direction. Although TLRs have been shown to inhibit negative regulatory cells such as Tregs, the relationship between TLRs and myeloid-derived suppressor cells (MDSCs) is less clear [42,43]. Our findings support the MyD88 pathway in modulating infiltrating myeloid-derived suppressor cells, which have been implicated in tumor immune evasion and progression and may explain the decrease in NK cells that we observed [25,44]. It is quite possible that distinct TLR pathways in the context of different tumors and tumor characteristics can specifically shape and program the tumor infiltrating microenvironment. It is unclear the specificity of upstream TLRs utilizing MyD88 in prostate cancer and the bias between MyD88-dependent and -independent pathways upon their activation. We expect future work will categorize the various PRR signaling pathways that will differentially regulate the prostate immune tumor microenvironment.

We observed no significant difference in canonical NF-κB activation comparing prostates of MyD88$^{+/+}$ TRAMP$^{Tg+/-}$ compared to MyD88$^{-/-}$ TRAMP$^{Tg+/-}$ mice. These data suggest that MyD88-independent pathways may exert the majority activation of NF-κB, which has been implicated in development of castrate resistant prostate cancer. A prior report in a subcutaneous model of prostate cancer showed that loss of IKKβ in immune cells prevented metastasis and delayed castration resistance in part through lymphotoxin expression, which can activate non-canonical NF-κB through the LTβ receptor [45,46]. Future directions will specifically examine the mechanistic nature of canonical versus non-canonical NF-κB signaling pathways and their influence in TILs, to examine if a dichotomous relationship exists. Care may need to be exercised in designing therapeutic TLR agonists that will preferentially activate the canonical versus non-canonical pathway in balancing anti-tumor and pro-tumor effects.

One of the criticisms of the TRAMP tumor model is the high percentage of neuroendocrine differentiation

compared to human prostate cancers. In our studies, we did not observe any neuroendocrine differentiation, which appears more common when crossed to the FvB background. An alternative $PTEN^{loxp/loxp}$ x PB-$Cre4^{+}$ mouse model has been suggested to more closely mimic the human disease [47]. Indeed, prostates from $PTEN^{loxp/loxp}$ x PB-$Cre4^{+}$ show an expansion of CD11b+ Gr1+ MDSCs [40]. However, the majority of immunological studies have utilized the TRAMP model. Another limitation of our system is that we cannot discriminate loss of MyD88 in the immune system, stroma, or prostate epithelial tissues although expression was highest in the stroma. Future directions will utilize models that can combine different genotypes in the immune, tumor, and stromal environments that will define the role of MyD88 and other PRR signaling components in these distinct compartments. Preliminary studies have shown that a kidney implantation model holds promise in dissecting out the various compartments [48].

CONCLUSIONS

The composition of the tumor microenvironment can alter tumor growth by mediating tumor surveillance and mediating negative immune regulators. We have provided evidence that MyD88 signaling pathways can alter the tumor immune microenvironment and development of prostate cancer. Future studies will need to clarify the mechanisms involved and whether activation of MyD88-dependent pathways can reverse our observations. Defining the role of tumor immune surveillance in the prostate cancer microenvironment will contribute towards the basic comprehension of tumor immunology as well as the development and enhancement of novel therapeutics, vaccines, and immune adjuvants against prostate cancer.

ACKNOWLEDGMENTS

The authors thank the UCLA Broad Stem Cell Research Center Flow Cytometry Core and the UCLA Translational Pathology Core Laboratory for providing core support.

REFERENCES

1. Davidsson S, Fiorentino M, Andrén O, Fang F, Mucci LA, Varenhorst E, Fall K, Rider JR. Inflammation, focal atrophic lesions, and prostatic intraepithelial neoplasia with respect to risk of lethal prostate cancer., Cancer Epidemiol. Biomarkers Prev 2011;20:2280–22877.
2. Sfanos KS, Bruno TC, Meeker AK, De Marzo AM, Isaacs WB, Drake CG. Human prostate-infiltrating CD8+ T lymphocytes are oligoclonal and PD-1 +. Prostate 2009;69:1694–1703.
3. Brigati C, Noonan DM, Albini A, Benelli R. Tumors and inflammatory infiltrates: Friends or foes? Clin Exp Metastasis. 2002;19:247–258.
4. Sfanos KS, Hempel HA, De Marzo AM. The role of inflammation in prostate cancer. Adv Exp Med Biol 2014;816:153–181.
5. Wu C-T, Hsieh C-C, Lin C-C, Chen W-C, Hong J-H, Chen M-F. Significance of IL-6 in the transition of hormone-resistant prostate cancer and the induction of myeloid-derived suppressor cells. J Mol Med (Berl) 2012;90:1343–1355.
6. Sfanos KS, Bruno TC, Maris CH, Xu L, Thoburn CJ, DeMarzo AM, et al. Phenotypic analysis of prostate-infiltrating lymphocytes reveals TH17 and Treg skewing. Clin Cancer Res 2008;14:3254–3261.
7. Rigamonti N, Bellone M. Prostate cancer, tumor immunity and a renewed sense of optimism in immunotherapy. Cancer Immunol Immunother 2012;61:453–468.
8. Yu M, Wang H, Ding A, Golenbock DT, Latz E, Czura CJ. HMGB1 signals through toll-like receptor (TLR) 4 and TLR2. Shock 2006;26:174–179.
9. Ellerman JE, Brown CK, de Vera M, Zeh HJ, Billiar T, Rubartelli A, et al. Masquerader: High mobility group box-1 and cancer. Clin Cancer Res 2007;13:2836–2848.
10. Vogl T, Tenbrock K, Ludwig S, Leukert N, Ehrhardt C, van Zoelen MAD, et al. Mrp8 and Mrp14 are endogenous activators of Toll-like receptor 4, promoting lethal, endotoxin-induced shock. Nat Med 2007; 13:1042–1049.
11. Cheng N, He R, Tian J, Ye PP, Ye RD. Cutting edge: TLR2 is a functional receptor for acute-phase serum amyloid A. J Immunol 2008; 181:22–26.
12. Le L, Chi K, Tyldesley S, Flibotte S, Diamond DL, Kuzyk MA. et al. Identification of serum amyloid A as a biomarker to distinguish prostate cancer patients with bone lesions. Clin Chem 2005;51:695–707.
13. Chen G-Y, Tang J, Zheng P, Liu Y. CD24 and Siglec-10 selectively repress tissue damage-induced immune responses. Science 2009; 323:1722–1725.
14. Kawai T, Akira S. TLR signaling. Cell Death Differ 2006;13: 816–825.
15. Chin AI, Miyahira AK, Covarrubias A, Teague J, Guo B, Dempsey PW. Toll-like receptor 3-mediated suppression of TRAMP prostate cancer shows the critical role of type I interferons in tumor immune surveillance. Cancer Res 2010;70:2595–2603.
16. Zheng SL, Augustsson-Bälter K, Chang B, Hedelin M, Li L, Adami HO, Bensen J, Li G, Johnasson JE, Turner AR, Adams TS, Meyers DA, Isaacs WB, Xu J, Grönberg H. Sequence variants of toll-like receptor 4 are associated with prostate cancer risk: Results from the CAncer Prostate in Sweden Study. Cancer Res 2004;64:2918–2922.
17. Sun J, Wiklund F, Zheng SL, Chang B, Bälter K, Li L, Adami HO, Liu W, Tolin A, Turner AR, Meyers DA, Isaacs WB, Xu J, Grönberg H. Sequence variants in Toll-like receptor gene cluster (TLR6-TLR1-TLR10) and prostate cancer risk. J Natl Cancer Inst 2005;97:525–532.
18. Stevens VL, Hsing AW, Talbot JT, Zheng SL, Sun J, Chen J, Thun MJ, Xu J, Calle EE, Rodriguez C. Genetic variation in the toll-like receptor gene cluster (TLR10-TLR1-TLR6) and prostate cancer risk. Int J Cancer 2008;123:2644–2650.
19. Sun J, Wiklund F, Hsu F-C, Bälter K, Zheng SL, Johansson J-E. Interactions of sequence variants in interleukin-1 receptor-

associated kinase4 and the toll-like receptor 6-1-10 gene cluster increase prostate cancer risk. Cancer Epidemiol Biomarkers Prev 2006; 15:480–485.

20. Zhang H, Chin AI. Role of Rip2 in development of tumor-infiltrating MDSCs and bladder cancer metastasis. PLoS One 2014;9:e94793.
21. Greenberg NM, DeMayo F, Finegold MJ, Medina D, Tilley WD, Aspinall JO. et al. Prostate cancer in a transgenic mouse. Proc Natl Acad Sci USA 1995;92:3439–3443.
22. Hurwitz AA, Foster BA, Allison JP, Greenberg NM, Kwon ED. The TRAMP mouse as a model for prostate cancer. Curr Protoc Immunol 2001;Chapter 20.
23. Pietras EM, Miller LS, Johnson CT, O'Connell RM, Dempsey PW, Cheng G. A MyD88-dependent IFN-γR-CCR2 signaling circuit is required for mobilization of monocytes and host defense against systemic bacterial challenge. Cell Res 2011;21:1068–1079.
24. Yeh I-T, Reddick RL, Kumar AP. Malignancy arising in seminal vesicles in the transgenic adenocarcinoma of mouse prostate (TRAMP) model. Prostrate 2009;69:755–760.
25. Khaled YS, Ammori BJ, Elkord E. Myeloid-derived suppressor cells in cancer: Recent progress and prospects. Immunol Cell Biol 2013;91:493–502.
26. Hoesel B, Schmid JA. The complexity of NF-κB signaling in inflammation and cancer. Mol Cancer 2013;12:86.
27. Zhang L, Charron M, Wright WW, Chatterjee B, Song CS, Roy AK, Brown TR. Nuclear factor-kappaB activates transcription of the androgen receptor gene in Sertoli cells isolated from testes of adult rats. Endocrinology 2004;145:781–789.
28. Zhang L, Altuwaijri S, Deng F, Chen L, Lal P, Bhanot UK, Korets R, Wenske S, Lilja HG, Chang C, Scher HI, Gerald WL. NF-kappaB regulates androgen receptor expression and prostate cancer growth. Am J Pathol 2009;175:489–499.
29. Jain G, Voogdt C, Tobias A, Spindler K-D, Möller P, Cronauer V, Marienfeld RB. IκB kinases modulate the activity of the androgen receptor in prostate carcinoma cell lines. Neoplasia 2012;14:178–189.
30. Nadiminty N, Lou W, Sun M, Chen J, Yue J, Kung H-J, Evans CP, Zhou Q, Gao AC. Aberrant activation of the androgen receptor by NF-kappaB2/p52 in prostate cancer cells. Cancer Res 2010; 70:3309–3319.
31. Ochi A, Nguyen AH, Bedrosian AS, Mushlin HM, Zarbakhsh S, Barilla R, Zambirinis CP, Fallon NC, Rehman A, Pylayeva-Gupta Y, Badar S, Hajdu CH, Frey AB, Bar-Sagi D, Miller G. MyD88 inhibition amplifies dendritic cell capacity to promote pancreatic carcinogenesis via Th2 cells. J Exp Med 2012; 209:1671–1687.
32. Qiu J, Wang X, Guo X, Zhao C, Wu X, Zhang Y. Toll-like receptor 9 agonist inhibits ERalpha-mediated transactivation by activating NF-kappaB in breast cancer cell lines. Oncol Rep 2009;22:935–941.
33. Hofmann MA, Kors C, Audring H, Walden P, Sterry W, Trefzer U. Phase 1 evaluation of intralesionally injected TLR9-agonist PF-3512676 in patients with basal cell carcinoma or metastatic melanoma. J Immunother 2008;31:520–527.
34. Kim YH, Girardi M, Duvic M, Kuzel T, Link BK, Pinter-Brown L, Rook AH. Phase I trial of a Toll-like receptor 9 agonist, PF-3512676 (CPG 7909), in patients with treatment-refractory, cutaneous T-cell lymphoma. J Am Acad Dermatol 2010;63: 975–983.
35. Zent CS, Smith BJ, Ballas ZK, Wooldridge JE, Link BK, Call TG, Shanafelt TD, Bowen DA, Kay NE, Witzig TE, Weiner GJ. Phase I clinical trial of CpG oligonucleotide 7909 (PF-03512676) in patients with previously treated chronic lymphocytic leukemia. Leuk Lymphoma 2012; 53:211–217.
36. Vacchelli E, Galluzzi L, Eggermont A, Fridman WH, Galon J, Sautès-Fridman C, Tartour E, Zitvogel L, Kroemer G. Trial watch: FDA-approved Toll-like receptor agonists for cancer therapy. Oncoimmunology 2012; 1:894–907.
37. Rakoff-Nahoum S, Medzhitov R. Regulation of spontaneous intestinal tumorigenesis through the adaptor protein MyD88. Science 2007; 317:124–127.
38. Wang L, Zhu R, Huang Z, Li H, Zhu H. Lipopolysaccharide-induced toll-like receptor 4 signaling in cancer cells promotes cell survival and proliferation in hepatocellular carcinoma. Dig Dis Sci 2013;58:2223–2236.
39. Greten FR, Eckmann L, Greten TF, Park JM, Li Z-W, Egan LJ. et al. IKKbeta links inflammation and tumorigenesis in a mouse model of colitis-associated cancer. Cell 2004;118:285–296.
40. Vogl T, Liberg D, Olsson A, Bjo P, Wikstro P, Ka E. et al. S100A9 Interaction with TLR4 Promotes Tumor Growth. PLoS One 2012;7:1–11.
41. Nagarajan UM, Sikes J, Prantner D, Andrews CW, Frazer L, Goodwin A, Snowden JN, Darville T. MyD88 deficiency leads to decreased cell gamma interferon production and T cell recruitment during Chlamydia muridarum genital tract infection, but a predominant Th1 response and enhanced monocytic inflammation are associated with infection resolution. Infect Immun 2011; 79:486–498.
42. van Maren WWC, Jacobs JFM, de Vries IJM, Nierkens S, Adema GJ. Toll-like receptor signalling on Tregs: To suppress or not to suppress? Immunology 2008; 124:445–452.
43. Lechner MG, Epstein AL. A new mechanism for blocking myeloid-derived suppressor cells by CpG. Clin Cancer Res 2011; 17:1645–1648.
44. Ostrand-Rosenberg S, Sinha P. Myeloid-derived suppressor cells: Linking inflammation and cancer. J Immunol 2009; 182:4499–4506.
45. Razani B, Reichardt AD, Cheng G. Non-canonical NF-κB signaling activation and regulation: Principles and perspectives. Immunol Rev 2011;244:44–54.
46. Ammirante M, Luo J-L, Grivennikov S, Nedospasov S, Karin M. B-cell-derived lymphotoxin promotes castration-resistant prostate cancer. Nature 2010;464:302–305.
47. Wang S, Gao J, Lei Q, Rozengurt N, Pritchard C, Jiao J, Thomas GV, Li G, Roy-Burman P, Nelson PS, Liu X, Wu H. Prostate-specific deletion of the murine Pten tumor suppressor gene leads to metastatic prostate cancer. Cancer Cell 2003;4:209–221.
48. Goldstein AS, Drake JM, Burnes DL, Finley DS, Zhang H, Reiter RE, Huang J, Witte ON. Purification and direct transformation of epithelial progenitor cells from primary human prostate. Nat Protoc 2011;6:656–667.

CHAPTER III

MYD88-DEPENDENT SIGNALING IN PROSTATE CANCER MODULATES MDSC INFILTRATION AND ACTIVITY

ABSTRACT

The role of immune signaling in cancer is complex and conflicting. Inflammatory signaling can drive an anti-tumor response, but chronic inflammation is strongly tied to tumorigenesis and many tumors exploit mechanisms of immunosuppression to block an anti-tumor response. The most well-characterized of inflammatory pathways is the Toll-like receptor (TLR) pathway, and mutations in TLRs are associated with a higher risk of prostate cancer.

We have previously reported the impact of TLR signaling disruption on tumor growth and progression in the TRAMP model of prostate cancer. The adaptor protein MyD88 is an essential component of signaling for almost all TLRs, so loss of MyD88 abrogates most TLR signaling. Absence of MyD88-dependent signaling in TRAMP prostate tumors resulted in a more aggressive disease, likely driven by increased infiltration of $CD11b^{+}Gr\text{-}1^{+}$ MDSCs (myeloid-derived suppressor cells) when compared to $MyD88^{+/+}$ tumors.

The goal was to identify an explicit link between MyD88-dependent signaling and MDSC accumulation, at some level likely tied to chemokines that promote MDSC recruitment. Various chemotactic agents were expressed by the tumors, but the most promising was S100A9, a TLR4 ligand also known to directly recruit MDSCs to tumors. S100A9 activity indicates that MyD88-dependent signaling may play a role within the MDSCs themselves. *In vitro* differentiation of MDSCs from bone marrow skewed towards the granulocytic subset (gMDSCs) in $MyD88^{-/-}$ cells, supporting an internal role for MyD88 signaling. $MyD88^{-/-}$ MDSCs also showed an increased sensitivity to chemotaxis mediated by S100A9 and an increase in Arg-1 expression following S100A9 stimulation. We conclude that MyD88-dependent signaling may play an essential role in regulating the population of tumor-infiltrating cells by reducing MDSC activity and MDSC response to S100A9-mediated chemotaxis, thus limiting prostate tumor progression.

INTRODUCTION

Prostate cancer is the second most common cancer for men in the US, with 2.9 million men currently living with prostate cancer[1]. One in six men will be diagnosed in their lifetime, and, while localized disease is highly survivable, the 5-year survival for metastatic disease is 29.3%.

The role of inflammation in the development and progression of cancer was originally proposed by Rudolf Virchow in 1863. However, inflammatory signaling still continues to show both pro- and anti-tumor effects in a variety of models[2-7]. Within prostate cancer, chronic inflammation has been identified as a common feature in tumor-adjacent tissue[8], and some SNPs in TLR genes increase the risk of prostate cancer[9].

Previous work in our lab[10] has focused on the role of the adaptor protein MyD88 in murine prostate cancer using the established TRAMP model[11-12]. We showed that MyD88-dependent signaling is important for regulating the tumor-infiltrating immune populations and that loss of this signaling led to a more immunosuppressive tumor microenvironment and a more advanced disease.

Specifically, myeloid derived suppressor cells (MDSCs) appeared to play an important role, as TRAMP tumors lacking MyD88 showed a significantly increased MDSC population. These cells are part of a heterogeneous group of cells with similar suppressive activity but different lineages [13-14]. MDSCs are typically identified as $CD11b^{+}Gr\text{-}1^{+}$ cells, though Gr-1 can be further broken down into Ly6G and Ly6C. The granulocytic lineage of MDSCs is $CD11b^{+}Ly6G^{+}Ly6C^{mid/lo}$, while the monocytic lineage is $CD11b^{+}Ly6G^{-}Ly6C^{hi}$. Both subpopulations inhibit T cell activation and

NK cell differentiation, and both are associated with more aggressive tumors and worsened survival[15-16].

Recruitment of MDSCs, both in infection and disease models, is well-characterized. Many secreted proteins have been identified as promoting MDSC differentiation and recruitment[17]: members of the CCL and CXCL families of chemokines[18-20]; interleukins IL-1β, -5, -6, and -13[21-23]; and colony stimulating factors (M-CSF, G-CSF, GM-CSF)[24-25].

We aim to determine the mechanistic link between MyD88 signaling and MDSC population changes in prostate cancer, with the hope that any mechanism be more broadly applicable. Only by teasing out the complex interactions mediated by inflammatory signaling in cancer can we understand how to exploit those interactions to design therapeutics.

MATERIALS & METHODS

Tumor model

MyD88$^{+/+}$ TRAMP$^{Tg-/-}$, MyD88$^{+/+}$ TRAMP$^{Tg+/-}$, MyD88$^{-/-}$ TRAMP$^{Tg-/-}$, and MyD88$^{-/-}$ TRAMP$^{Tg+/-}$ male mice were previously sacrificed at 30 weeks of age[10], with lungs, liver, and abdominal lymph nodes grossly inspected for metastases. Whole prostates with seminal vesicles were removed, fixed in formalin, or embedded in OCT.

Immunofluorescence and Immunohistochemistry

Immunofluorescence was performed on OCT-embedded tissue. Sections were fixed in 4% paraformaldehyde for 10min and then blocked for 1hr with either standard (5% BSA and 5% goat serum in PBS) or specific, when using mouse primary antibodies, (M.O.M kit block, Vector Labs) reagents. Sections were stained overnight at 4°C with FITC anti-CD11b (M1/70, BD Bioscience), PE anti-Gr-1 (RB6-8C5, BD Bioscience), anti-CD49b (DX5, Biolegend), and FITC anti-CD3e (145-2C11, BD Bioscience) at 1:500. Secondary antibody staining using goat anti-rat Al568 (Invitrogen) was performed, with incubation at 1:1000 for 1hr. Sections were counterstained with DAPI and mounted using Vectorshield (Vector Labs). Images were assessed by fluorescence microscopy using an Axio Imager 2 (Zeiss).

Immunohistochemistry was performed on formalin-fixed and paraffin-embedded tissues. Sections were deparaffinized and rehydrated before blocking for one hour in 5% BSA and 5% goat serum in PBS. Sections were stained with anti-S100A9 at 1:500 (SC-20173, Santa Cruz), followed by incubation with biotinylated goat anti-rabbit antibodies at 1:750 using the ABC kit (Vector Labs).

Sections were developed using streptavidin-conjugated HRP and substrate, counterstained with hematoxylin, then dehydrated and mounted with Cytoseal 60 (Richard-Allan Scientific). Images were assessed by light microscopy using an Axio Imager 2 (Zeiss).

In vitro MDSC differentiation

WT and MyD88$^{-/-}$ C57Bl/6 mice were sacrificed at 8-12 weeks, and bone marrow was harvested from the femurs and tibiae. Bone marrow was dispersed by fine needle aspiration in PBS before red blood cells were lysed with ACK buffer. Once counted, cells were plated at 1x10^6 cells per ml in M-CSF media (RPMI with 10% fetal calf serum and 1% penicillin/streptomycin solution, plus 20% L929 conditioned media) and incubated overnight. The following day, non-adherent cells were harvested and recounted.

Those cells were replated in specific stimulation buffers: M-CSF+GM-CSF (M-CSF media described above with 10 ng/ml) or G-CSF+GM-CSF (RPMI complete media with 10 ng/ml G-CSF and 10 ng/ml GM-CSF). Media was changed after 3 days, and only adherent cells were reserved. Cells were harvested on day 5 for flow cytometric analysis.

Transwell migration assay

Following *in vitro* differentiation, 1-5x10^5 cells were plated in 100 μl of media on cell culture plate inserts (Corning 24-well plate, 6.5 mm transwell, 5.0 μm pore). 600 μl of media (with or without a chemokine) was placed in the bottom of the well. Cells were incubated for 24 hours at 37°C, at which point, the transwell insert was carefully removed. The cell concentration within the bottom of the well was used to quantify the amount of migration, and the experimental results were

compared to a control with no chemokine. Results were reported as fold change in migration from the control, as has been described previously[26-28].

Quantitative PCR

Total RNA extracted from frozen prostate tissue was used to synthesize cDNA using High Capacity cDNA Reverse Transcription Kits (Applied Biosystems). Relative gene expression was determined using SYBR Green PCR Master Mix (Applied Biosystems) on a Viia 7 system (Applied Biosystems), normalized to GAPDH as a reference gene, using the comparative threshold cycle method. Primer sets for the following genes were used:

Gene	Forward Primer	Reverse Primer
Arg-1	5'-AACACGGCAGTGGCTTTAACC -3'	5'- GGTTTTCATGTGGCGCATTC-3'
iNOS	5'-GCTGGAAGCCACTGACACTTCG-3'	5'- CGAGATGGTCAGGGTCCCCT-3'
CCL2	5'-GAAGGAATGGGTCCAGACAT-3'	5'-ACGGGTCAACTTCACATTCA-3'
CCL3	5'-ACTGCCTGCTGCTTCTCCTACA-3'	5'-AGGAAAATGACACCTGGCTGG-3'
CCL5	5'-CCTCACCATCATCCTCACTGCA-3'	5'-TCTTCTCTGGGTTGGCACACAC-3'
CXCL1	5'-CCAACACAGCACCATGATCC-3'	5'-CCTCGCGACCATTCTTG-3'
G-CSF	5'-CTCAACTTTCTGCCCAGAGG-3'	5'-AGCTGGCTTAGGCACTGTGT-3'
GM-CSF	5'-GCCATCAAAGAAGCCCTGAA-3'	5'-GCGGGTCTGCACACATGTTA-3'
IL-1b	5'-CACAGCAGCACATCAACAAG-3'	5'-GTGCTCATGTCCTCATCCTG-3'
IL-4	5'-GGATGTGCCAAACGTCCTC-3'	5'-GAGTTCTTCTTCAAGCATGGAG-3'
IL-13	5'-ATGAGTCTGCAGTATCCCG-3'	5'-CCGTGGCAGACAGGAGTGTT-3'
S100A9	5'-GTTGATCTTTGCCTGTCATGAG-3'	5'-AGCCATTCCCTTTAGACTTGG-3'

RESULTS

Increased infiltration of MDSCs

Prostates of all genotypes were stained for CD11b and Gr-1 **(Figure 1A)**. While $CD11b^{+}$ cells are found sparsely in both normal and Tg prostates, co-stained cells are abundant in $MyD88^{-/-}$ $TRAMP^{Tg+/-}$ prostates, as reported previously[10].

Prostates were also co-stained for CD3e and CD49b **(Figure 1B)**; $CD49b^{+}$ single staining defines the NK cell population, and double staining with CD3e more specifically stains the NKT cell population. As is expected, the large population of MDSCs in the $MyD88^{-/-}$ tumor coincides with reduced NK cell presence.

An established function of MDSCs is to suppress NK cell differentiation and activity[29-31]. There does not appear to be any significant difference in NKT cell populations in WT vs. $MyD88^{-/-}$ tumors, though there are few cells present at all. The observed effect on tumor-infiltrating populations recapitulates previous data.

Chemokine-mediated MDSC recruitment

An increase in MDSCs within the tumor microenvironment does not automatically suggest a role for MyD88-dependent signaling. However, there is an extensive body of literature on the many chemokines that have a role in MDSC recruitment, both generally and within a cancer model[32-43]. We selected the most relevant chemokines and observed the expression of these proteins in prostate tissue from all four mouse genotypes **(Figure 2A)**.

Two major expression trends presented themselves. *IL-1β, IL-13, CCL2, CCL3*, and *CXCL1* were highly expressed in only the MyD88$^{-/-}$ TRAMP tumors, with low expression in the rest. In another set of genes, *G-CSF, GM-CSF* and *S100A9* all showed low expression in the non-transgenic prostates but increased expression in both the categories of TRAMP prostates, with no difference in expression between the MyD88$^{+/+}$ and MyD88$^{-/-}$ tumors.

Predictions for a recruitment mechanism

The chemokine expression data suggest two possible mechanisms **(Table 1)** explaining the increased MDSC recruitment seen in MyD88$^{-/-}$ tumors: the "expression" model and the "sensitivity" model.

In the expression model, more of the essential chemokine(s) responsible for MDSC recruitment will be found in the tumor microenvironment. That necessitates a chemokine-secreting cell near the tumor responsible for the increased expression. The loss of MyD88-dependent signaling would be relevant in that chemokine-secreting cell or another activating cell upstream. Therefore, the effect of MyD88-dependent signaling could be directly regulating MDSC recruitment or indirectly functioning to activate chemokine-secreting cells.

In the sensitivity model, the same chemokine expression is observed in both MyD88$^{+/+}$ and MyD88$^{-/-}$ tumors. The putative chemokine-secreting cell from the previous model is not necessarily influenced by MyD88-dependent signaling here. Instead, the MyD88$^{-/-}$ MDSCs are more sensitive to the chemotactic effects of the protein. The same amount of chemokine recruits more MDSCs

when MyD88-dependent signaling is disrupted. Here, the role for MyD88 signaling is within the MDSC and downstream of the chemokine stimulation.

All of the tested chemokines activate various pathways known to promote an inflammatory response (MAPK, JAK/STAT, AKT, NF-kB)[17,32,37,44-46]. These pathways are also known to influence each other through signaling crosstalk and downstream transcriptional changes, meaning that the loss of MyD88-dependent signaling would likely have downstream consequences even if the chemokine signaling did not specifically require MyD88. Obviously, this complicates the search for a specific mechanism regulating MDSC recruitment in this case, but the goal would be to find a direct connection between a chemokine and MyD88-dependent signaling.

S100A9

After a careful analysis of chemokine-related signaling, one protein stands out as having a direct signaling axis involving MyD88. S100A9 is both a robust recruiter of MDSCs to the tumor microenvironment[47-49] and a well-studied endogenous ligand for TLR4[50-52], which promotes signaling through MyD88.

S100A9 also displays significantly increased mRNA expression within the TRAMP tumors (**Figure 2A**). Protein expression within the tumor microenvironment was confirmed by immunohistochemistry **(Figure 2B)**. We see no significant difference in the expression of S100A9 within $MyD88^{+/+}$ and $MyD88^{-/-}$ tumors, though the non-transgenic prostates had reduced expression. These data preliminarily support the "sensitivity" model, which is defined by inherent

MyD88-dependent signaling within MDSCs. To probe the cells themselves, we needed to generate MDSCs *in vitro*.

In vitro *differentiation*

Mouse bone marrow from WT and MyD88$^{-/-}$ mice was stimulated with various colony stimulating factors to promote differentiation of MDSCs, as described previously[53-55]. MDSC subpopulations were analyzed, using surface biomarkers, to characterize their differentiation[56]. MDSCs derived from a granulocytic lineage are CD11b^{+} Ly6G^{+} Ly6C^{mid}, while MDSCs from a myeloid lineage are defined as CD11b^{+} Ly6G^{-} Ly6C^{hi}. While the differences between these subpopulations are not fully understood, they appear to be functionally similar and equally able to suppress T cell activation[56].

Differentiation of MyD88$^{-/-}$ bone marrow with G-CSF+GM-CSF shows a skewing of the subpopulations when compared to the WT bone marrow **(Figure 3A,B)**. Cells lacking MyD88-dependent signaling appear to favor the granulocytic subset, with a corresponding decrease in the myeloid subset. The MDSCs differentiated *in vitro* did show a difference in expression of *Arg-1* and *iNOS*, indicating a change in the immunosuppressive activity **(Figure 3C)**. Generally, MyD88-/- MDSCs showed the same expression of *Arg-1* but a significant decrease in the expression of *iNOS*. This decrease in *iNOS* expression can be attributed to the skewing of differentiation toward g-MDSCs, which favor ROS production over NO. Additionally, stimulation of these MDSCs with various TLR ligands did not have any effect on the functionality, except in the case of S100A9. Stimulation by S100A9 increased the expression of both genes from the control MyD88$^{-/-}$ cells, indicating a potential role for S100A9 to activate MDSCs as well.

Taken together, these changes imply that MyD88-dependent signaling plays a role within MDSCs themselves. In the context of the models described previously, this would indicate that MyD88$^{-/-}$ MDSCs may be inherently more sensitive to chemotactic proteins due to some alteration of internal signaling.

The chemotactic response of WT and MyD88$^{-/-}$ MDSCs (derived *in vitro*) was measured using a standard trans-well migration assay[26-28]. The response to S100A9 was compared to other standard TLR ligands **(Table 2)**. Both HMGB1 and S100A9 are damage-associated molecular patterns (DAMPs), endogenous ligands that stimulate TLR signaling in the case of internal injury or cell death[57-60]. From this panel of ligands, only S100A9 showed a significant ability to promote chemotaxis. Most compellingly, the migration induced by S100A9 was markedly increased in MyD88$^{-/-}$ MDSCs as compared to WT **(Figure 3D)**.

We can therefore postulate a mechanism linking MyD88-dependent signaling to MDSC recruitment to the tumor **(Figure 4)**. Cells from the prostate tumor, surrounding stromal cells, or infiltrating immune cells secrete chemokines that promote MDSC chemotaxis. This includes S100A9, which binds to TLR4 on MDSCs. Loss of downstream MyD88 signaling induces a stronger chemotactic response to S100A9 than if MyD88 signaling was intact. An increased response to S100A9 leads to an increase in MDSC recruitment to the tumor. The increase in MDSC infiltration promotes tumor growth and limits any anti-tumor immune activity.

DISCUSSION

Role of MyD88

We report here that disruption of MyD88-dependent signaling results in the increased recruitment of myeloid-derived suppressor cells (MDSCs) to the tumor microenvironment in murine prostate cancer. Tumors showed increased expression of chemokines that are known to drive MDSC recruitment, though in some cases the exact expression scheme differed. MDSCs derived *in vitro* indicate that MyD88-dependent signaling is essential within the MDSC population to regulate subset differentiation and migration.

Crucially, the chemokine S100A9 produced an elevated recruitment response in cells lacking MyD88 signaling. As S100A9 is known to bind TLR4, the data elucidate a mechanism where a dysregulated chemotactic response to S100A9 leads to an overabundance of tumor-infiltrating MDSCs **(Figure 4)**. The end result is that prostate tumors in MyD88$^{-/-}$ animals show greater evidence of immunosuppression and advanced disease.

RAGE and TLR signaling

Existing literature also clarifies the role of MyD88 in chemotactic signaling. In fact, the ability of S100A9 to recruit MDSCs has been specifically linked to downstream RAGE signaling and not TLR4 activation[56]. Chen et al. definitively show that blockade of TLR4 does not prevent S100A9-induced RAW cell migration, while migration was inhibited by RAGE blockade[61]. RAGE blockade has been shown to suppress tumor growth and metastasis in glioma, breast, and prostate cancers as well[62-64].

Compellingly, RAGE does not appear to rely on MyD88-dependent signaling, while TLR4 signals heavily (but not exclusively) through MyD88. RAGE can also directly activate MAPK (ERK1/2, p38, SAPK/JNK), PI3K/Akt, and cell migration (RhoA, Rac-1, Cdc42) pathways[65], and RAGE was shown to oppose MyD88 signaling in a liver resection model[66]. Therefore, disrupted MyD88-dependent signaling may bias S100A9-induced activation towards RAGE, increasing the MDSC response to chemotaxis.

Tasquinimod

The drug tasquinimod (TASQ) was first introduced as an anti-angiogenic agent in animal models of prostate cancer[67], but it was quickly shuttled into clinical trials for patients with metastatic castration-resistant prostate cancer (mCRPC)[68]. Tasquinimod was found to bind S100A9 and prevent binding to both RAGE and TLR4, reducing angiogenesis and tumor growth by modulating MDSCs[69]. It also significantly slowed patient progression and improved progression-free survival in phase II trials[70-71].

Due to the success of TASQ in early trials, a phase III trial was undertaken using TASQ as a single agent in chemotherapy-naïve men with mCRPC. While progression-free survival was significantly improved, overall survival was not affected[72]. Unfortunately, the mediocre results of the phase III trial led partners Active Biotech and Ipsen to discontinue all prostate cancer studies.

Given the data presented here, we may not expect an S100A9 inhibitor to function robustly as a single agent. When MyD88 signaling is disrupted, a significant increase in tumor-infiltrating

MDSCs is observed, which produces only a modest increase in tumor progression. Depleting MDSCs alone may not be the most effective way to utilize the drug. In a field so rife with combinatorial therapies, TASQ is likely better-equipped to succeed as a complement therapy. In fact, TASQ previously showed significant enhancement to a prostate cancer tumor vaccine (SurVax M)[73]. Prostate cancer has typically shown poor responses to immunotherapies, other than Sipuleucel-T[74-76]. By reducing the immunosuppressive activity perpetuated by MDSCs, other immunotherapies may begin to show increased efficacy.

FIGURES

Figure 3.1. MyD88$^{-/-}$ TRAMP tumors show increased infiltration of CD11b^{+}Gr-1^{+} MDSCs. Prostates from MyD88$^{+/+}$ and MyD88$^{-/-}$ mice, expressing or not expressing the TRAMP transgene, were embedded in OCT and frozen. Sections were stained by immunofluorescence with **(A)** CD11b and Gr-1 to show MDSCs or **(B)** CD3ε and CD49b to show T cells, NK cells, and NKT cells. DAPI was added to visualize the nuclei. Representative prostates from multiple mice are shown as merged fluorescence images (400x or 1600x). Staining was quantified by mean positive-staining cells per field for 10 high-powered fields. All *p*-values were determined by two-tailed Student *t*-test, with statistical significance defined as $p<0.05$.

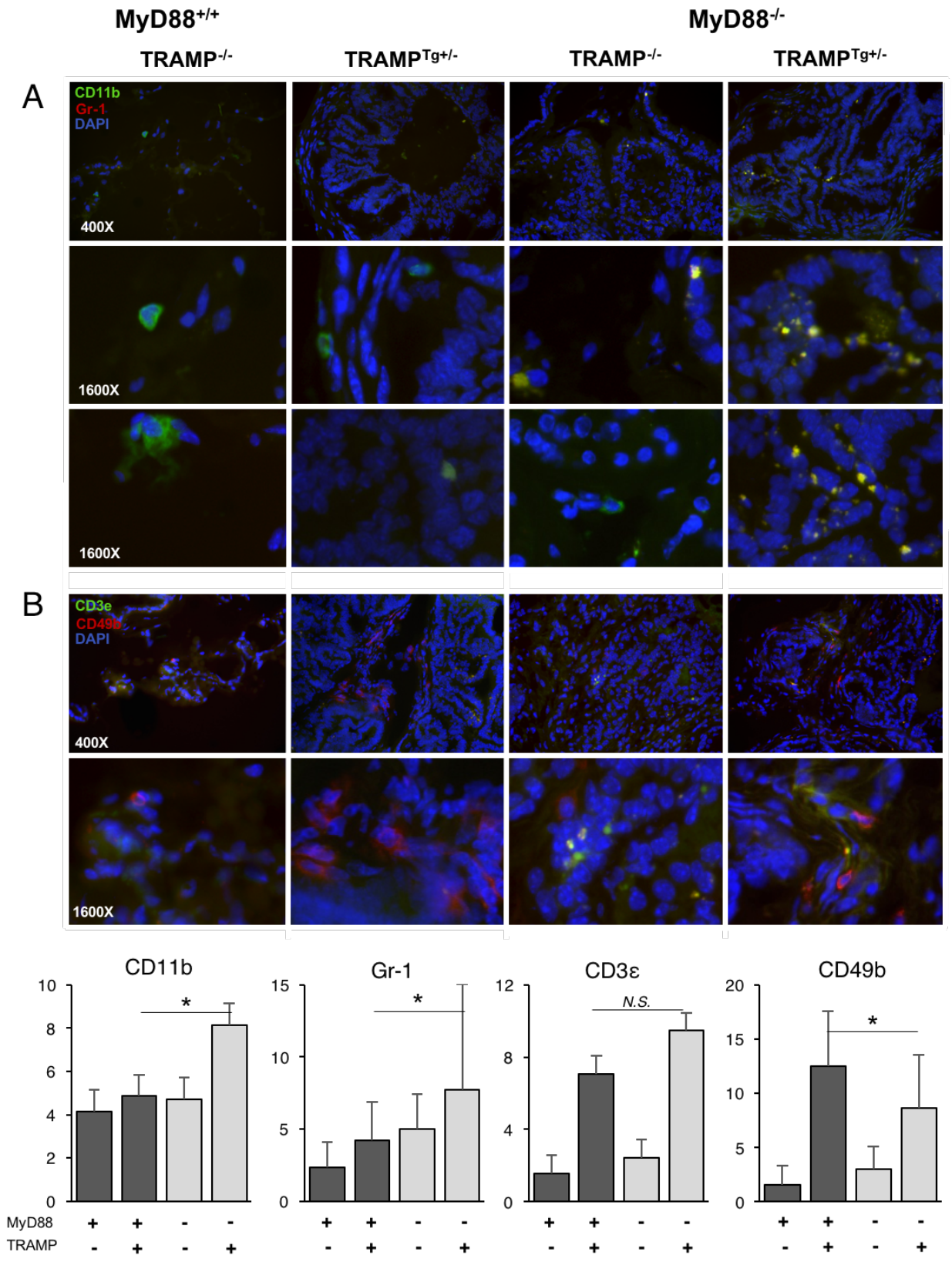
MyD88+/+
MyD88-/-
TRAMP-/-
TRAMPTg+/-
TRAMP-/-
TRAMPTg+/-
A
CD11b
Gr-1
DAPI
400X
1600X
1600X
B
CD3e
CD49b
DAPI
400X
1600X
CD11b
Gr-1
CD3ε
CD49b
*
*
N.S.
*
MyD88
TRAMP

Figure 3.2. Loss of MyD88-dependent signaling results in increased recruitment driven by chemokine expression in the tumor microenvironment. (A) Normal prostate and tumor samples were analyzed by qPCR to determine the expression of various known chemokines. The graphs depicted are representative experiments (n=2), with three animals per tumor category and one per normal prostate. Error bars represent standard deviation values, and all *p*-values were determined by two-tailed Student *t*-test, with statistical significance defined as $p<0.05$. **(B)** Prostate sections were stained by immunohistochemistry using anti-S100A9 antibodies to measure protein expression in mouse prostates. Representative prostates from multiple mice are shown (n=2).

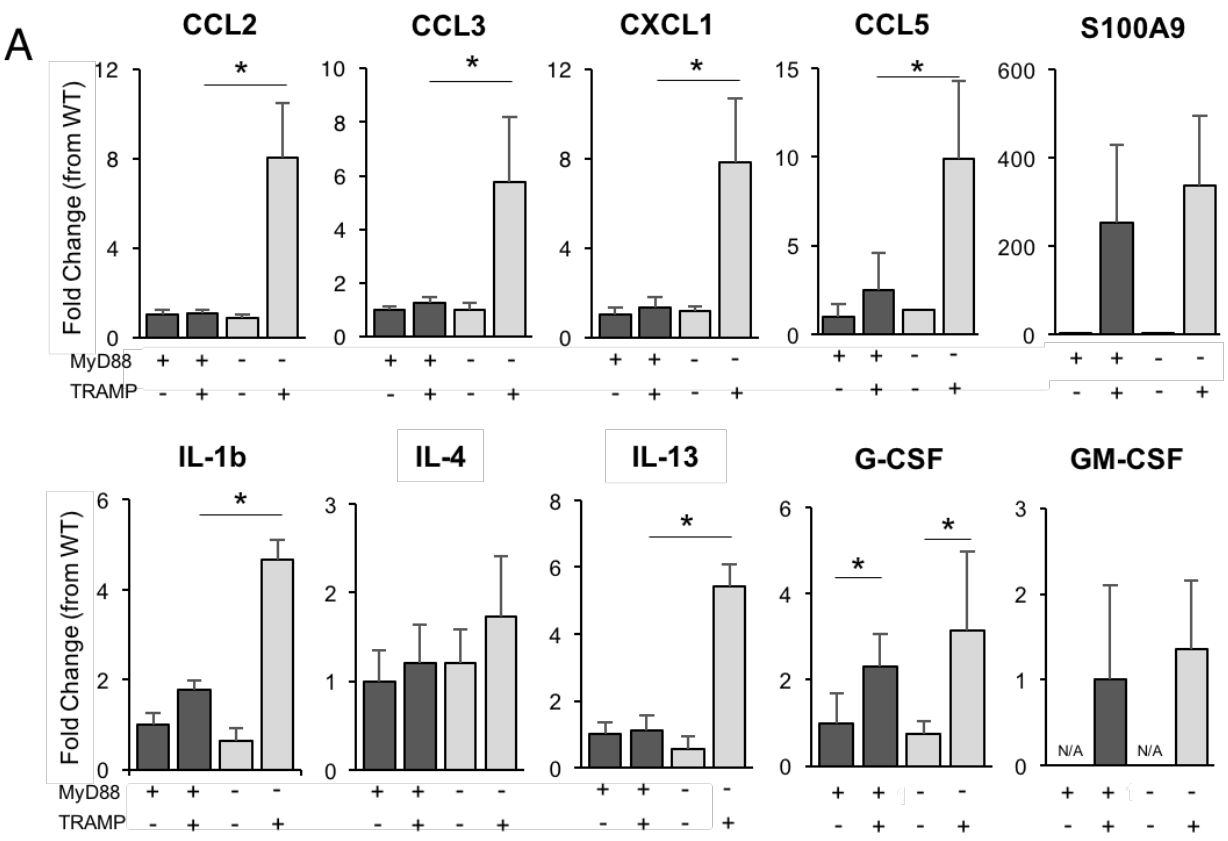
A
CCL2
CCL3
CXCL1
CCL5
S100A9
Fold Change (from WT)
MyD88
TRAMP
IL-1b
IL-4
IL-13
G-CSF
GM-CSF
N/A
N/A

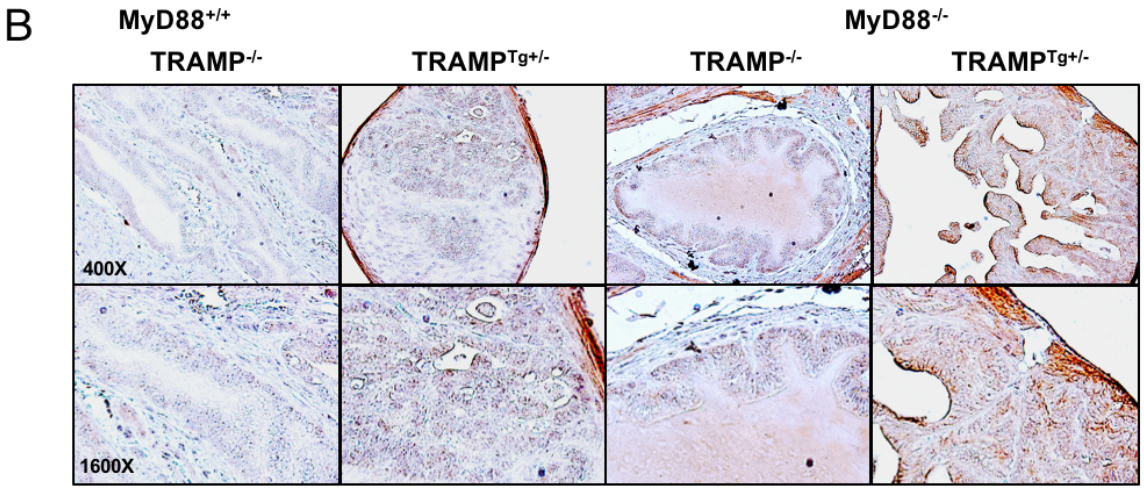
B
MyD88+/+
MyD88-/-
TRAMP-/-
TRAMPTg+/-
TRAMP-/-
TRAMPTg+/-
400X
1600X

Figure 3.3. Loss of MyD88 signaling within MDSCs skews *in vitro* differentiation in favor of gMDSCs and alters response to various stimuli. Mouse bone marrow was differentiated *in vitro* and then stained with APC-CD11b, FITC-Ly6C, and PE-Ly6C for analysis by flow cytometry. **(A)** $CD11b^+$ cells were gated based on the combination of Ly6G and Ly6C expression into gMDSC ($Ly6G^+$ $Ly6C^{mid}$) and mMDSC ($Ly6G^-$ $Ly6C^{hi}$) subpopulations. **(B)** The proportion of each subpopulation found within the $CD11b^+$ differentiated cells was quantified. Representative experiment (n=3) is shown. Columns depict differentiated bone marrow samples from four mice, and error bars represent standard deviation values. All *p*-values were determined by two-tailed Student *t*-test, with statistical significance defined as $p<0.05$. **(C)** Differentiated MDSCs were stimulated for 24 hours with known TLR ligands. The expression of MDSC functional genes Arg-1 and iNOS were analyzed by qPCR. Representative experiment is shown (n=2). **(D)** Differentiated MDSCs were placed in the upper well of a trans-well plate, while a chemokine or other protein was added to the media of the lower well. After 24 hours, the change in migration due to chemotaxis was observed, as compared to the control. MDSCs were pooled from multiple differentiated samples (n=4-6). The mean of two experiments is shown, and error bars represent standard deviation values.

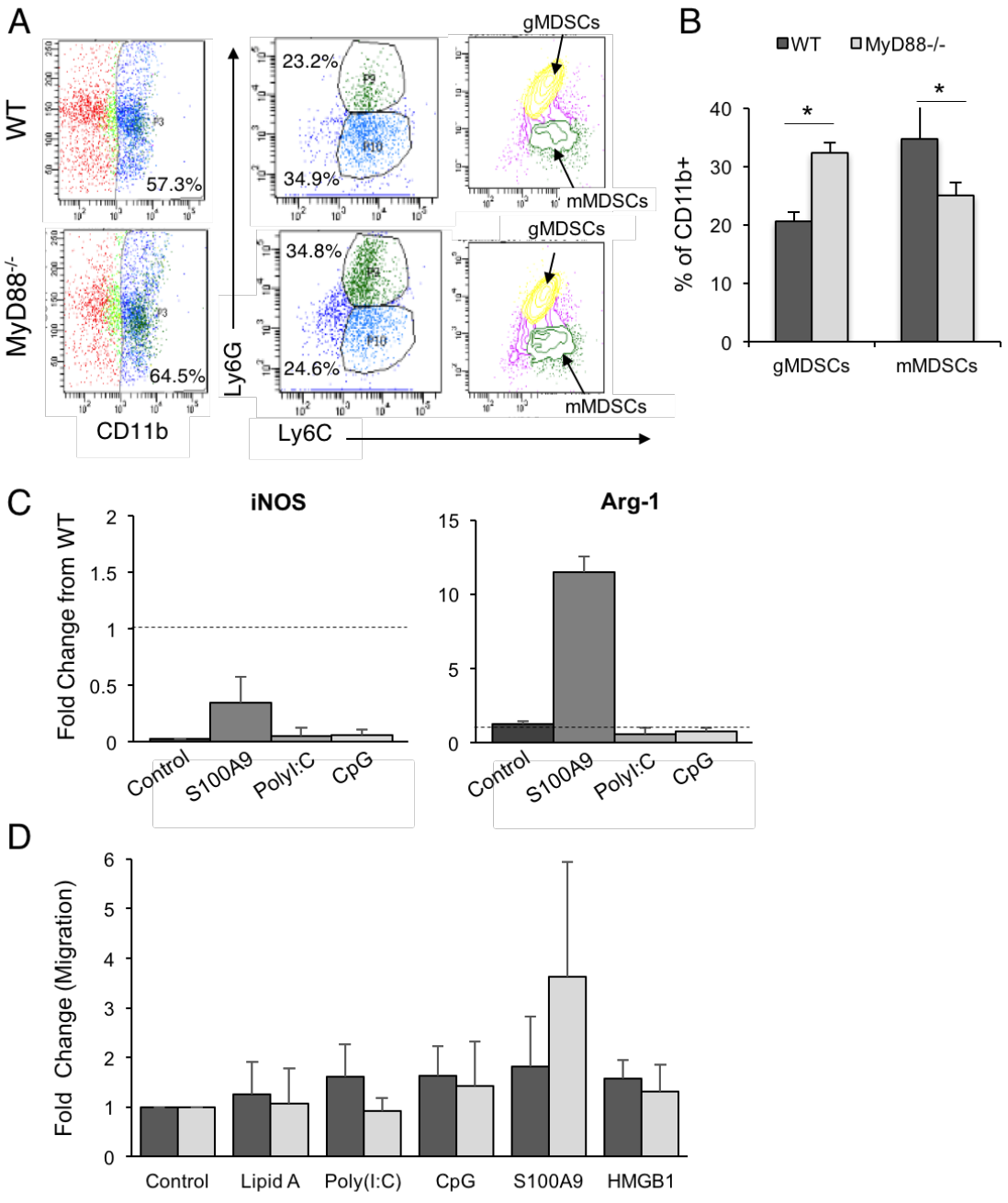
A
WT
MyD88-/-
57.3%
64.5%
23.2%
34.9%
34.8%
24.6%
gMDSCs
mMDSCs
CD11b
Ly6G
Ly6C
B
WT
MyD88-/-
% of CD11b+
gMDSCs
mMDSCs
C
iNOS
Arg-1
Fold Change from WT
Control
S100A9
Poly:C
CpG
D
Fold Change (Migration)
Control
Lipid A
Poly(I:C)
CpG
S100A9
HMGB1

Figure 3.4. Model of MDSC recruitment to the tumor microenvironment. (A) In prostate tumors of $MyD88^{+/+}$ mice, immune populations in the tumor microenvironment are diverse, with T cells, NK cells, and other populations present. This is contrasted with **(B)** tumors in $MyD88^{-/-}$ mice, where many more MDSCs are observed around the tumor, and NK cell differentiation and tumor infiltration are disrupted. S100A9 expression within the tumor recruits MDSCs, but $MyD88^{-/-}$ MDSCs are more sensitive to S100A9-mediated chemotaxis. Therefore, $MyD88^{-/-}$ tumors see a drastic increase in MDSC infiltration and a corresponding effect on tumor progression.

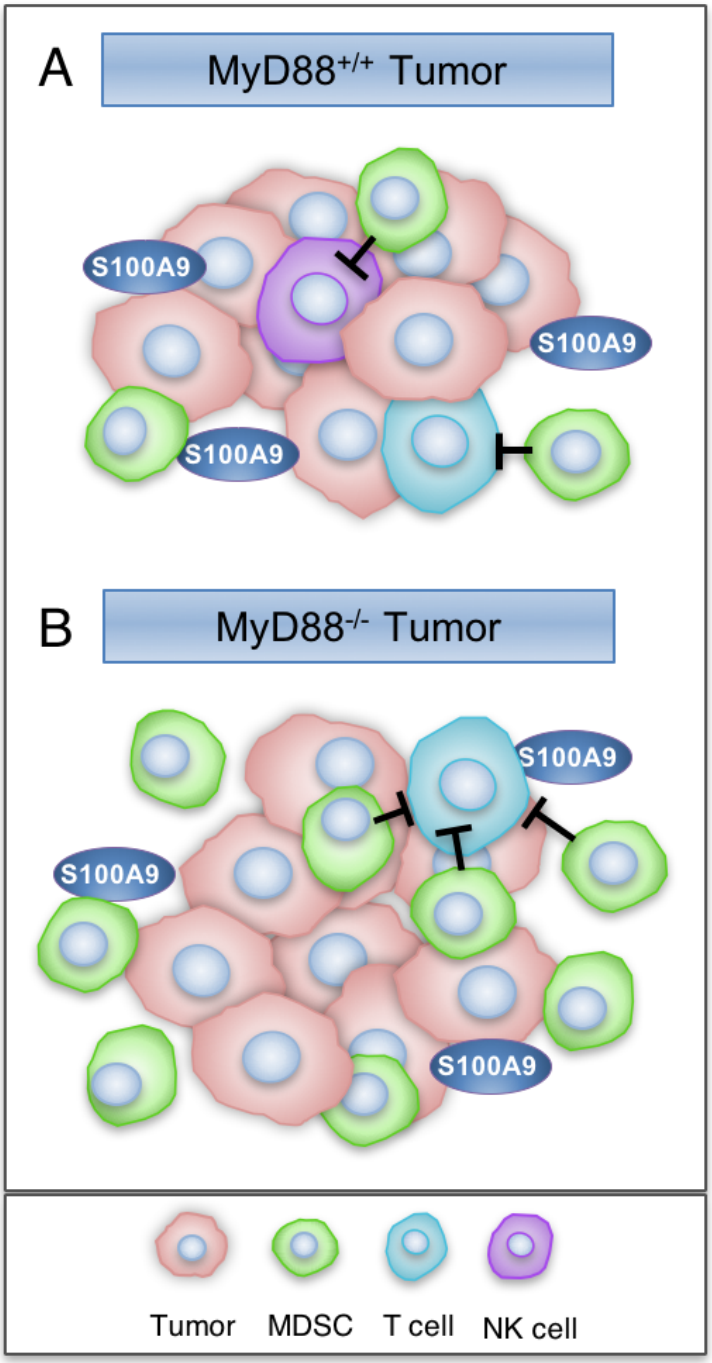
A
MyD88+/+ Tumor
S100A9
S100A9
S100A9
B
MyD88-/- Tumor
S100A9
S100A9
S100A9
Tumor
MDSC
T cell
NK cell

Table 3.1. Potential mechanisms underlying MDSC recruitment.

Expression	Sensitivity
More chemokine in tumor microenvironment	Same amount of chemokine
More chemokine secreted by upstream cell	No change in upstream secretion
MyD88 role upstream of MDSCs	MDSCs are more sensitive to chemokine
	MyD88 role within MDSC

Table 3.2. Toll-like receptor ligands.

Ligand	Receptor	MyD88-dependent	Source
Poly(I:C)	TLR3	No	Exogenous (PAMP)
CpG	TLR9	Yes	Exogenous (PAMP)
Lipid A	TLR4	Partially	Exogenous (PAMP)
S100A9	TLR4/RAGE	Partially	Endogenous (DAMP)
HMGB1	TLR2/TLR4/RAGE	Partially	Endogenous (DAMP)

REFERENCES

1. Howlader, N. et al. SEER Cancer Statistics Review, 1975-2013, National Cancer Institute. Bethesda, MD, http://seer.cancer.gov/csr/1975_2013/, based on November 2015 SEER data submission, posted to the SEER web site, April 2016.

2. Ochi, A. et al. (2012). MyD88 inhibition amplifies dendritic cell capacity to promote pancreatic carcinogenesis via Th2 cells. JEM 209(9), 1671-87.

3. Aviello, G. et al. (2014). MyD88 adaptor-like (Mal) regulates intestinal homeostasis and colitis-associated colorectal cancer in mice. American Journal of Physiology 306(9), G769-78.

4. Ammirante, M. et al. (2010). B-cell-derived lymphotoxin promotes castration-resistant prostate cancer. Nature 464(11), 302-5.

5. Greten, F.R. et al. (2004). IKKb links inflammation and tumorigenesis in a mouse model of colitis-associated cancer. Cell 118, 285-96.

6. Chin, A.I. et al. (2010). Toll-like receptor 3-mediated suppression of TRAMP prostate cancer demonstrates the critical role of Type I interferons in tumor immune surveillance. Cancer Res 70(7), 2595-603.

7. Rakoff-Nahoum, S. & Medzhitov, R. (2007). Regulation of spontaneous intestinal tumorigenesis through the adaptor protein MyD88. Science 317, 124-7.

8. Davidsson et al. (2011) Inflammation, focal atrophic lesions, and PIN with respect to risk of lethal prostate cancer. Cancer Epidemiol Biomarkers Prev.

9. Sfanos et al. *The role of inflammation in prostate cancer*. (2014).

10. EM Peek, W Song, H Zhang, J Huang, AI Chin (2015). Loss of MyD88 leads to more aggressive TRAMP prostate cancer and influences tumor infiltrating lymphocytes. *Prostate* 75(5):463-73.

11. Greenberg, N. et al. (1995). Prostate cancer in a transgenic mouse. PNAS, 92(8), 3439-43.

12. Hurwitz, A. et al. (2001). The TRAMP mouse as a model for prostate cancer. Current Protocols in Immunology, chapter 20.

13. Damuzzo, V. et al. (2015). Complexity and challenges in defining myeloid-derived suppressor cells. Cytometry. Part B, Clinical Cytometry, 88(2), 77–91.

14. Mantovani, A. (2010). The growing diversity and spectrum of action of myeloid-derived suppressor cells. European Journal of Immunology, 40(12), 3317-20.

15. Liu, C. et al. (2007). Expansion of spleen myeloid suppressor cells represses NK cell cytotoxicity in tumor-bearing host. Blood, 109(10), 4336-42.

16. Movahedi, K. et al. (2008). Identification of discrete tumor-induced myeloid-derived suppressor cell subpopulations with distinct T cell-suppressive activity. Blood, 111(8), 4233-44

17. Sevko, A. & Umansky, V. (2013). Myeloid-Derived Suppressor Cells Interact with Tumors in Terms of Myelopoiesis, Tumorigenesis and Immunosuppression: Thick as Thieves. J. Cancer 4, 3–11.

18. Fridlender, Z. et al. (2010). CCL2 blockade augments cancer immunotherapy. Cancer Research, 70(1), 109-18.

19. Huang, B. et al. (2007). CCL2/CCR2 pathway mediates recruitment of myeloid suppressor cells to cancers. Cancer Letters, 252(1), 86-92.

20. Zollo, M. et al. (2012). Targeting monocyte chemotactic protein-1 synthesis with bindarit induces tumor regression in prostate and breast cancer animal models. Clinical & Experimental Metastasis, 29(6), 585-601.

21. Song, X. et al. (2005). CD11b+/Gr-1+ immature myeloid cells mediate suppression of T cells in mice bearing tumors of IL-1-secreting cells. Journal of Immunology, 175(12), 8200-8208.

22. Boneberg, E. & Hartung, T. (2003). Febrile temperatures attenuate IL-1 release by inhibiting proteolytic processing of the preform and influence Th1/Th2 balance by favoring Th2 cytokines. Journal of Immunology, 171(2), 664-668.

23. Gabitass, R. et al. (2011). Elevated myeloid-derived suppressor cells in pancreatic, esophageal, and gastric cancer are an independent prognostic factor and are associated with significant elevation of the Th2 cytokine interleukin-13. Cancer Immunology & Immunotherapy, 60(10), 1419-30.

24. Barreda, D. et al. (2004). Regulation of myeloid development and function by colony stimulating factors. Developmental and Comparative Immunology, 28(5), 509-54.

25. Bot, F. et al. (1990). Synergistic effects between GM-CSF and G-CSF or M-CSF on highly enriched human marrow progenitor cells. Leukemia, 4(5), 325-8.

26. Hiratsuka, S. et al. (2006). Tumor-mediated upregulation of chemoattractants and recruitment of myeloid cells predetermines lung metastasis. Nat. Cell Biol. 8, 1369–75.

27. Sroussi, H. Y. et al. (2007). Oxidation of methionine 63 and 83 regulates the effect of S100A9 on the migration of neutrophils in vitro. J. Leukoc. Biol. 81(3), 818–824.

28. Manitz, M.-P. et al. (2003). Loss of S100A9 (MRP14) results in reduced interleukin-8-induced CD11b surface expression, a polarized microfilament system, and diminished responsiveness to chemoattractants in vitro. Mol. Cell. Biol. 23, 1034–43.

29. Elkabets, M. et al. (2010). IL-1b regulates a novel myeloid-derived suppressor cell subset that impairs NK cell development and function. European Journal of Immunology, 40(12), 3347-57.

30. Dasgupta, S. et al. (2005). Inhibition of NK cell activity through TGF-1 by down-regulation of NKG2D in a murine model of head and neck cancer. Journal of Immunology, 175(8), 5541-5550.

31. Li, H. et al. (2008). Cancer-expanded myeloid-derived suppressor cells induce anergy of NK cells through membrane-bound TGF-1. Journal of Immunology, 182(1), 240-249.

32. Kusmartsev, S., & Gabrilovich, D. I. (2006). Effect of tumor-derived cytokines and growth factors on differentiation and immune suppressive features of myeloid cells in cancer. Cancer Metastasis Reviews, 25(3), 323–31.

33. Sawanobori, Y. et al. (2008). Chemokine-mediated rapid turnover of myeloid-derived suppressor cells in tumor-bearing mice. Blood, 111(12), 5457-66.

34. Cornish, C. J. et al. (1996). S100 protein CP-10 stimulates myeloid cell chemotaxis without activation. J. Cell. Physiol. 166, 427–37.

35. Zhao, X. et al. (2012). TNF signaling drives myeloid-derived suppressor cell accumulation. Journal of Clinical Investigation, 122(11), 4094-104.

36. Bunt, S. et al. (2007). Reduced inflammation in the tumor microenvironment delays the accumulation of myeloid-derived suppressor cells and limits tumor progression. Cancer Research, 67(20), 10019-26.

37. Ichikawa, M. et al. (2011). S100A8/A9 activate key genes and pathways in colon tumor progression. Molecular Cancer Research, 9(2), 133-48.

38. Lesokhin, A. et al. (2012). Monocytic CCR2+ myeloid-derived suppressor cells promote immune escape by limiting activated CD8 T-cell infiltration into the tumor microenvironment. Cancer Research, 72(4), 876-86.

39. Molon, B. et al. (2011). Chemokine nitration prevents intratumoral infiltration of antigen-specific T cells. Journal of Experimental Medicine, 208(10), 1949-62.

40. Dolcetti, L. et al. (2010). Hierarchy of immunosuppressive strength among myeloid-derived suppressor cell subsets is determined by GM-CSF. European Journal of Immunology, 40(1), 22–35.

41. Lechner, M. G. et al. (2011). Functional characterization of human Cd33+ and Cd11b+ myeloid-derived suppressor cell subsets induced from peripheral blood mononuclear cells co-cultured with a diverse set of human tumor cell lines. Journal of Translational Medicine, 9, 90.

42. Morales, J. et al. (2010). GM-CSF is one of the main breast tumor-derived soluble factors involved in the differentiation of CD11b-Gr1-bone marrow progenitor cells into myeloid-derived suppressor cells. Breast Cancer Research and Treatment, 123(1), 39-49.

43. Waight, J. et al. (2011). Tumor-derived G-CSF facilitates neoplastic growth through a granulocytic myeloid-derived suppressor cell-dependent mechanism. PLoS One, 6(11), e27690.

44. Chintakuntlawar, A. & Chodosh, J. (2010). Chemokine CXCL1/KC and its receptor CXCR2 are responsible for neutrophil chemotaxis in adenoviral keratitis. Journal of Interferon & Cytokine Research, 29(10), 657-66.

45. Numata, A. et al. (2005). Signal transducers and activators of transcription 3 augments the transcriptional activity of CCAAT/enhancer-binding protein alpha in granulocyte colony-stimulating factor signaling pathway.

46. Stanley, E. et al. (1997). Biology and action of colony-stimulating factor-1. Molecular Reproduction and Development, 46(1), 4-10.

47. Gabrilovich & Hurwitz. (2014). Tumor-Induced Immune Suppression: Mechanisms and Therapeutic Reversal.

48. Cheng, P. et al. (2008). Inhibition of dendritic cell differentiation and accumulation of myeloid-derived suppressor cells in cancer is regulated by S100A9 protein. Journal of Experimental Medicine. 205(10), 2235-49.

49. Eue, I. (2002). S100A8, S100A9 and the S100A8/A9 heterodimer complex specifically bind to human endothelial cells: identification and characterization of ligands for the myeloid-related proteins

S100A9 and S100A8/A9 on human dermal microvascular endothelial cell line-1 c. Int. Immunol. 14, 287–297.

50. Sinha, P. et al. (2008). Proinflammatory S100 proteins regulate the accumulation of myeloid-derived suppressor cells. J. Immunol. 181, 4666–75.

51. Ehrchen, J. M. et al. (2009). The endogenous Toll-like receptor 4 agonist S100A8/S100A9 (calprotectin) as innate amplifier of infection, autoimmunity, and cancer. J. Leukoc. Biol. 86, 557–566.

52. Kallberg, E. et al. (2012). S100A9 interaction with TLR4 promotes tumor growth. PLoS One, 7(3), e34207.

53. Liechtenstein, T. et al. (2014). A highly efficient tumor-infiltrating MDSC differentiation system for discovery of anti-neoplastic targets, which circumvents the need for tumor establishment in mice. Oncotarget, 5(17), 7843–57.

54. Priceman, S. J. et al. (2010). Targeting distinct tumor-infiltrating myeloid cells by inhibiting CSF-1 receptor: combating tumor evasion of antiangiogenic therapy. Blood, 115(7), 1461–71.

55. Solito, S. et al. (2011). A human promyelocytic-like population is responsible for the immune suppression mediated by myeloid-derived suppressor cells. Blood, 118(8), 2254–2265.

56. Youn, J.-I. et al. (2008). Subsets of myeloid-derived suppressor cells in tumor-bearing mice. Journal of Immunology (Baltimore, Md.: 1950), 181(8), 5791–802.

57. Leanderson, T. & Ivars, F. (2014). S100A9 and tumor growth. Oncoimmunology 1, 1404–1405.

58. Todorova, J. et al. (2012). High mobility group B1 protein interacts with its receptor RAGE in tumor cells but not in normal tissue. Oncology Letters 3:214-8.

59. Tsung, A. et al. (2007). HMGB1 release induced by liver ischemia involves Toll-like receptor 4-dependent reactive oxygen species production and calcium-mediated signaling. JEM 204(12), 2913-23.

60. Yu, M. et al (2006). HMGB1 signals through toll-like receptor (TLR) 4 and TLR2. Shock 26(2), 174-9.

61. Chen, B. et al. (2015). S100A9 induced inflammatory responses are mediated by distinct damage associated molecular patterns (DAMP) receptors in vitro and in vivo. PLoS One, 10(2), e0115828.

62. Taguchi, A. et al. (2000). Blockade of RAGE-amphoterin signalling suppresses tumour growth and metastases. Nature, 405(6784), 354-60.

63. Nasser, M. et al. (2015). RAGE mediates S100A7-induced breast cancer growth and metastasis by modulating the tumor microenvironment. Cancer Research, 75(6), 974-85.

64. Bao, J. et al. (2015). AGE/RAGE/Akt pathway contributes to prostate cancer cell proliferation by promoting Rb phosphorylation and degradation. Am J Cancer Res, 5(5), 1741-50.

65. Xie, J. et al. (2013). Cellular signaling of the receptor for advanced glycation end products (RAGE). Cellular Signaling 25(11), 2185-97.

66. Zeng, S. et al. (2012). Opposing roles of RAGE and MyD88 signaling in extensive liver resection. FASEB Journal, 26(2), 882-93.

67. Isaacs, J.T. et al. (2006). Identification of ABR-215050 as lead second generation quinoline-3-carboxamide anti-angiogenic agent for the treatment of prostate cancer. Prostate 66, 1768-78.

68. Bratt, O. et al. (2009). Open-label, clinical phase I studies of tasquinimod in patients with castration-resistant prostate cancer. Br J Cancer 101, 1233–40.

69. Raymond, E. et al. (2014). Mechanisms of action of tasquinimod on the tumor microenvironment. Cancer Chemotherapy and Pharmacology 73(1), 1-8.

70. Pili, R. et al. (2011). Phase II randomized double blind placebo-controlled study to determine the efficacy of tasquinimod in asymptomatic patients with metastatic castrate-resistant prostate cancer. J Clin Oncol 29, 4022-8.

71. Armstrong, A.J. et al. (2013). Long-term survival and biomarker correlates of tasquinimod efficacy in a multicenter randomized study of men with minimally symptomatic metastatic castration-resistant prostate cancer. Clin Cancer Res 19(24), 6891-901.

72. Sternberg, C.N. et al. (2016). A Phase 3, randomized, double-blind, placebo-controlled study of tasquinimod (TAQ) in men with metastatic castration-resistant prostate cancer (mCRPC), secondary endpoints. J Clin Oncol 34 (suppl2S; abstr 239).

73. Shen, L. et al. (2015). Tasquinimod modulates suppressive myeloid cells and enhances cancer immunotherapies in murine models. Cancer Immunol Res 3,136.

74. Kantoff, P.W. et al. (2010). Sipuleucel-T immunotherapy for castration-resistant prostate cancer. NEJM 363, 411-22.

75. Kwon, E.D. et al. (2014). Ipilimumab versus placebo after radiotherapy in patients with metastatic castration-resistant prostate cancer that had progressed after docetaxel chemotherapy (CA184-043): a multicentre, randomised, double-blind, phase 3 trial. Lancet Oncol 15, 700-12.

76. Topalian, S.L. et al. (2012). Safety, activity, and immune correlates of anti-PD-1 antibody in cancer. NEJM 366, 2443-54.

CHAPTER IV

STROMAL MODULATION OF BLADDER CANCER-INITIATING CELLS IN A SUBCUTANEOUS TUMOR MODEL

Elizabeth M. Peek, David R. Li, Hanwei Zhang, Hyun Pyo Kim, Baohui Zhang, Isla P. Garraway, and Arnold I. Chin (2012). Stromal modulation of bladder cancer-initiating cells in a subcutaneous tumor model. *American Journal of Cancer Research* 2(6): 745-751.

Am J Cancer Res 2012;2(6):745-751
www.ajcr.us /ISSN:2156-6976/ajcr0000156

Original Article

Stromal modulation of bladder cancer-initiating cells in a subcutaneous tumor model

Elizabeth M Peek[1,2,3*], David R Li[1,2*], Hanwei Zhang[1,2], Hyun Pyo Kim[1,2], Baohui Zhang[1], Isla P Garraway[1,4], Arnold I Chin[1,2,4]

[1]*UCLA Department of Urology, Los Angeles, California;* [2]*Eli & Edythe Broad Center of Regenerative Medicine & Stem Cell Research, UCLA, Los Angeles, California;* [3]*Molecular Biology Institute at UCLA, Los Angeles, California;* [4]*Jonsson Comprehensive Cancer Center, UCLA, Los Angeles, California.* **Elizabeth M Peek and David R Li contributed equally to this work.*

Received October 24, 2012; Accepted November 19, 2012; Epub November 20, 2012; Published November 30, 2012

Abstract: The development of new cancer therapeutics would benefit from incorporating efficient tumor models that mimic human disease. We have developed a subcutaneous bladder tumor regeneration system that recapitulates primary human bladder tumor architecture by recombining benign human fetal bladder stromal cells with SW780 bladder carcinoma cells. As a first step, SW780 cells were seeded in ultra low attachment cultures in order to select for sphere-forming cells, the putative cancer stem cell (CSC) phenotype. Spheroids were combined with primary human fetal stromal cells or vehicle control and injected subcutaneously with Matrigel into NSG mice. SW780 bladder tumors that formed in the presence of stroma showed accelerated growth, muscle invasion, epithelial to mesenchymal transition (EMT), decreased differentiation, and greater activation of growth pathways compared to tumors formed in the absence of fetal stroma. Tumors grown with stroma also demonstrated a greater similarity to typical malignant bladder architecture, including the formation of papillary structures. In an effort to determine if cancer cells from primary tumors could form similar structures *in vivo* using this recombinatorial approach, putative CSCs, sorted based on the $CD44^{+}CD49f^{+}$ antigenic profile, were collected and recombined with fetal bladder stromal cells and Matrigel prior to subcutaneous implantation. Retrieved grafts contained tumors that exhibited the same structure as the original primary human tumor. Primary bladder tumor regeneration using human fetal bladder stroma may help elucidate the influences of stroma on tumor growth and development, as well as provide an efficient and accessible system for therapeutic testing.

Keywords: Bladder cancer, cancer stem cell (CSC), subcutaneous tumor model, stroma, sphere

Introduction

Bladder cancer is the second most common genitourinary malignancy, with transitional cell carcinoma representing 90% of the cases [1]. Although BCG immunotherapy is effective in up to 75% of patients [2], treatments for bladder cancer have not significantly advanced in the last 30 years. Advances in therapeutics heavily depend on disease models. Subcutaneous models involving the direct injection of bladder tumor cells suffer from the inability of the tumor to form biologically relevant architecture [3]. Conversely, transgenic models [4-6] lack flexibility and require a longer incubation period. Here, we present a subcutaneous bladder tumor model with the ability to create papillary architecture, a model that may uniquely support the development of therapeutics.

The last few decades of cancer research have focused on the identification of oncogenes and tumor suppressors involved in the emergence of tumors. The effects of the surrounding stromal tissue have been largely ignored until recently. While the quantity of stroma does not appear to correspond with malignancy [7], signaling between tumor and stromal tissue is important for the formation of a complex tumor microenvironment and can influence the phenotype of the tumor [8].

Tumor cells are known to directly influence their surrounding stroma through invasion and angio-

genesis [9]. Growth factors such as VEGF, EGF, FGF, and TGF-β, as well as other cytokines, modulate the tumor microenvironment to promote a more permissive stroma and facilitate tumor growth [10, 11]. We postulated that tumor-adjacent stroma influences both the growth and differentiation of malignant cells.

Recent strides have been made in the identification and characterization of cancer stem cells (CSCs), the cancer-initiating cells within the tumor. By targeting CSCs specifically with new therapies, the risk of tumor recurrence is expected to be greatly reduced [12], justifying the inclusion of and focus on CSCs in any new tumor model. Breast cancer stem cells have been demonstrated to engage in stromal remodeling [13], but a more focused view of the interaction between CSCs and the surrounding stroma is necessary.

Stem cells have been shown to grow in three-dimensional spheroids in culture [14, 15]. This culture system has proven effective at growing cancer stem cells as well [16-18] and allowed for the culture of immortalized cell lines with cancer stem cell properties. For this study, we utilized the SW780 transitional bladder carcinoma cell line, which we found form spheres when grown in serum-free media. These cells exhibit the cancer-initiating cell phenotype, defined as $CD44^{+}CD49f^{+}$. When combined with fetal bladder mesenchymal cells in a novel subcutaneous model, the SW780 spheroids develop tumors that recapitulate primary tumor architecture. Therefore, the addition of stroma to a tumor model may promote both larger and less differentiated tumors.

Materials and methods

Cell lines and tumor samples

The SW780 immortalized human urinary bladder cell line (ATCC #CRL-2169) and the HT-1376 immortalized human urinary bladder cell line (ATCC #CRL-1472) were used in our *in vitro* and *in vivo* models. SW780 monolayer cells were maintained in RPMI 1640 with L-glutamine supplemented with 10% fetal bovine serum (FBS), and 1% penicillin/streptomycin. Sphere cultures for staining and implantation were maintained in floating culture as previously described [19, 20] on uncoated plates in RPMI 1640 with L-glutamine supplemented with 2% B-27 serum-free, 1% Pen/Strep, 2 μg/ml heparin, 20 ng/ml FGF, and 20 ng/ml EGF. When passaged, spheres were gravity-separated for 15-20 minutes before fresh media was added. Fresh bladder tumor samples were surgically resected, immediately suspended in PBS or DMEM, and maintained at 4°C until processed. Tumors were digested in 0.25% collagenase IV-DMEM for 4 hours and plated as above. Experiments were performed under IRB approved protocol #11-001363.

Acquisition, isolation, and culture of fetal bladder stroma

Human fetal bladder tissue was acquired from 16-17 week gestation specimens in accordance with federal and state guidelines. Fetal bladder, prostate, and urethra were removed *en bloc*. A portion of the specimen was fixed in formalin and paraffin-embedded to confirm correct anatomic localization. The remainder of the tissue was mechanically and enzymatically digested as previously described [21]. Dissociated bladder cell suspensions were sequentially filtered through 100-micron and 40-micron filters, and then passed through a 23-gauge needle. Cells were counted with a hemocytometer and resuspended in RPMI supplemented with 10% FBS and 1% Pen/Strep, and Methyltrienolone R1881 (Sigma) for culture in vitro. After 3 passages, cells were cryopreserved and thawed/expanded as needed for use in recombination assays.

Sphere formation efficiency assay

To quantify the percentage of cells that produce spheres, we adapted a previously described MatriGel culture system [22]. SW780 monolayer cells using 0.05% Trypsin-EDTA incubated at 37°C for 5-6 minutes before quenching with RPMI 1640 with L-glutamine supplemented with 10% FBS. Media was replaced with sphere media and cells were resuspended at 2.5×10^4 cells/mL. 40 μL of cell mixture was then mixed with 60 μL ice-cold MatriGel, and well-mixed. 100 μL of MatriGel mixture was then pipetted around the rim of a chilled 12-well plate. Plate was then swirled to evenly distribute the mixture around the edges and incubated at 37°C for 30 minutes to allow the MatriGel to set. 1 mL of sphere media was then gently added to the center of each well. 500 μL of media was aspirated and replaced with fresh

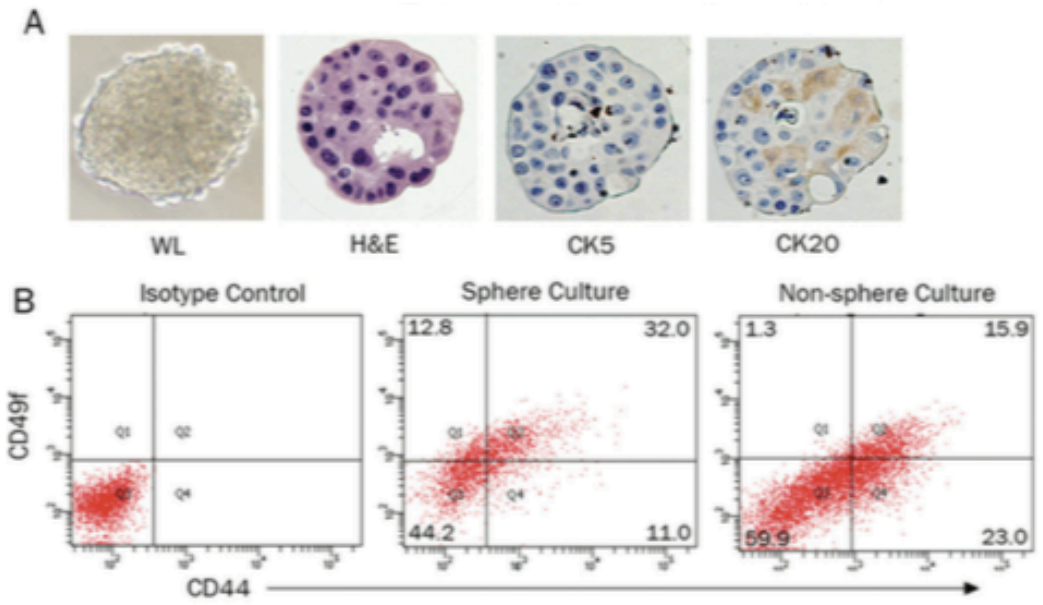

Figure 1. Spherical cultures express both luminal and basal markers. SW780 spheres from serum-free culture were fixed and bisected for IHC (A). Sections were stained with basal (CK5) and luminal (CK20) cell markers, as well as H&E. Representative views are shown, and images were captured at 400X magnification. SW780 spheres were dissociated and compared to SW780 cells grown in monolayer by flow cytometry (B). Cells were stained with anti-CD44-PE and anti-CD49f-FITC antibodies or isotype controls.

sphere media every three days. Spheres were counted at 7 days and 14 days.

Immunohistochemistry

Paraffin-embedded sections were stained with hematoxylin and eosin (H&E) for histological analysis. Immunohistochemistry was performed using antibodies against CK5/6 (Invitrogen), CK20 (DAKO), CD44 (eBioscience), EGFR (BIOCARE), pS6 (Cell Signaling), E-cadherin (BD Biosciences), and N-cadherin (ZYMED). Slides were probed with biotinylated goat anti-rabbit or goat anti-mouse secondary antibodies and with streptavidin conjugated to HRP. Photographs were taken using an Axio Imager 2 (Zeiss).

Flow cytometry

Cell surface marker analysis was performed by flow cytometry using the LSR II (BD Biosciences). Cells were incubated with antibodies against CD44 conjugated to PE (BD Biosciences) and against CD49f conjugated to FITC (BD Biosciences). Mouse IgG antibodies conjugated with each fluorochrome were used as isotype controls.

Subcutaneous tumor model

Non-obese diabetic severe combined immunodeficient gamma (NSG) mice between 6 and 8 weeks old were used for *in vivo* subcutaneous tumor growth experiments. Approximately 10^5 monolayer cells were suspended in 0.1 mL of media for inoculation. Cultured SW780 spheres and patient-derived spheres were prepared for xenograft implantation by first gravity-separating spheres for 15-20 minutes. Approximately 500 spheres were suspended in 0.1 mL of media for inoculation, and an equal quantity of Matrigel (BD Biosciences) was added. All mice were inoculated subcutaneously in the lower flank. Mice were monitored daily, and tumor growth was observed. Mice were sacrificed when tumor size reached 1 cm.

Results

Spherical cultures exhibit a cancer stem cell phenotype

To establish the validity of spheres as a cancer stem cell culture method, SW780 cells were grown in a Matrigel suspension and allowed to form spheres. The efficiency of sphere forma-

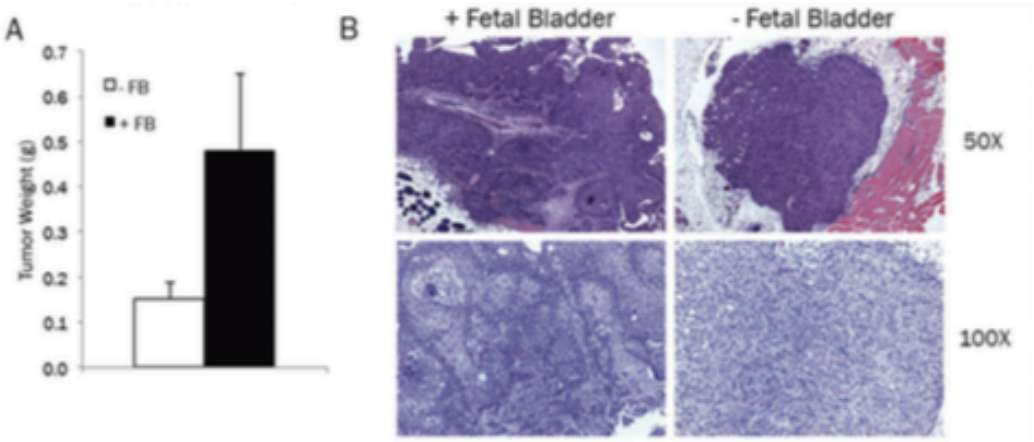

Figure 2. Stromal influence promotes increased tumor growth and invasiveness. NSG mice were implanted subcutaneously with SW780 spheres with and without the presence of fetal bladder stroma. After 4 weeks, tumors were harvested and weighed (A) (n=7 mice/group, $P < 0.001$). Nearby satellite tumors were also included in this weight. Error bars indicate standard deviation from the mean. Tumor sections were stained with H&E for histology. Tissue architecture (B) was compared in representative images captured at 50-100X magnification. Evidence of muscle invasion (C) was noted in images captured at 400X magnification.

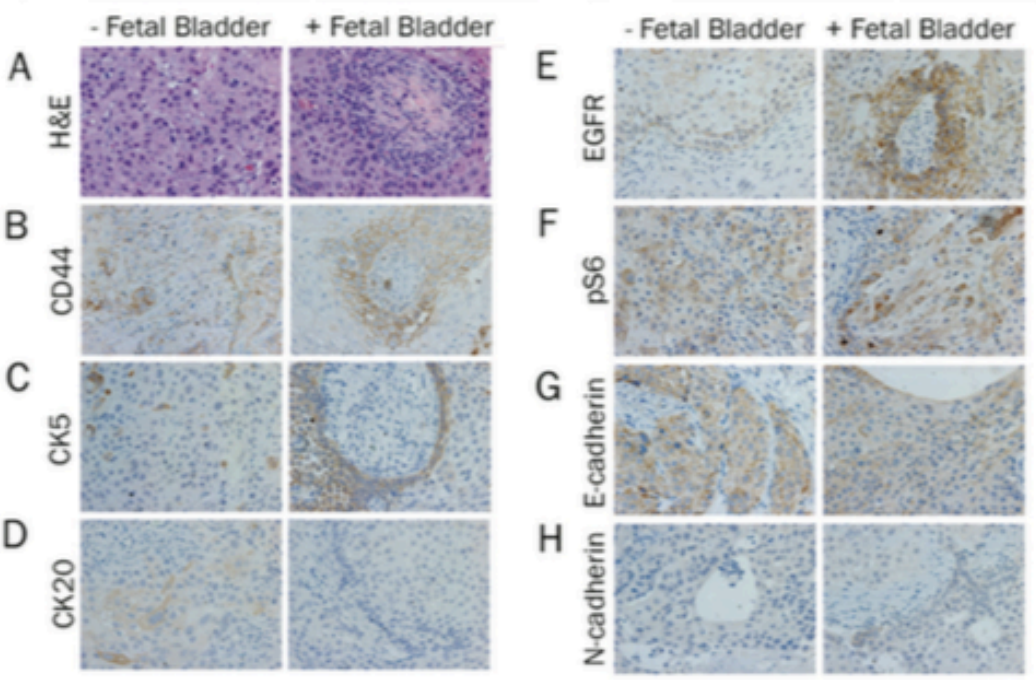

Figure 3. Tumors formed in the presence of stroma are less differentiated and functionally distinct. NSG mice were implanted subcutaneously with SW780 spheres with and without the presence of fetal bladder. After 4 weeks, tumors were harvested and embedded in paraffin for IHC. Slides were stained with H&E (A) for histology, as well as differentiation markers CD44, CK5, and CK20 (B-D). Tumor sections were also stained for functional markers: EGFR, pS6, E-cadherin, and N-cadherin (E-H). Representative views are shown, and images were captured at 400X magnification.

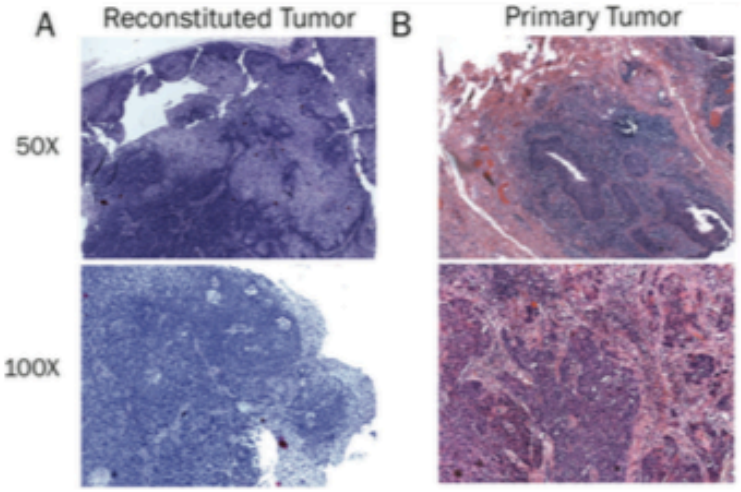

Figure 4. Subcutaneous model using human cells recapitulates both murine and primary tumor architecture. Primary human bladder tumor was sorted to isolate the $CD44^{+}CD49f^{+}$ population. Cells were combined with human fetal bladder and injected subcutaneously into NSG mice. Tumor sections were stained with H&E for histology (A). Pathology slides from the original human bladder tumor were stained with H&E for histology (B). Representative views are shown, captured at 50X and 100X magnification.

tion was measured at 2-4% (data not shown). Spheres from floating culture were fixed and sectioned for staining with basal and luminal markers to determine the cell phenotype (**Figure 1A**). The spheres showed expression of CK20, a luminal marker, towards the center and expression of the basal marker CK5 in the periphery. SW780 spheres were also shown to have a more undifferentiated phenotype than monolayer cells by measuring cell surface levels of the stem cell markers CD44 and CD49f (**Figure 1B**).

Stromal influence on tumor growth and function

To test the influence of stromal cells on tumors in an *in vivo* model, NSG mice were challenged subcutaneously with spheres with or without human fetal bladder stroma. Tumors were harvested, weighed, and stained. Supporting the assertion that the influence of stroma creates a more aggressive tumor, mice challenged with spheres and fetal bladder mesenchyme developed larger tumors than mice challenged with spheres alone (**Figure 2A**). The tumors with stroma present also showed evidence of invasion into the muscle (**Figure 2C**) and surrounding satellite tumors (data not shown), which were not observed in tumors formed without the influence of stroma. Histological analysis (**Figure 2B, 3A**) showed that tumors formed in the presence of stroma grew papillary architecture, creating a malignant bladder-like structure in the subcutaneous compartment.

The tumors that included fetal bladder also showed higher expression of basal markers CD44 (**Figure 3B**) and CK5 (**Figure 3C**), while conversely, the expression of the luminal marker CK20 is decreased (**Figure 3D**). This indicates the presence of less differentiated malignant cells, which are associated with more advanced tumors [23].

The stromal-influenced tumors expressed more EGFR (**Figure 3E**) and pS6 ribosomal protein (**Figure 3F**), indicating an increase in growth factor signaling. A decrease in E-cadherin (**Figure 3G**), suggested an early stage of epithelial-to-mesenchymal transition (EMT) although we did not observe a corresponding increase in N-cadherin (**Figure 3H**). Both early EMT and activation of growth pathways would be expected in a more advanced tumor.

Primary human bladder tumor was also used to validate this model. A primary tumor was sorted to isolate $CD44^{+}CD49f^{+}$ cells previously described as the cancer stem cell population [24]. NSG mice were challenged with sorted cells combined with fetal bladder. The resulting tumor (**Figure 4A**) not only formed papillary architecture comparative to the murine model (**Figure 2B**), but the architecture recapitulated the structure of the original primary tumor (**Figure 4B**).

Discussion

With this work, we suggest a model for bladder cancer that creates a subcutaneous tumor that

exhibits typical human bladder tumor architecture. It maintains the benefits of subcutaneous implantation while gaining more physiological relevance, allowing comparisons to orthotopic or induced models.

The use of spheres to seed the tumor is validated by their demonstrated expression of the cancer stem cell (CSC) phenotype and their ability to express markers of both basal and luminal cells (**Figure 1**). As CSCs have the ability to differentiate into the heterogeneous malignant cell types found in a tumor [25], they are ideal for implantation. Their use isolates the model from extraneous factors and increases tumor-forming efficiency, as seen in breast cancer with $CD44^{+}CD49^{hi}$ cells [24].

Within the framework of this model, we can also explore the stromal contribution to tumor growth and progression. Fetal bladder induced significantly accelerated tumor growth (**Figure 2A**). The tumors were also less differentiated, showed signs of EMT, and began invading the surrounding muscle (**Figure 2C, 3**), indicating a more advanced disease. The effects appear to be mediated, at least partially, by stromal activation of growth pathways (**Figure 3E, 3F**), as has been previously observed [26, 27].

For this tumor model to be physiologically relevant, it should mimic typical bladder tissue architecture. With the addition of the stromal component, the tumors effectively recreated malignant bladder tissue (**Figure 2B**). Similar effects were seen when primary human CSCs were used in place of a cell line (**Figure 4A**). Most significantly, the model recapitulated the architecture seen in the primary tumor (**Figure 4B**).

This novel model of subcutaneous bladder cancer presents a unique opportunity to analyze the influence of the surrounding stroma to tumor growth. The elucidation of the role of stroma represents a significant area of research interest, and a subcutaneous model is particularly well suited to disentangle the contribution of malignant cells and stroma to the tumor microenvironment.

Acknowledgments

The authors thank the UCLA Broad Stem Cell Research Center Flow Cytometry Core Resource and the UCLA Translational Pathology Core Laboratory for providing core support. Funding for this research was provided by American Association of Cancer Research 10-20-14, the Prostate Cancer Foundation, Department of Defense PC073073, and the Jean Perkins Foundation.

Address correspondence to: Dr. Arnold I Chin, Department of Urology, University of California at Los Angeles, 10833 Le Conte Avenue, P.O. Box 951738, Los Angeles, CA 90095-1738. Phone: 310-206-4022; Fax: 310-206-5343; E-mail: aichin@ucla.edu

References

[1] Kim B, Choi HJ, Kim MH and Cho KS. Recurrence patterns of bladder transitional cell carcinoma after radical cystectomy. Acta Radiol 2012; 53: 943-949.

[2] Alexandroff AB, Jackson AM, O'Donnell MA and James K. BCG immunotherapy of bladder cancer: 20 years on. Lancet 1999; 353: 1689-1694.

[3] Chan E, Patel A, Heston W and Larchian W. Mouse orthotopic models for bladder cancer research. BJU Int 2009; 104: 1286-1291.

[4] Zhang ZT, Pak J, Shapiro E, Sun TT and Wu XR. Urothelium-specific expression of an oncogene in transgenic mice induced the formation of carcinoma in situ and invasive transitional cell carcinoma. Cancer Res 1999; 59: 3512-3517.

[5] Grippo PJ and Sandgren EP. Highly invasive transitional cell carcinoma of the bladder in a simian virus 40 T-antigen transgenic mouse model. Am J Pathol 2000; 157: 805-813.

[6] Mo L, Zheng X, Huang HY, Shapiro E, Lepor H, Cordon-Cardo C, Sun TT and Wu XR. Hyperactivation of Ha-ras oncogene, but not Ink4a/Arf deficiency, triggers bladder tumorigenesis. J Clin Invest 2007; 117: 314-325.

[7] Dvorak HF, Senger DR and Dvorak AM. Fibrin as a component of the tumor stroma: origins and biological significance. Cancer Metastasis Rev 1983; 2: 41-73.

[8] Kuperwasser C, Chavarria T, Wu M, Magrane G, Gray JW, Carey L, Richardson A and Weinberg RA. Reconstruction of functionally normal and malignant human breast tissues in mice. Proc Natl Acad Sci U S A 2004; 101: 4966-4971.

[9] Gururajan M, Posadas EM and Chung LW. Future perspectives of prostate cancer therapy. Transl Androl Urol 2012; 1: 19-32.

[10] Mueller MM and Fusenig NE. Friends or foes - bipolar effects of the tumour stroma in cancer. Nat Rev Cancer 2004; 4: 839-849.

[11] Rowley D and Barron DA. The reactive stroma microenvironment and prostate cancer progression. Endocr Relat Cancer 2012 Oct 30; 19: R187-204. doi: 10.1530/ERC-12-0085. Print 2012.

[12] Basile KJ and Aplin AE. Resistance to chemotherapy: short-term drug tolerance and stem cell-like subpopulations. Adv Pharmacol 2012; 65: 315-334.

[13] Parashurama N, Lobo NA, Ito K, Mosley AR, Habte FG, Zabala M, Smith BR, Lam J, Weissman IL, Clarke MF and Gambhir SS. Remodeling of endogenous mammary epithelium by breast cancer stem cells. Stem Cells 2012; 30: 2114-2127.

[14] Reynolds BA and Weiss S. Clonal and population analyses demonstrate that an EGF-responsive mammalian embryonic CNS precursor is a stem cell. Dev Biol 1996; 175: 1-13.

[15] Dontu G, Abdallah WM, Foley JM, Jackson KW, Clarke MF, Kawamura MJ and Wicha MS. In vitro propagation and transcriptional profiling of human mammary stem/progenitor cells. Genes Dev 2003; 17: 1253-1270.

[16] Ponti D, Costa A, Zaffaroni N, Pratesi G, Petrangolini G, Coradini D, Pilotti S, Pierotti MA and Daidone MG. Isolation and in vitro propagation of tumorigenic breast cancer cells with stem/progenitor cell properties. Cancer Res 2005; 65: 5506-5511.

[17] Lang SH, Sharrard RM, Stark M, Villette JM and Maitland NJ. Prostate epithelial cell lines form spheroids with evidence of glandular differentiation in three-dimensional Matrigel cultures. Br J Cancer 2001; 85: 590-599.

[18] Fang D, Nguyen TK, Leishear K, Finko R, Kulp AN, Hotz S, Van Belle PA, Xu X, Elder DE and Herlyn M. A tumorigenic subpopulation with stem cell properties in melanomas. Cancer Res 2005; 65: 9328-9337.

[19] Hemmati HD, Nakano I, Lazareff JA, Masterman-Smith M, Geschwind DH, Bronner-Fraser M and Kornblum HI. Cancerous stem cells can arise from pediatric brain tumors. Proc Natl Acad Sci USA 2003; 100: 15178-15183.

[20] Garraway IP, Sun W, Tran CP, Perner S, Zhang B, Goldstein AS, Hahm SA, Haider M, Head CS, Reiter RE, Rubin MA and Witte ON. Human prostate sphere-forming cells represent a subset of basal epithelial cells capable of glandular regeneration in vivo. Prostate 2010; 70: 491-501.

[21] Jiao J, Hindoyan A, Wang S, Tran LM, Goldstein AS, Lawson D, Chen D, Li Y, Guo C, Zhang B, Fazli L, Gleave M, Witte ON, Garraway IP and Wu H. Identification of CD166 as a surface marker for enriching prostate stem/progenitor and cancer initiating cells. PLoS One 2012; 7: e42564.

[22] Guo C, Zhang B and Garraway IP. Isolation and characterization of human prostate stem/progenitor cells. Methods Mol Biol 2012; 879: 315-326.

[23] Mete O and Asa SL. Pathological definition and clinical significance of vascular invasion in thyroid carcinomas of follicular epithelial derivation. Mod Pathol 2011; 24: 1545-1552.

[24] Meyer MJ, Fleming JM, Lin AF, Hussnain SA, Ginsburg E and Vonderhaar BK. CD44posCD49fhiCD133/2hi defisnes xenograft-initiating cells in estrogen receptor-negative breast cancer. Cancer Res 2010; 70: 4624-4633.

[25] van der Horst G, Bos L and van der Pluijm G. Epithelial plasticity, cancer stem cells, and the tumor-supportive stroma in bladder carcinoma. Mol Cancer Res 2012; 10: 995-1009.

[26] Korc M. Pancreatic cancer-associated stroma production. Am J Surg 2007; 194: S84-86.

[27] Hadari Y and Schlessinger J. FGFR3-targeted mAb therapy for bladder cancer and multiple myeloma. J Clin Invest 2009; 119: 1077-1079.

CHAPTER V

SYNERGY OF HISTONE-DEACETYLASE INHIBITOR AR-42 WITH CISPLATIN IN BLADDER CANCER

David R. Li, Hanwei Zhang, **Elizabeth M. Peek**, Wang Song, Lin Du, Gang Li, Arnold I. Chin (2015). Synergy of histone-deacetylase inhibitor AR-42 with cisplatin in bladder cancer. *Journal of Urology* 194(2):547-55.

Synergy of Histone-Deacetylase Inhibitor AR-42 with Cisplatin in Bladder Cancer

David R. Li, Hanwei Zhang, Elizabeth Peek, Song Wang, Lin Du, Gang Li and Arnold I. Chin*

From the Department of Urology (DRL, HZ, AIC), Eli and Edythe Broad Stem Cell Research Center (HZ, AIC), Molecular Biology Institute (EP, AIC), Department of Biostatistics (LD, GL) and Jonsson Comprehensive Cancer Center (GL, AIC), University of California-Los Angeles, Los Angeles, California, and Urology Center, First Hospital of Jilin University (SW), Changchun, People's Republic of China

Purpose: Cisplatin based chemotherapy regimens form the basis of systemic bladder cancer treatment, although they show limited response rates and efficacy. Recent molecular analysis of bladder cancer revealed a high incidence of mutations in chromatin regulatory genes, suggesting a therapeutic avenue for histone deacetylase inhibitors. We investigated the ability of the novel histone deacetylase inhibitor AR-42 to synergize with cisplatin in preclinical models of bladder cancer.

Materials and Methods: We assessed the ability of the pan-histone deacetylase inhibitor AR-42 with and without cisplatin to destroy bladder cancer cells by survival and apoptosis assays in vitro, and by growth and differentiation in an in vivo xenograft model. We also assessed the response to the bladder cancer stem cell population by examining the effect of AR-42 on the $CD44^{+}CD49f^{+}$ population with and without cisplatin. Synergy was calculated using combination indexes.

Results: The AR-42 and cisplatin combination synergistically destroyed bladder cancer cells via apoptosis and it influenced tumor growth and differentiation in vivo. When tested in the $CD44^{+}CD49f^{+}$ bladder cancer stem cell population, AR-42 showed greater efficacy with and without cisplatin.

Conclusions: AR-42 may be an attractive novel histone deacetylase inhibitor with activity against bladder cancer. Its efficacy in bladder cancer stem cells and synergy with cisplatin warrant further clinical investigation. Our in vitro and animal model studies provide preclinical evidence that AR-42 may be administered in conjunction with cisplatin based chemotherapy to improve the treatment of bladder cancer in patients.

Key Words: urinary bladder neoplasms, histone deacetylase inhibitors, cisplatin, apoptosis, chromatin

Abbreviations and Acronyms

CI = combination index
CK = cytokeratin
HDAC = histone deacetylase
IC_{50} = percent of maximal inhibitory concentration
NaB = sodium butyrate
NSG = Nod-*scid* IL-2Rgamma^{null}
PI = propidium iodide
TSA = trichostatin A
VA = valproic acid

Accepted for publication February 23, 2015.
Study received animal care and use committee approval.
Supported by the Broad Stem Cell Research Center Scholars in Translational Medicine, Perkins Foundation and STOP Cancer.
* Correspondence: Department of Urology, University of California-Los Angeles, 10833 Le Conte Ave., P.O. Box 951738, Los Angeles, California 90095 (telephone: 310-206-4022; FAX: 310-206-5343; e-mail: aichin@ucla.edu).

BLADDER cancer affects more than 54,000 men and 17,000 women in the United States annually, making it the fourth most common cancer in men and the ninth most common cancer in women.[1] Primary chemotherapy is the mainstay of locally advanced and metastatic disease while neoadjuvant chemotherapy is indicated for muscle invasive urothelial carcinoma before radical cystectomy. Since its approval by the FDA (Food and Drug Administration) in 1978, platinum containing chemotherapeutic cis-diamminedichloroplatinum, or cisplatin, has formed the backbone of primary bladder cancer regimens in combination with methotrexate,

0022-5347/15/1942-0547/0
THE JOURNAL OF UROLOGY®

http://dx.doi.org/10.1016/j.juro.2015.02.2918
Vol. 194, 547-555, August 2015
Printed in U.S.A.

vinblastine and doxorubicin or gemcitabine, in part through its ability to induce apoptosis.[2] Limitations of cisplatin based therapy for bladder cancer reflect its limited response rate (40% to 50%) as well as its dose limiting nephrotoxicity and neurotoxicity.[3]

Histone acetylation and deacetylation have a critical role in chromatin formation and gene regulation. Histone acetylation relaxes the chromatin structure into transcriptionally active euchromatin while the opposing effect occurs upon deacetylation. HDAC inhibitors represent a class of compounds that disrupts the function of histone deacetylases, of which there are 4 classes and more than 11 subtypes. HDAC inhibitor function leads to the hyperacetylation of histone as well as nonhistone proteins.[4] Recently interest has focused on the antitumor ability of HDAC inhibitors to interfere with cancer cell proliferation through mechanisms such as cell cycle arrest, apoptosis and the induction of cellular differentiation.[5] Currently the HDAC inhibitors vorinostat and romidepsin are approved as treatment of cutaneous T-cell lymphoma.[6,7]

Bladder cancer is an attractive disease for the use of HDAC inhibitors. Chromatin structure modulation may be a critical step in bladder cancer progression because increased expression of HDAC-1 and 2 is linked to high grade noninvasive urothelial carcinoma. Data from TCGA (The Cancer Genome Atlas) revealed that 76% of the bladder tumors analyzed had an inactivating mutation in at least 1 chromatin regulatory gene.[8,9] In previous studies using VA, TSA and belinostat the bladder cancer cell lines were inhibited through cell cycle blockade, induction of apoptosis and reduced tumor growth in in vivo bladder cancer models.[10–13] This suggests the possibility that HDAC inhibitors may synergize with the apoptotic effects of cisplatin and potentially increase clinical efficacy and the overall response rate.

AR-42 is a class I (HDAC 1, 2, 3 and 8) and class IIb (HDAC 6 and 10) HDAC inhibitor with activity against multiple cancer types, including chronic lymphocytic and acute myeloid leukemia, B-cell lymphoma, prostate and ovarian cancer, and human glioma cells.[14] In fact AR-42 has the distinct ability to target leukemic stem cells while preserving normal hematopoietic stem and progenitor cells. Although it is a phenylbutyrate derivative, AR-42 shows increased activity even at sub μM concentrations.[15] AR-42 is currently being evaluated in phase I/IIa clinical trials for hematological malignancies (unpublished data).

We provide essential preclinical data on the potential efficacy of AR-42 in bladder cancer. We hypothesized that the therapeutic ability of AR-42 against bladder cancer would be enhanced by synergy with cisplatin in vitro and in vivo.

MATERIALS AND METHODS

Bladder Cancer Cell Lines

The 2 human urothelial carcinoma cell lines SW780 (CRL-2169) and HT1376 (CRL-1472, ATCC®) were maintained as monolayer cultures in RPMI 1640 with L-glutamine supplemented with 10% fetal bovine serum and 1% penicillin/streptomycin.

Flow Cytometry

Cells stained with anti-CD44 (559942/550989), anti-CD49f (555735) and isotype controls were analyzed on the LSR II flow cytometer (BD™). $CD44^{+}CD49f^{+}$ cells were sorted using the FACSAria™ cell sorter.

In Vitro Drug Viability Assay

SW780 and HT1376 cells cultured in 96-well plates at 5,000 per well were treated in triplicate for 48 hours with a titration of cisplatin and 1 of 4 HDAC inhibitors, including AR-42, NaB (303410-5G), VA (P4543-10G, Sigma-Aldrich®) and TSA (9950S, Cell Signaling Technology®). At 48 hours MTT was added. The preparations were incubated for 2 hours at 37C, dissolved in dimethyl sulfoxide and quantitated against a standard curve using an Infinite® M1000 Pro spectrophotometer.

On combination drug assays cisplatin was titrated with individual HDAC inhibitors at a constant ratio based on the IC_{50} concentration of each drug. The ratio of cisplatin to the HDAC inhibitors AR-42, NaB, VA and TSA was 5:1, 1:75, 1:75 and 80:1, respectively.

Time course combinations were performed using certain treatment regimens during 48 hours, including 1) cisplatin and AR-42 for 0 to 24 hours, 2) cisplatin and AR-42 for 24 to 48 hours, 3) cisplatin for 0 to 24 hours and AR-42 for 24 to 48 hours, and 4) AR-42 for 0 to 24 hours and cisplatin for 24 to 48 hours. All cells were washed and plated with fresh treatments or medium at the 24-hour mark.

In Vivo Tumor Model and Therapy

Total SW780 cells or a sorted $CD44^{+}CD49f^{+}$ fraction of SW780 cells were combined with human fetal bladder mesenchyma in a 1:10 ratio, mixed with Matrigel™ in a 1:1 ratio and subcutaneously implanted in NSG mice.[16] At the onset of a palpable tumor on day 15 treatments were started in 1 of 4 groups, including 1) vehicle control, 2) 50 mg/kg AR-42 intraperitoneally 3 times per week, 3) 1.5 mg/kg cisplatin intraperitoneally weekly and 4) combined AR-42 and cisplatin. Tumor size was measured and tumor volume was estimated by multiplying width, length and depth by a factor of 0.4. The mice were sacrificed and the tumors were weighed and fixed in formalin.

Histology and Immunohistochemistry

Representative formalin fixed, paraffin embedded tissues were sectioned at 0.4 μm. Histology was assessed after hematoxylin and eosin staining. Immunohistochemistry was performed on sections that were deparaffinized and rehydrated, and then blocked for 1 hour in 5% bovine serum albumin and 5% goat serum in phosphate buffered saline. Sections were stained with CK5 at 1:5,000 (ab53121, Abcam®) and CK20 at 1:300 (M7019, Dako™) followed by incubation with biotinylated goat anti-rabbit or goat anti-mouse secondary antibodies at 1:750 using

an avidin-biotin complex kit (Vector Laboratories, Burlingame, California). Sections were developed with streptavidin conjugated horseradish peroxidase and substrate, counterstained with hematoxylin, and dehydrated and mounted with Cytoseal™ 60. Images were assessed by light microscopy using an Axio Imager 2 (Carl Zeiss Microscopy, Thornwood, New York) and quantitated by the percent stained in deciles per high power field (400×).

Apoptosis Assay

To assay the apoptosis rate SW780 monolayer cells were treated with IC_{75} doses of 20 μM cisplatin and/or 5 μM AR-42 for 24 hours. Apoptosis was assessed by flow cytometry on the LSR II device using annexin V and PI staining with the Apoptosis Assay Kit (Biotium, Hayward, California) according to manufacturer instructions. We identified live cells by negative staining for annexin V and PI, early apoptotic cells by positive staining for annexin V but negative staining for PI, and late apoptotic cells by positive staining for annexin V and PI.

Statistics

One-way and 2-way ANOVA, and post hoc analysis were performed for group comparisons. Log transformations were done for tumor volume to improve normality. IC_{50} values of single drug treatments were calculated using CalcuSyn 2.1 (Biosoft®). The CI was calculated for each combination drug treatment at IC_{50}, IC_{75} and IC_{90} points using CalcuSyn, version 2.1. CI less than 1.0 indicates synergistic interaction between drugs, values around 1.0 indicate an additive relationship and values greater than 1.0 reflect an antagonistic interaction.

RESULTS

Bladder Cancer Cell Susceptibility to HDAC Inhibition

To test SW780 and HT1376 cell sensitivity to cisplatin and HDAC inhibition the cells were treated with a titration of cisplatin or one of the 4 HDAC inhibitors AR-42, NaB, VA or TSA. Cells were assessed for viability and IC_{50} was calculated (fig. 1, *A*). SW780 cells appeared more sensitive to all agents than HT1376 cells, which could have been due in part to the source of the cell lines. SW780 cells were derived from a low grade tumor while HT1376 cells were derived from a high grade tumor, potentially explaining the decreased drug sensitivity. The IC_{50} concentrations of NaB and VA showed significantly greater minimum effective doses than those of AR-42 and TSA, potentially limiting efficacy in vivo (fig. 1, *B*).

Synergy between Cisplatin and HDAC Inhibitors

We next investigated combination treatment with cisplatin and each of the HDAC inhibitors to explore synergistic effects on cell viability (fig. 2, *A*). Cisplatin plus AR-42 and cisplatin plus NaB showed synergy at IC_{50} and IC_{90} dose levels as determined by combination index calculations and visualized in isobolograms (fig. 2, *B*). Cisplatin plus VA and cisplatin plus TSA showed synergy at IC_{50} but not at IC_{90} doses (see table).

A

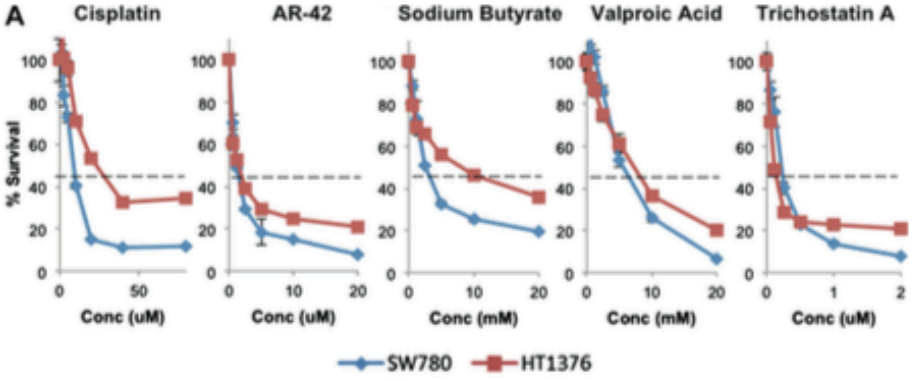

B

Drug	SW780 IC50	HT1376 IC50
Cisplatin	8.5 uM	30.5 uM
AR-42	1.4 uM	1.4 uM
Sodium Butyrate	3.8 mM	8.5 mM
Valproic Acid	6.0 mM	7.4 mM
Trichostatin A	0.25 uM	0.12 uM

Figure 1. Viability according to MTT incorporation in SW780 and HT1376 cells treated for 48 hours with titrated doses of single cisplatin and HDAC inhibitor drugs (*A*). Dashed horizontal lines indicate IC_{50} (*Conc*). Data represent mean of triplicate preparations and represent 3 independent experiments. Bars indicate SD. Calculated IC_{50} concentrations (*B*). *uM*, μM.

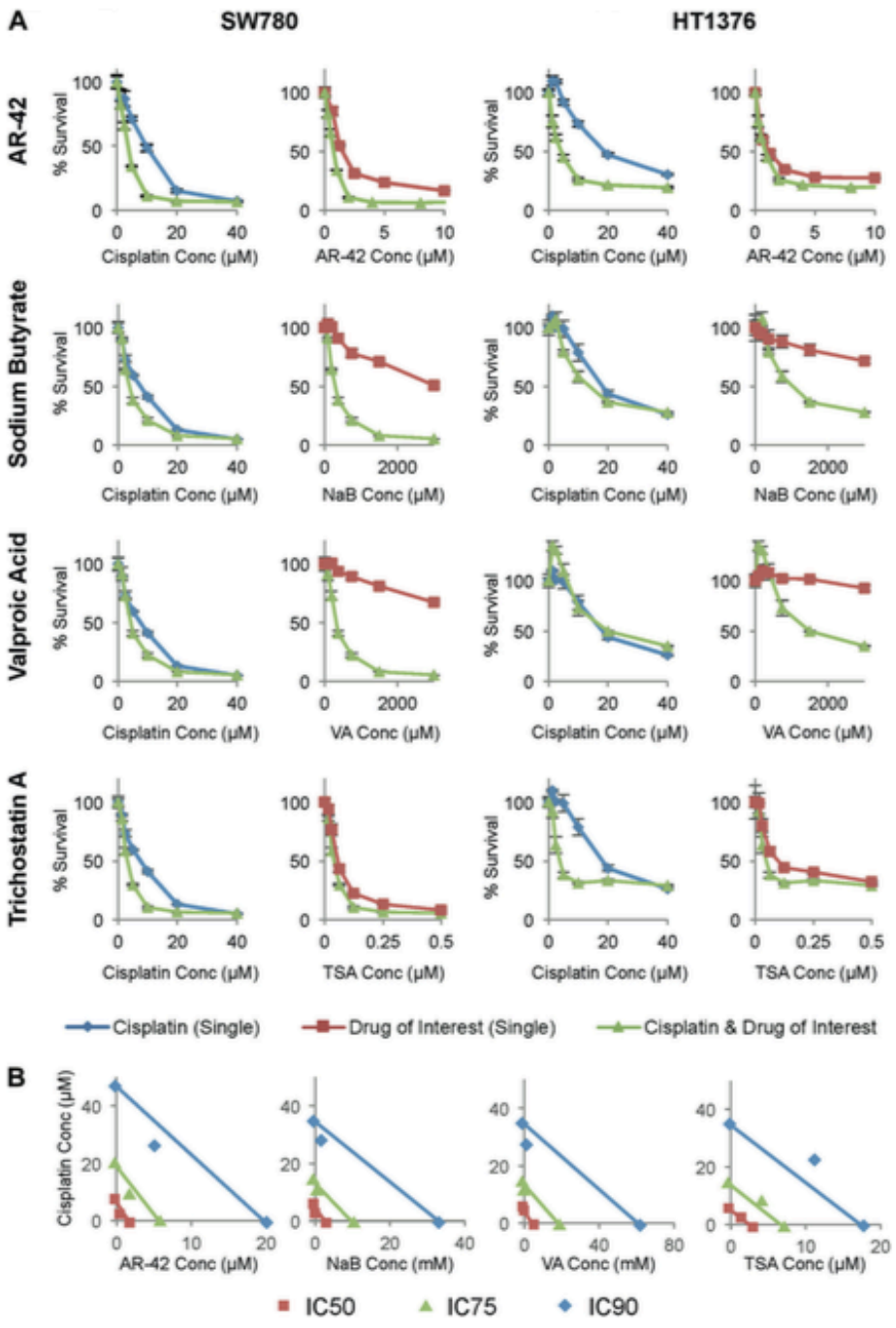

Figure 2. Cisplatin synergized with HDAC inhibitors, including novel broad-spectrum classes I and 2b HDAC inhibitor AR-42. Cisplatin was combined with AR-42, NaB, VA and TSA at ratio of 5:1, 1:75, 1:75 and 80:1, respectively, as determined by each IC_{50} (*Conc*) (*A*). Viability was measured by MTT incorporation in SW780 and HT1376 cells treated for 48 hours. Green curves represent combined therapies. Blue curves represent cisplatin alone. Red curves indicate HDAC inhibitor alone. Data represent mean of triplicate presentations and represent 3 independent experiments. Bars indicate SD. Isobolograms created with CalcuSyn show relationship of cisplatin and each HDAC inhibitor in SW780 cells (*B*). Combination data points on diagonal, lower left and upper right indicate additive, synergistic and antagonistic effects, respectively.

CI of cisplatin plus AR-42, NaB, VA or TSA in SW780 and HT1376 cells by IC

Cisplatin Combination (dose)	SW780 CI*	HT1376 CI*
AR-42:		
IC_{50}	0.581	0.376
IC_{90}	0.419	0.709
NaB:		
IC_{50}	0.229	0.871
IC_{90}	0.629	0.988
VA:		
IC_{50}	0.728	0.981
IC_{90}	1.021	5.566
TSA:		
IC_{50}	0.685	0.764
IC_{90}	1.431	3.957

*Value less than 1 indicates synergy.

Cancer Stem Cell Population More Sensitive to Combined Cisplatin and AR-42

Cancer stem cells are more chemotherapy resistant.[17] Because AR-42 had efficacy in leukemic stem cells,[14] we assessed the response of AR-42 against bladder cancer stem cell populations. We analyzed SW780 cells by flow cytometry using the expression of CD44 and CD49f, which are surface markers characteristic of bladder cancer stem cells.[18] This established that approximately a third of the SW780 monolayer populations were $CD44^+CD49f^+$. To examine whether AR-42 had higher affinity to target the bladder cancer stem cell population SW780 cells were treated with cisplatin, AR-42 and cisplatin plus AR-42 at IC_{75} concentrations. Flow cytometry was then done to examine the expression of stem cell surface markers in surviving populations. The percent of $CD44^+CD49f^+$ cells remained similar at 27% to 30% after cisplatin treatment but the percent of $CD44^+CD49f^+$ cells decreased significantly after treatment with AR-42 alone and combined with cisplatin (fig. 3). This suggests that compared to cisplatin alone AR-42 may increase the susceptibility of the bladder cancer stem cell population to treatment.

In Vivo AR-42 Decreased Tumor Growth

To examine the effects of cisplatin and AR-42 on bladder cancer in vivo growth and differentiation we treated NSG mice implanted with a subcutaneous xenograft consisting of SW780 cells combined with fetal bladder mesenchymal cells. The cisplatin plus AR-42 combination led to a decreased rate of tumor growth and reduced tumor size with a significant decrease in tumor volume after combined treatment vs treatment with AR-42 or cisplatin alone (fig. 4, *A*). To test the effects of treatment in the cancer stem cell population we sorted SW780 cells and implanted the same number of $CD44^+CD49f^+$ fraction cells with fetal bladder mesenchyma. Compared to tumors derived from wild-type SW780 cells the $CD44^+CD49f^+$ SW780 tumors grew larger but were more sensitive to AR-42 treatment. Cisplatin plus AR-42 significantly decreased tumor growth compared to treatment with AR-42 or cisplatin alone (fig. 4, *B*).

We examined tumor differentiation by staining with basal CK (CK5) and luminal CK (CK20). Changes in tumor differentiation significantly differed between cisplatin only and cisplatin plus AR-42 treatment in tumors derived from native SW780 cells and from the $CD44^+CD49f^+$ fraction of SW780 cells. Adding AR-42 decreased basal cell expression, as shown by CK5 staining, and increased luminal cell expression, as characterized by CK20 staining. This suggests that AR-42 treatment may lead to more tumor differentiation than that of untreated or cisplatin treated tumors (fig. 4, *C*).

Cisplatin and AR-42

Combination Enhanced Apoptosis. To evaluate the effects of combined cisplatin and AR-42 in apoptosis induction we examined apoptotic activity using a flow cytometry based assay. We found increased apoptosis in the combination treated population compared to that in cells treated with AR-42 or cisplatin alone (fig. 5, *A*).

No Difference in Sequence. Clinically the sequence of combination drug delivery may be important and affect the synergic effects. Thus, we performed in vitro studies to test differences in cell viability based on the sequence of cisplatin and AR-42 administration. During 48 hours concurrent administration in the first or second half of the treatment period yielded no difference in cell viability compared to treatments with 1 drug administered in the first 24 hours followed by the second drug in the next 24 hours (fig. 5, *B*). This finding suggests that the mechanism of synergy between cisplatin and AR-42 is not sequence dependent.

DISCUSSION

Bladder cancer treatments have remained essentially unchanged for decades with limited patient options. Cisplatin forms the basis of bladder cancer chemotherapy but it is limited by its efficacy and toxicity. However, recent understanding of its molecular subtypes, molecular targets and widespread development of novel immune and targeted therapies, such as those targeting the PD-1/PDL-1 axis, are encouraging and have made inroads in bladder cancer therapy.[9,19,20]

VA combined with cisplatin in bladder cancer cell lines previously demonstrated the synergistic effects of HDAC inhibitors.[2,21] However, a phase II trial of VA in prostate cancer revealed significant neurotoxicity whether administered intravenously or orally.[22] TSA remains in preclinical development and

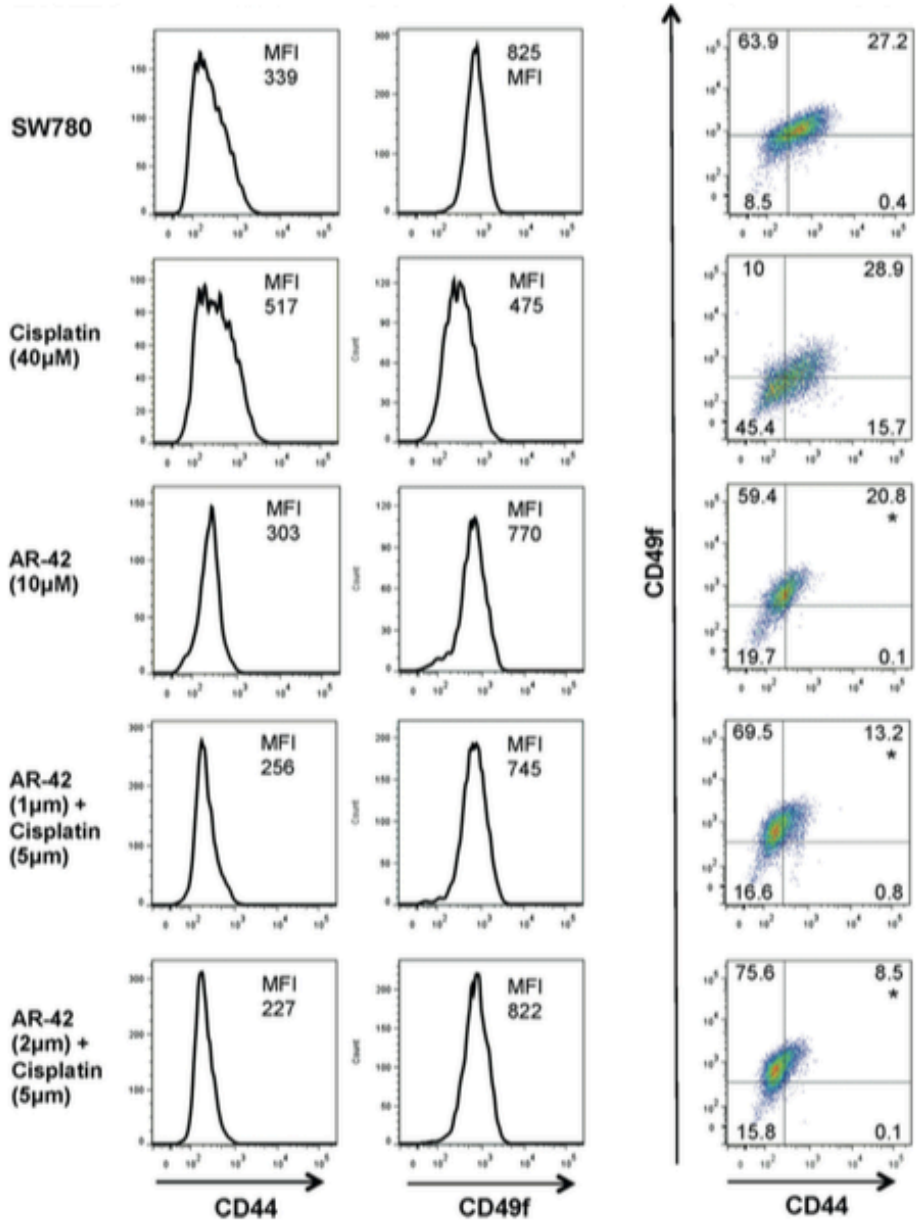

Figure 3. Cisplatin and AR-42 combination decreased $CD44^{+}CD49f^{+}$ population. SW780 cells treated with indicated doses of cisplatin and AR-42 to achieve approximately IC_{75} doses were examined by flow cytometry to assess CD44 and CD49f expression in surviving population. Higher 2 μM AR-42 dose was combined with cisplatin to evaluate dose response. Data represent 3 independent experiments. *MFI*, median fluorescence intensity. Asterisk indicates $CD44^{+}CD49f^{+}$ cell group comparisons statistically significantly different (1-way ANOVA $p < 0.05$).

NaB requires a mM concentration to achieve a measurable response. Because AR-42 has shown efficacy for multiple cancers, including cancer stem cells in particular,[14] we chose it as a promising HDAC inhibitor for analysis. To our knowledge we report for the first time that the novel HDAC inhibitor AR-42 synergizes with cisplatin against bladder cancer cells in vitro and in an in vivo tumor model.

Bladder cancer stem cells, which are marked by the surface markers $CD44^{+}$ and $CD49f^{+}$, represent

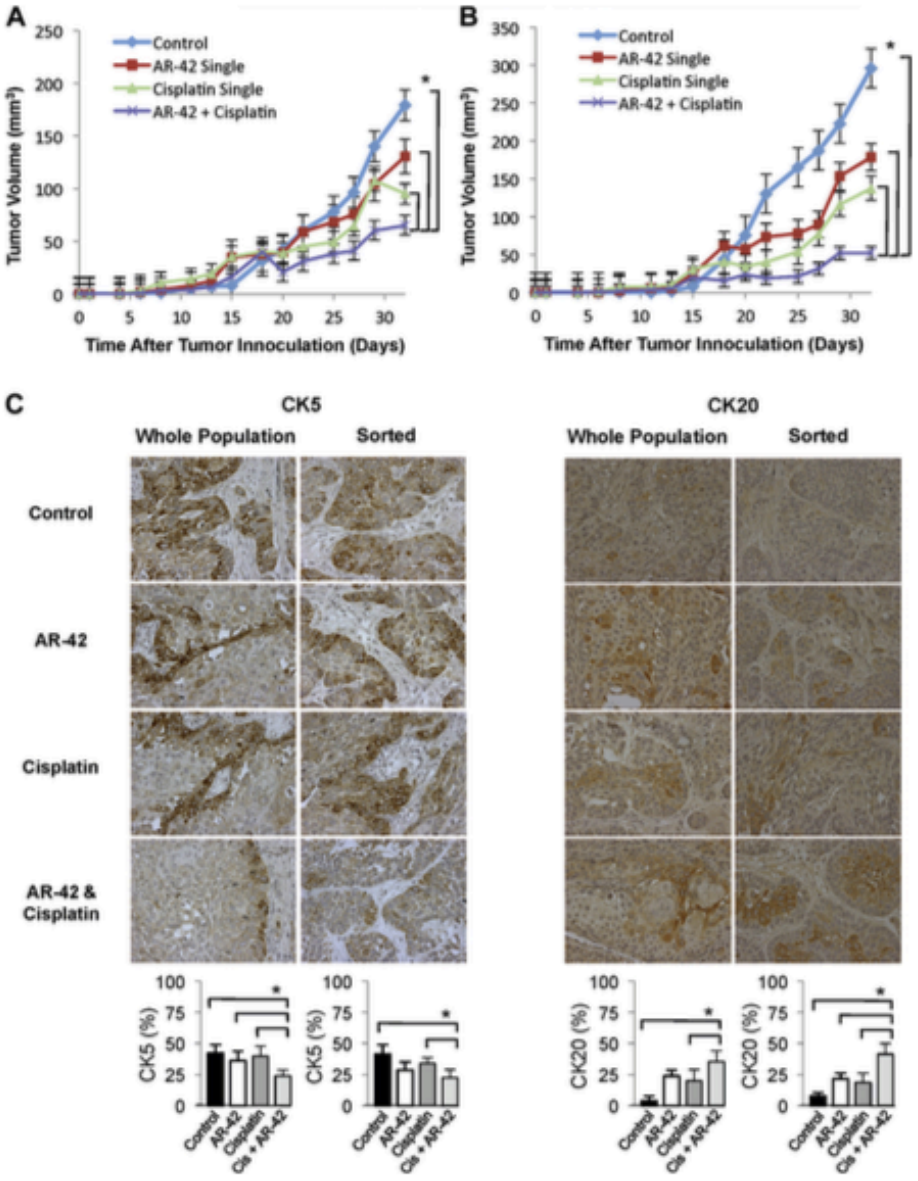

Figure 4. In vivo combined cisplatin and AR-42 decreased tumor size relative to single treatment or untreated tumors in NSG mice implanted with unsorted (*A*) or $CD44^+CD49f^+$ enriched (*B*) SW780 cells mixed with fetal bladder mesenchymal cells in Matrigel suspension. Treatments began on day 15 after palpable tumor first presented. Curves indicate mean of 6 tumors. Bars indicate SEM. Asterisk indicates statistically significant (2-way ANOVA $p < 0.05$). Representative unsorted and $CD44^+CD49f^+$ enriched tumors (*C*). CK5 and CK20 staining, reduced from ×400. *Cis*, cisplatin. Columns indicate mean of percent positive staining cells in 4 representative sections at 400× magnification. Bars indicate SD. Asterisk indicates statistically significant (1-way ANOVA $p < 0.05$).

a hierarchical organization of cells that can reconstitute all cell types of a specific tumor.[18] Their resistance to chemotherapy may explain recurrence after latency periods. Studies suggest that more poorly differentiated tumors, which are marked by the basal surface markers $CK14^+CK5^+$ and the surface marker profile $CD90^+CD44^+CD49f^+$, have a worse prognosis than less differentiated luminal subtypes that express luminal CK ($CK20^+$) and the associated surface markers $CD90^-CD44^-CD49f^+$.[23] These subtypes were validated in large-scale analyses of patient expression patterns.[9,19]

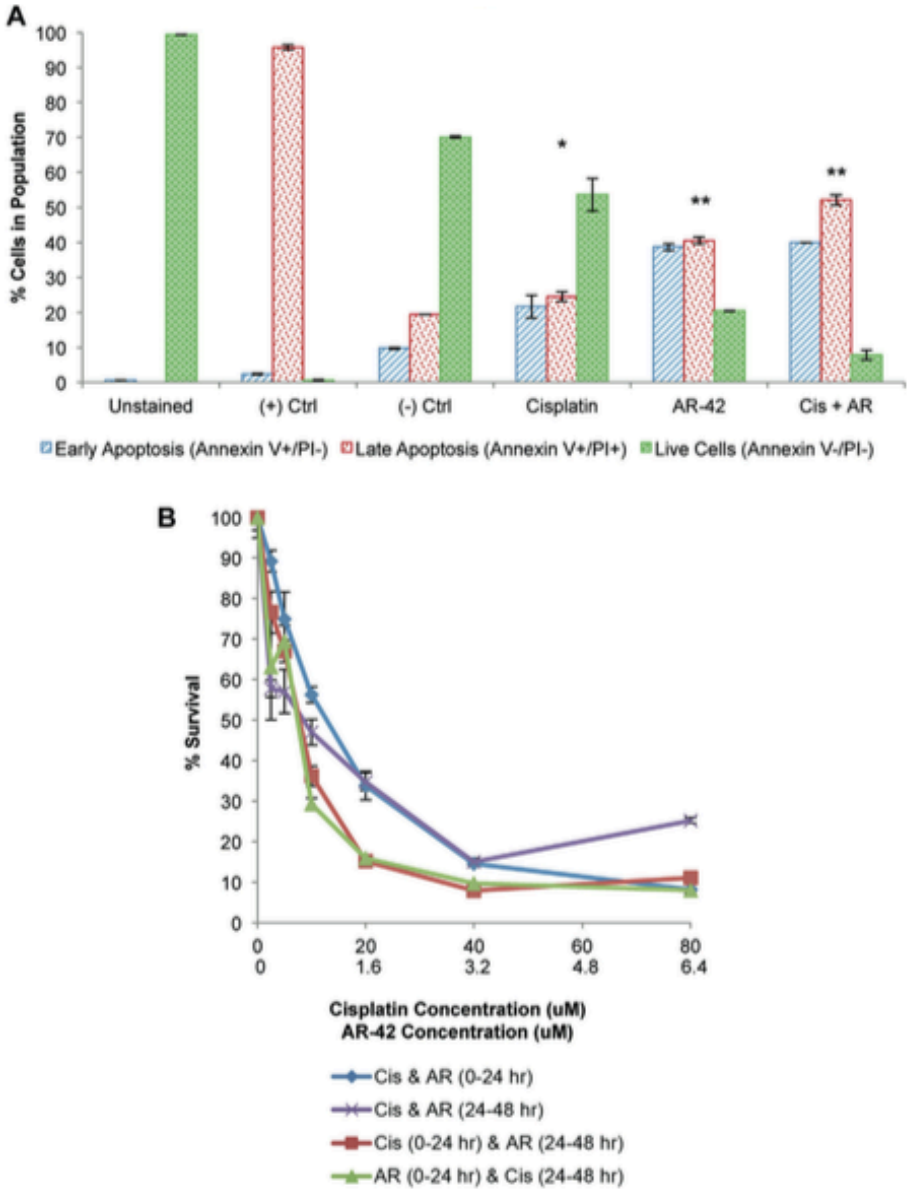

Figure 5. SW780 cells treated with cisplatin (*Cis*), AR-42 (*AR*) or cisplatin plus AR-42 for 24 hours showed enhanced apoptosis on annexin V and PI staining followed by flow cytometry (*A*). Annexin V^+PI^- cells were considered early apoptotic cells (blue bars). Annexin V^+PI^+ cells were considered late apoptotic cells (red bars). Live cells were unstained (green bars). *Ctrl*, control. Single asterisk indicates statistical significance between all populations and other treatment groups (1-way ANOVA $p < 0.05$). Double asterisks indicate statistical significance between all populations and other treatment groups except early apoptotic cells between AR-42 and AR-42 plus cisplatin (1-way ANOVA $p < 0.05$). SW780 cells were treated with varying cisplatin and AR-42 concentrations for 48 hours (*B*). Viability was assessed by MTT incorporation. Curves indicate mean of triplicate preparations and represent 2 independent experiments (not significant according to 1-way ANOVA $p < 0.05$).

The efficacy of HDAC inhibitors in stem cells is supported by recent evidence showing that HDAC-1 and 2 may be critical in embryonic stem cell self-renewal, in part by maintaining expression of the transcription factors Oct4, Nanog, Esrrb and Rex1.[14,24] AR-42 previously showed efficacy for specifically targeting leukemic stem cells.[14] Our results suggest that AR-42 has improved ability to destroy

the $CD44^{+}CD49f^{+}$ population of bladder cancer cells compared to cisplatin. Treatment with combined AR-42 and cisplatin may lead to more differentiated and, therefore, less aggressive tumors.

Study limitations include the use of bladder cell lines as a surrogate for evaluating primary bladder cancer. The subcutaneous model may also not reflect the bladder microenvironment. However, we noted inconsistencies in generating orthotopic xenografts using human bladder cancer cell lines compared to our established murine models and the subcutaneous model facilitated the measurement of tumor growth. To our knowledge the potential targets of AR-42 to nonhistone proteins has not been addressed. An important future direction is to explore its mechanisms and expand the understanding of bladder cancer biology. Reports of HDAC inhibitors mediating autophagy and the potential inhibition of autophagy by cisplatin in melanoma cells must also be explored.[25,26]

CONCLUSIONS

In our objective to provide a preclinical analysis of the efficacy of AR-42 in bladder cancer we identified the ability of AR-42 to synergize with cisplatin to augment the destruction of bladder cancer cells in vitro and in vivo, and preferentially target the cancer stem cell population. This synergistic effect may not only improve cisplatin efficacy but also improve its overall response rate or allow for a lower cisplatin dose to be used. This remains a subject of future study. Whether these observations translate clinically to long-term durable responses must be tested in future clinical trials. In the future we may select the use and sequence of novel therapies for bladder cancer based on molecular and genetic markers.

ACKNOWLEDGMENTS

ARNO Therapeutics provided AR-42 through a Material Transfer Agreement.

REFERENCES

1. Siegel R, Naishadham D and Jemal A: Cancer statistics, 2013. CA Cancer J Clin 2013; **63:** 11.
2. Von der Maase H, Hansen SW, Roberts JT et al: Gemcitabine and cisplatin versus methotrexate, vinblastine, doxorubicin, and cisplatin in advanced or metastatic bladder cancer: results of a large, randomized, multinational, multicenter, phase III study. J Clin Oncol 2000; **18:** 3068.
3. Drayton RM and Catto JWF: Molecular mechanisms of cisplatin resistance in bladder cancer. Expert Rev Anticancer Ther 2012; **12:** 271.
4. Witt O, Deubzer HE, Milde T et al: HDAC family: what are the cancer relevant targets? Cancer Lett 2009; **277:** 8.
5. Shankar S and Srivastava RK: Histone deacetylase inhibitors: mechanisms and clinical significance in cancer: HDAC inhibitor-induced apoptosis. Adv Exp Med Biol 2008; **615:** 261.
6. Prince HM and Dickinson M: Romidepsin for cutaneous T-cell lymphoma. Clin Cancer Res 2012; **18:** 3509.
7. Siegel D, Hussein M, Belani C et al: Vorinostat in solid and hematologic malignancies. J Hematol Oncol 2009; **2:** 31.
8. Poyet C, Jentsch B, Hermanns T et al: Expression of histone deacetylases 1, 2 and 3 in urothelial bladder cancer. BMC Clin Pathol 2014; **14:** 10.
9. Cancer Genome Atlas Research Network: Comprehensive molecular characterization of urothelial bladder carcinoma. Nature 2014; **507:** 315.
10. Buckley MT, Yoon J, Yee H et al: The histone deacetylase inhibitor belinostat (PXD101) suppresses bladder cancer cell growth in vitro and in vivo. J Transl Med 2007; **5:** 49.
11. Vallo S, Xi W, Hudak L et al: HDAC inhibition delays cell cycle progression of human bladder cancer cells in vitro. Anticancer Drugs 2011; **22:** 1002.
12. Qu W, Kang YD, Zhou MS et al: Experimental study on inhibitory effects of histone deacetylase inhibitor MS-275 and TSA on bladder cancer cells. Urol Oncol 2010; **28:** 648.
13. Ozawa A, Tanji N, Kikugawa T et al: Inhibition of bladder tumour growth by histone deacetylase inhibitor. BJU Int 2010; **105:** 1181.
14. Guzman ML, Yang N, Sharma KK et al: Selective activity of the histone deacetylase inhibitor AR-42 against leukemia stem cells: a novel potential strategy in acute myelogenous leukemia. Mol Cancer Ther 2014; **13:** 1979.
15. Sharma S, Symanowski J, Wong B et al: A phase II clinical trial of oral valproic acid in patients with castration-resistant prostate cancers using an intensive biomarker sampling strategy. Transl Oncol 2008; **1:** 141.
16. Peek EM, Li DR, Zhang H et al: Stromal modulation of bladder cancer-initiating cells in a subcutaneous tumor model. Am J Cancer Res 2012; **2:** 745.
17. Zhang Y, Wang Z, Yu J et al: Cancer stem-like cells contribute to cisplatin resistance and progression in bladder cancer. Cancer Lett 2012; **322:** 70.
18. Chan KS, Espinosa I, Chao M et al: Identification, molecular characterization, clinical prognosis, and therapeutic targeting of human bladder tumor-initiating cells. Proc Natl Acad Sci U S A 2009; **106:** 14016.
19. Choi W, Porten S, Kim S et al: Identification of distinct basal and luminal subtypes of muscle-invasive bladder cancer with different sensitivities to frontline chemotherapy. Cancer Cell 2014; **25:** 152.
20. Powles T, Eder JP, Fine GD et al: MPDL3280A (anti-PD-L1) treatment leads to clinical activity in metastatic bladder cancer. Nature 2014; **515:** 558.
21. Wang D, Jing Y, Ouyang S et al: Inhibitory effect of valproic acid on bladder cancer in combination with chemotherapeutic agents in vitro and in vivo. Oncol Lett 2013; **6:** 1492.
22. Kulp SK, Chen CS, Wang DS et al: Antitumor effects of a novel phenylbutyrate-based histone deacetylase inhibitor, (S)-HDAC-42, in prostate cancer. Clin Cancer Res 2006; **12:** 5199.
23. Volkmer J-P, Sahoo D, Chin RK et al: Three differentiation states risk-stratify bladder cancer into distinct subtypes. Proc Natl Acad Sci U S A 2012; **109:** 2078.
24. Jamaladdin S, Kelly RDW, O'Regan L et al: Histone deacetylase (HDAC) 1 and 2 are essential for accurate cell division and the pluripotency of embryonic stem cells. Proc Natl Acad Sci U S A 2014; **111:** 9840.
25. Del Bello B, Toscano M, Moretti D et al: Cisplatin-induced apoptosis inhibits autophagy, which acts as a pro-survival mechanism in human melanoma cells. PLoS One 2013; **8:** e57236.
26. Robert T, Vanoli F, Chiolo I et al: HDACs link the DNA damage response, processing of double-strand breaks and autophagy. Nature 2011; **471:** 74.